PHASE SENSITIVE SPECTRAL DOMAIN INTERFEROMETRY FOR LABEL FREE BIOMOLECULAR INTERACTION ANALYSIS AND BIOSENSING APPLICATIONS

by

SAJAL CHIRVI

Presented to the Faculty of the Graduate School of

The University of Texas at Arlington in Partial Fulfillment

of the Requirements

for the Degree of

DOCTOR OF PHILOSOPHY

THE UNIVERSITY OF TEXAS AT ARLINGTON

August 2012

ACKNOWLEDGEMENTS

I would like to thank my mentor Dr. Digant Davé for his supervision and support. He has encouraged and challenged me throughout my doctoral program. I would also like to thank him for his efforts in making me an independent researcher.

I would also like to thank my committee members Drs. Georgios Alexandrakis, Robert Bachoo, J.C. Chiao, Young-tae Kim and Kytai Truong Nguyen for their guidance and valuable inputs throughout my dissertation work.

I would like to thank UTA and UTSW for providing excellent research facilities with competitive and supportive environment.

My sincere thanks are also due to my parents, Mrs. Teja Chirvi & Mr Ashok Kumar Chirvi, who believed in me and supported and encouraged me at every phase of my Ph.D. I would also like to acknowledge the support, love and encouragement of my brother Jewel Chirvi, sister Twinkle Chirvi and my niece Raynee Makroo, who have been there with me through thick and thin and took over my share of responsibilities while I was away from home. In the end I would like to thank my husband, Dharmendra Nadkar who has suffered and survived my tantrums throughout my Ph.D work. He has been there for me during ups and downs in my research and personal life.

At the end I would like to thank God for it is he who guided and showed me path towards success.

July 19, 2012

ABSTRACT

PHASE SENSITIVE SPECTRAL DOMAIN INTERFEROMETRY
FOR LABEL FREE BIOMOLECULAR INTERACTION
ANALYSIS AND BIOSENSING APPLICATIONS

Sajal Chirvi, PhD

The University of Texas at Arlington, 2012

Supervising Professor: Digant P. Davé.

Biomolecular interaction analysis (BIA) plays vital role in wide variety of fields, which include biomedical research, pharmaceutical industry, medical diagnostics, and biotechnology industry. Study and quantification of interactions between natural biomolecules (proteins, enzymes, DNA) and artificially synthesized molecules (drugs) is routinely done using various labeled and label-free BIA techniques.

Labeled BIA (Chemiluminescence, Fluorescence, Radioactive) techniques suffer from steric hindrance of labels on interaction site, difficulty of attaching labels to molecules, higher cost and time of assay development. Label free techniques with real time detection capabilities have demonstrated advantages over traditional labeled techniques. The gold standard for label free BIA is surface Plasmon resonance (SPR) that detects and quantifies the changes in refractive index of the ligand-analyte complex molecule with high sensitivity. Although SPR is a highly sensitive BIA technique, it requires custom-made sensor chips and is not well suited for highly multiplexed BIA required in high throughput applications. Moreover implementation of SPR on various biosensing platforms is limited.

In this research work spectral domain phase sensitive interferometry (SD-PSI) has been developed for label-free BIA and biosensing applications to address limitations of SPR and other label free techniques. One distinct advantage of SD-PSI compared to other label-free techniques is that it does not require use of custom fabricated biosensor substrates. Laboratory grade, off-the-shelf glass or plastic substrates of suitable thickness with proper surface functionalization are used as biosensor chips. SD-PSI is tested on four separate BIA and biosensing platforms, which include multi-well plate, flow cell, fiber probe with integrated optics and fiber tip biosensor. Sensitivity of 33 ng/ml for anti-IgG is achieved using multi-well platform. Principle of coherence multiplexing for multi-channel label-free biosensing applications is introduced. Simultaneous interrogation of multiple biosensors is achievable with a single spectral domain phase sensitive interferometer by coding the individual sensograms in coherence-multiplexed channels. Experimental results demonstrating multiplexed quantitative biomolecular interaction analysis of antibodies binding to antigen coated functionalized biosensor chip surfaces on different platforms are presented.

TABLE OF CONTENTS

LIST OF ILLUSTRATIONS

LIST OF TABLES

CHAPTER 1

INTRODUCTION

1.1 Background and Significance

Biomolecular interaction analysis (BIA) plays vital role in life science research and clinical applications [1]. The host of biomolecular interaction occurring in a body drives and controls cellular function. BIA allows measuring interactions that occur between proteins, enzymes, DNA, antibodies or cell receptors. Antibodies in the body form complexes with foreign antigens to eliminate them from body. Drug molecules bind to cell receptors to illicit an antagonistic or agonist response [2]. The experimental study of functional proteomic interactions occurring within the body improves understanding at cellular level for most of the biological processes[2-4]. BIA is a multi-parameter quantitative and qualitative technique for studying binding affinity, binding kinetics, specificity and concentration analysis of protein-protein interactions[3]. Information from BIA can be used to gauge state of health of an individual, introduce new drug to market or early diagnostics from concentration analysis of multi-biomarker detection [5, 6]

The application area for biosensing is quite diverse and is expanding at a very high pace. The need for reliable and sensitive sensing modality for medical diagnostics, multi-marker detection and biosafety among others has further enabled the sensing field to mature [7-10]. Biosensors are also of paramount importance in pharmaceutical industry for drug discovery and screening[11-14]. As an example, there might be many test candidates for anti-cancer drug developed by pharmaceutical industry. The drugs can be tested for a target by biosensors. And if the drug has the desired characteristics, it can then be further tested on animal models [15]. The real time binding interactions provide information during hit finding, secondary screening,

lead optimization and lead selection. This information is vital for characterizing, optimizing and evaluating the drug candidate[16].

The biosensor essentially consists of biological-recognition system (bioreceptor) and transducer. The interaction of bioreceptor with analyte produces a change that is detected by a transducer. Transducer changes this physiochemical activity into a measurable signal. Depending on the type of bioreceptor, the sensors can be classified as immuno-biosensor, enzyme biosensor or nucleic acid/DNA. Based on type of transduction method, biosensors can be classified as optical, electrochemical, thermal, mass detection methods [17]. The information that can be extracted from the biosensor generally is the binding affinity of the analyte with ligand, the concentration of analyte, binding dynamics of the molecules, conformational changes in the protein, quantification of cancer biomarkers.

The study of BIA parameters is done in cell based and biochemical based assays[18, 19]. In biochemical-based assays, the target is immobilized on plate though coupling chemistry. The analyte protein is first extracted from cell and then characterized by incubating on the plate. The biochemical assays needs protein purification and extraction steps. In cell based assays the target protein is in their native form on the cell. Cell based assays eliminate need of purification and can also provide information about cytotoxicity and intracellular and extracellular targets. Also as the target of interest is unaltered, BIA yields data that represents natural physiological state [20].

The functioning of biosensors depends on the affinity binding of cells receptors or biomolecules to their corresponding functional partners. The interactions between two biomolecules change some physical parameter that can be detected and quantified using biosensor. The physical parameter change can be mass, refractive index, size, or enthalpy. Different technologies are available in the markets that are sensitive to either one of the physical parameter changes that occurs during binding. The action of binding interaction causes a physical parameter change that proportionally changes some property of the measured signal.

For optical modalities, there can be change in phase, wavelength, reflectivity, intensity, or polarization state of the measured signal that can be quantified. The linear relationship between physical parameter change and change in measured signal parameter enables quantification of BIA parameters. As an example the action of target protein binding to immobilized surface protein on micro-cantilever changes the mass (physical parameter) on the cantilever surface that induces bending (change in property of measured signal). The radius of curvature of bending is quantified and is converted to mass change as a function of target protein attachment [21-23].

1.2 Current Detection Techniques

The techniques available to study the proteomic methods can be categorized in labeled and label-free techniques. The labeled techniques are based on fluorescence, chemiluminescence or radioactive labeling. The protein of interest is labeled and can be detected after binding with target protein. ELISA (enzyme linked immunosorbent assay), fluorescence and western blot are some of the techniques. These techniques are well established and use simple instrumentation[24, 25]. ELISA relies on the secondary probe for detection, has a lower dynamic range and cannot perform biomolecular interaction studies, which are important from drug discovery point of view [26]. The fluorescence based detection techniques have been very successful for qualitative analysis. The quantitative analysis for this detection technique is difficult due to quenching and bleaching at high concentrations. Due to the presence of secondary label, the natural binding interactions may be altered. For protein, labeling can interfere kinetic characteristics when binding to other protein[27]. Also, quantification of signal requires complex calibrations [28, 29].

Label free techniques measure analyte of interest without need of any labels. The shift from sensitive labeled techniques to label free techniques is primarily due to more realistic model to mimic in vivo environment. Labels introduce additional variable in the quantification of

the analyte i.e. it can interfere with the molecule of interest. By eliminating use of labels, time and resources can be saved. Label free techniques also detect analyte in the single step rather than relying on secondary or tertiary probes for detection. Multi-analyte detection, real time detection, sensitivity, quantification capability and determination of kinetic and affinity constants are the other attractive features for most of the label free detection techniques[30]. Label free techniques for BIA are based on acoustic, optical, isothermal titration calorimetric and electrochemical[31-33]. Label free optical detection techniques are discussed in more detail.

1.3 Label Free Optical Detection Techniques

There are various companies that have commercialized label free biosensing techniques using different transduction methods. Table 1 gives the details about few commercialized optical label free detection techniques available in market[12, 13, 30, 34-37].

The optical label free detection technique that is successful and has been commercialized (Biacore) is surface Plasmon resonance (SPR) [38, 39]. SPR detects and quantifies the changes in refractive index of the ligand-analyte complex molecule on the sensor substrate. SPR is a well-established method and widely used for BIA with the level of 200-Da small molecule [40, 41]. However, it typically requires polarization dependent source, metal coating process, and highly accurate angle rotation data acquisition stage, which increases total fabrication cost and also limit the high throughput capability[42]. Also, special attention needs to be paid to the background refractive index changes caused due to change in buffer composition or temperature.

Nanostructure optical grating based sensing is another biosensing technique commercialized by SRU biosystems. White light source incident on grating reflects only a single wavelength. After biomolecular interaction, the wavelength of reflected light increases which can be quantified. This system uses a proprietary optical grating within each well of microplate and is limited in small molecule affinity detection [3, 33].

Table 1.1 Sample commercialized label free optical techniques for biosensing

Platform	Company	Technology	Sensor, platform, throughput and sensitivity
Biacore 4000	GE healthcare	Surface Plasmon resonance	Requires nobel metal surface. Flow cell based platform Parallel analysis upto 16 targets Detection limit 100 pM
EpicTM	Corning	Resonant waveguide grating	Sensor is three layered Well plate based platform 40,000 wells in 8 hpurs Sensitivity of 5 pg/mm^2
Octet Red 384	Forte´Bio	Biolayer interferometry	Sensor with fabricated reference layer Fiber tip based platform Parallel analysis of 16 targets Sensitivity of 0.05µg/ml at 1000 rpm
BIND	SRU Biosystems	Nanostructured optical grating (photonic crystals)	Sensor with fabricated optical grating Well plate based detection 96 wells in 30 seconds Sensitivity of 0.1 pg/mm^2
AnaLight Nanoflex	Farfield group	Dual Polarisation Interferometry	Sensor has fabricated reference layer Flow cell based platform Parallel analysis of 3 channels Sensitivity of 0.1 pg/mm^2
BioOptix 104sa	BIOPTIX	SPR-enhanced common path interferometry (SPR-CPI) for microarray analysis	Gold coated sensor surface Flow cell based detection Parallel analysis of 4 spots Sensitivity of 0.2 pg/mm^2
dotLab mx system	Alexa	Grating based light diffraction	Coupling chemistry forms grating Flow cell based detection Labeled multiplexing for 12 targets Sensitivity of 17pg/ml for protein A
OWLS 120	OWLS Sensor	Optical grating coupler sensor technology	Fine optical grating on sensor Flow cell based detection Has potential for high throughput Sensitivity of 1ng/cm^2
Lightpath S8	Lamdagen Corporation	Based on localized surface plasmon resonance (LSPR)	Sensor has nobel metal nanostructure Well plate based platform Parallel analysis of 8 channels Sensitivity of 10 ng/ml for Protein A

Corning has commercialized the technology of resonant waveguide grating for biosensing. It is the first high throughput BIA platform. The technique works by illuminating

sensor by broadband light and measuring wavelength of reflected light. The biomolecular interaction changes resonant wavelength, which is quantified. System can detect antibody interactions in serum, and can work for complex samples. Three layer patented optical biosensor is used for sensing and this technique has shown limitations in small molecule affinity and detailed kinetic analysis [3, 43, 44]. ForteBio introduced Octet platform that works on Bio layer interferometry technique. In this interferometric technique, interference signal is generated from immobilized ligand layer and fabricated intrinsic layer. Binding of protein to ligand changes optical path length, which causes a wavelength shift. The wavelength shift is direct measure of change in thickness of biological layer [40, 41]. Using this technique crude sample can be used for analysis and fastest interactions in fluidics free environment are demonstrated[3]. Fiber probes used for BIA requires stringent functionalized thin film thickness ($\lambda/2$) which can create fabrication challenge.

Phase-sensitive low-coherence optical tomography [45, 46] has been used for tissue imaging for depth-resolved amplitude and quantitative phase images of transparent samples[27]. This technique has also been demonstrated for label-free biosensing with picometer-level thickness sensitivity due to implementation of common path geometry [47]. Spectral domain phase sensitive interferometric (SD-PSI) technique measures phase change in interferometric signal. Change in phase is a function of change in optical path length (OPL) that occurs as protein binds to immobilized ligand. Resolution of 10^{-10} rad is possible in spectral domain phase sensitive interferometric technique that demonstrates high sensitivity[27].

1.4 Spectral Domain-Phase Sensitive Interferometer for BIA

Spectral Domain-Phase Sensitive Interferometry (SD-PSI) is implemented for biosensing and BIA in proposed work [27, 48, 49]. Interferometric techniques can correlate optical phase shift to the biomolecule accumulation density on the surface of interrogation[29]. Spectrum of light that is reflected from the sample produces interference pattern. This modulated signal has a frequency that corresponds with optical path length difference between

top and the bottom surface of sensor. The interference between these two surfaces represents an accurate phase delay between them and yields optical thickness of the layer.

In SD-PSI, phase shift in the interference signal as the ligand binds to the protein is detected. SD-PSI in configured in common path geometry where reference and signal is generated from the same sample arm, which makes the assembly more robust by rejecting common mode noise. Using this detection technique, concentration quantification, real time interaction measurements and kinetic characterization with high sensitivity of the analyte can be obtained. The system has a capacity for making measurements using bulk optical system as well as with miniature fiber probe. SD-PSI can also be integrated to different platforms such as static multi-well plate, flow cell and fiber tip based setups, Multi-platform compatibility of SD-PSI platform makes the use of SD-PSI attractive for different applications areas. The system also has high-throughput capability to measure many biosensing interactions in parallel. This capability of the system can be targeted for pharmaceutical drug discovery and screening where real time detection of biomolecules is important because it provides the information about the binding affinity, biomolecule association and dissociation constants[50].

Some of the advantages of detection of biomolecular interaction using SD-PSI as compared to tabulated techniques are that the sensor surface can be a regular coverslip. Most of the tabulated techniques need stringent sensor fabrication design and calibration. For some of the tabulated techniques, reflectance needs to be calibrated as quantification is based on measurement of changes in reflectance as the binding occurs. In SD-PSI, phase is quantified which is independent of surface reflectivity. Also, any intensity fluctuations affect reflectance measurements whereas phase remains unaffected. Any unbound molecules or a local change in buffer refractive index does not affect measurements in SD-PSI. Also, the compatibility of different biosensing platforms with SD-PSI makes it attractive. High throughput detection can be performed using coherence and time division multiplexing. BIA on fiber probe tip with multiplexing capability makes this technique further attractive as potentially many fibers with

sensors at the tip can be packed together to detect hundreds of proteins simultaneously in a test sample.

1.5 Organization of Dissertation

This section summarizes the motivation, background and significance of BIA studies. It also gives an overview of current labeled and label free detection techniques that are currently available in market. Further, a need of label free SD-PSI is justified for study of BIA studies.

Chapter 2: Theory, characterization and calibration of spectral domain-phase sensitive interferometer (SD-PSI)

Performance metrics such as signal to noise ratio (SNR), phase noise and throughput of SD-PSI is characterized. SD-PSI measures phase shift due to material accumulation, which is directly proportional to OPL. OPL is product of refractive index and physical length of the attached material on sensor. For calibration of physical length, samples with fabricated thin film in nanometer range are used. For refractive index measurements, serial dilution of glycerol is quantified. Calibrations results help in validating optical path length (OPL) results obtained from SD-PSI.

Chapter 3: SD-PSI biosensing platforms.

Bulk SD-PSI setup and fiber based SD-PSI system is used for studying BIA of rabbit IgG and anti Rabbit IgG interaction. Bulk system uses bulk optics for optical interrogation of biomolecules. Two sensor platforms compatible with bulk system are multi-well static sensor and flow cell. For fiber-based detection, sample arm is miniaturized with integrated optics in a fiber probe. Multi-well static sensor, flow cell, fiber with attached sensor (fiber probe 1) and fiber tip sensing (fiber probe 2) are compatible platforms for fiber-based detection.

Chapter 4: Multiplexed biomolecular interaction analysis.

This section focuses on high throughput capability of SD-PSI. The capability of the system to detect different proteins in the sample simultaneously is demonstrated. Multiplexed detection is demonstrated using 4 coherence channels as proof of principle. Compatibility of

SD-PSI for coherence multiplexing is demonstrated using bulk and fiber based system. For bulk system, multiplexing is demonstrated using multi-well static sensor and flow cell. For fiber-based setup, multiplexing is demonstrated using fiber probe 1 and fiber probe 2.

Chapter 5: Conclusions and future work.

This chapter summarizes the contribution and gives further scope of detection sensitivity improvement. This section also gives future direction on the proposed work.

CHAPTER 2

THEORY, CHARACTERIZATION AND CALIBRATION OF SD-PSI

Interferometry is used in vast application areas of astronomy, fiber optics, metrology and biosensing. Interferometric measurements have redefined international standard of length in terms of speed of light [51]. Interferometry is used for accurate measurements of distances, displacements, vibrations and surface topologies [51]. Interference signal or Interferogram is formed when interference occurs between electromagnetic waves [52].

When light of same frequency is split in two paths, the split beams have exactly same properties. When the waves are reflected off sample and reference path, they are recombined. Interference occurs from superimposed reflection from the surfaces. Interference can either be constructive for which the waves reinforce each other (in phase) or destructive where waves cancel each other (out of phase). In optical interferometry, the light path from source is split into two, which travel similar paths. Any optical change experienced by one path changes the phase of the light signal which when recombined with light from other unchanged path creates an interesting phenomenon of Interference.

Depending on type of source used, Interferometry can be categorized into low coherence interferometry and Laser interferometry. Due to long coherence length of Lasers, interference signal produced in Laser interferometry does not need precise path length matching. However, any stray reflections in Laser Interferometry can also generate interference pattern, which can result in incorrect measurements [53, 54]. In low coherence interferometry, low coherence source with coherence length in micrometers is used. Low coherence length ensures that interference occurs only within coherence distance. The fringe visibility of interference pattern is maximum when the optical path length between two beams are matched perfectly, fringe visibility decreases as the optical path length increases and disappears

completely when optical path length (OPL) is greater than coherence length [55]. Hence, depth resolution depends on coherence length of source; shorter coherence length gives better spatial resolution.

Low coherence interferometry can be performed in time domain or in spectral domain. In time domain low coherence interferometry, depth probing is achieved using scanning mirror. Recorded interferogram is a function of reflector position. Spectral domain interferometry produces interferogram as a function of wavelength. The depth information is provided from coherence gating. As no mechanical moving parts are involved in spectral domain low coherence interferometry, the phase noise is drastically reduced [56-58].

Spectral Domain Low Coherence Interferometer (SD-LCI) is a non contact sensing modality [59]. The interference signal obtained from low coherence light source is spatially and temporally localized which allows for measurement of small distances reflected from different layers of the sample [60]. The spectral domain-LCI analyses superposition of spectrums reflected from sample and reference arms and hence uses spectrometer (spectrum analyzer) as the detection system. Using spectrometer, total intensity is measured as a function of wavelength[60].

Spectral domain low coherence interferometry can be implemented using two path or common path geometry. In two-path geometry, two beams travel in physically separated paths and recombine to produce interferogram. In common path geometry, two beams travel along same path and recombine to produce interferogram.

Figure 2.1 shows a simplified low coherence two path interferometric setup. As seen from the figure, light from broadband source is split into two beams using beam splitter. One beam travels towards the reference (mirror) and is reflected back. The other beam travels towards the sample and is reflected back. Essentially, LCI measures the echo time delay between the light backscattered from sample and reference path. These two beams are superimposed and create an interference pattern, which is detected by spectrometer.

Characterization of interference pattern gives the information about the sample. Phase noise from two path interferometer is in hundreds of nanometers and cannot be used for biomolecule quantification which needs noise less than picometer range for sensitive detection [61].

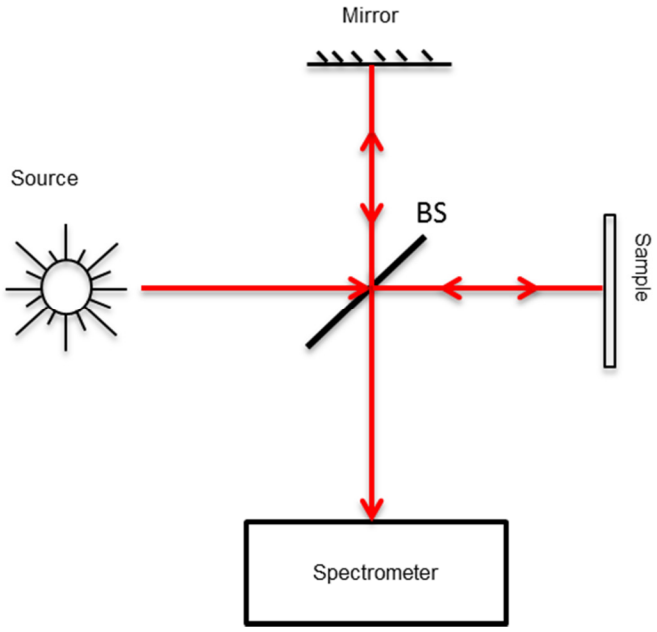

Figure 2.1 Low coherence two-path interferometric setup. Light from source is split in two using beamsplitter (BS) which after reflecting back from reference and sample path are recombined to produce interference fringes detected by spectrometer

In order to perform sensitive phase measurements using SD-LCI, a common path interferometric geometry is implemented. In this geometry, rather than two-path arrangement only one path geometry is used which is shown in figure 2.2. As seen from figure 2.2, both sample and reference beam travel along same path. The reference signal is generated from bottom of sample (coverslip) and sample signal is generated from top of sample. This geometry can help in quantification of phase changes that occur when there is any optical path length change in sample and hence helps in ultrasensitive detection [62]. As compared to two-path geometry, common path interferometry is resistant to environmental factors as it affects both reference and sample beams equally. Using this setup common mode noise is cancelled giving

the system higher stability and sensitivity. Also this geometry, does not have differential dispersion and polarization related issues [63].

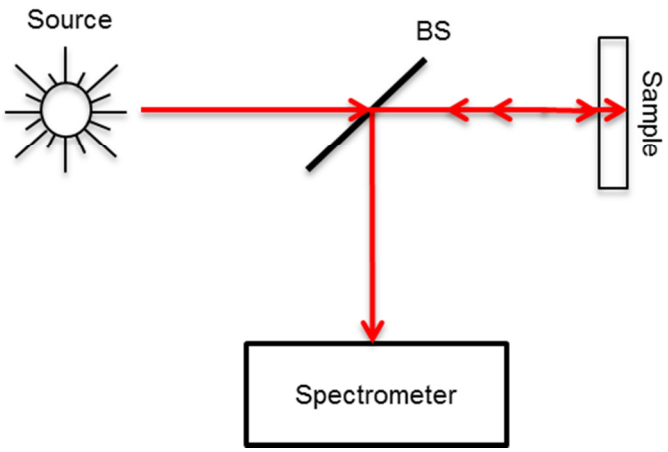

Figure 2.2 Low coherence single-path interferometric setup (common mode interferometry). Light from source is transmitted through beamsplitter (BS), which gets reflected back from top and bottom surface of sample and are recombined to produce interference fringes detected by spectrometer

Using this technique real time displacements measurements with sensitivity in picometer to nanometer range have been demonstrated [58]. Implementation of the technique for detection of biomolecules can be performed with high sensitivity as biomolecules are in nanometer range. Spectral domain phase sensitive interferometer (SD-PSI) in common path geometry is implemented for study of Biomolecular Interaction Analysis (BIA). Signal detected by spectrometer has interferometric component that contains information about amplitude and the phase of the sample. Extraction of phase information quantifies sub wavelength variations occurring in the sample [57, 58, 64]. The phase changes occur due to optical path length (OPL) changes in the sample. Optical path length is product of distance (l) traveled by light in media of given refractive index (n) and is given by

$$\Delta p = n * l \qquad (1)$$

2.1 Spectral Domain-Phase Sensitive Interferometry (SD-PSI)

Fiber optic configuration of spectral domain phase sensitive interferometry is implemented for BIA. Fiber optic configuration offers advantages of immunity by electromagnetic interference, flexibility of using them in different environmental conditions, and offers higher sensitivity [63].

2.1.1 Working Principle of SD-PSI for Biosensing

Figure 2.3 shows the cartoon illustration of the working principle of technique. Capture molecule/ligand (red) is immobilized on the aldehyde-coated coverslips that attaches amine group of protein covalently on the sensor surface before interrogation. During optical interrogation, light (yellow) incident on the coverslip is reflected from bottom of the coverslip (air-glass interface) and top of attached protein (ligand-buffer interface) as shown in figure 2.3. Two beams of reflected light interfere and the interference pattern (red) is recorded as shown on top right panel of figure 2.3. After incubation of analyte (blue) and binding with ligand, the source of reflective surface change. Reflections now occur at the glass-air interface and the analyte-buffer interface resulting in the interference signal, which is shifted with respect to the previous interference pattern as shown by bottom right panel of figure 2.3.

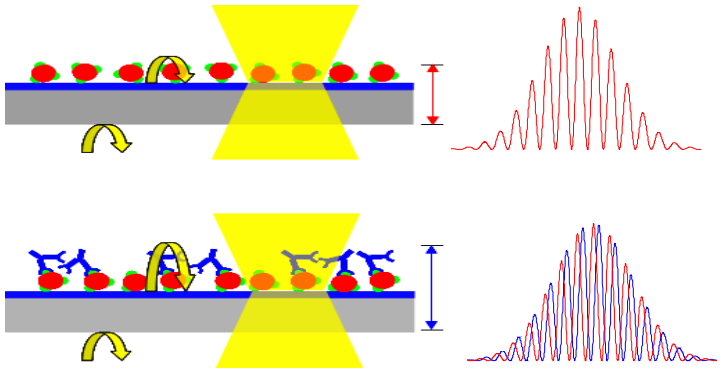

Figure 2.3 Cartoon illustration of working principle of SD-PSI. Upper panel shows the source of reflective surfaces for interference from immobilized protein (ligand). The bottom panel shows change in reflective surfaces after incubation of analyte causing shift in the interference pattern due to ligand-analyte complex formation.

The shift occurs due to the increase in the optical path length as a result of the physical increase in thickness caused by the analyte binding onto the ligand. The sub wavelength change in the length due to binding can be precisely quantified as change in phase. In this setup common path geometry of spectral domain interferometry is implemented and hence the sensor surface generates both sample and reference signal. Common path geometry has greater stability and is less sensitive to vibrations that in turn help in sensitive detection of analyte [65, 66].

When light is focused on the optically clear coverslip, light is reflected from the top surface of the coverslip and then again from the bottom surface of the coverslip. In spectral domain systems, the time varying signal along the optical axis is converted into the frequency Fourier domain[67].Then these two beams are combined to form interference signal. This interference signal can be mathematically represented by equation 2 [65, 68-70].

$$S(k) = S_0(k)\{R_1 + R_2 + \sqrt{R_1 R_2}|\mu(k)|\cos(4\pi\Delta p k)\} \qquad (2)$$

Where, $S_0(k)$ is incident spectral intensity, R_1 and $R_2$are reflectivities of two surfaces, μ_k is the spectral degree of coherence which is assumed one as the light exiting a single mode fiber is spatially coherent, Δp is optical path length difference between the two surfaces and k is the wave number. The cosine term is equation 2 causes modulation in the signal, which is function of optical path length difference between two reflective surfaces of the coverslip. Fourier transforming equation 2 can quantify the magnitude of the reflected light as a function of optical path length difference between two reflective surfaces of the sensor.

$$\Delta\varphi = \tan^{-}\left\{\frac{\mathrm{Im}\,F(S(k))}{\mathrm{Re}\,F(S(k))}\right\} = \frac{4\pi\Delta p}{\lambda_0} \qquad (3)$$

From equation 3, change in the phase of interference signal as analyte binds to captured protein can be precisely quantified which can be related to the change in the optical path length due to binding. Here λ_0 is center wavelength of the low coherence source.

The cumulative phase change that occurs when analyte is incubated depends on OPL change that in turn depends on size and refractive index of the analyte molecule binding on the surface. The OPL changes as number of analyte molecules binding to immobilized ligand in the optical interrogation volume changes. Quantification is carried out in linear region where OPL changes linearly as a function of concentration of analyte. The maximum phase change for a given analyte occurs when all the binding sites in the interrogation volume are captured by the analyte. When this occurs, monolayer of analyte on sensor surface is assumed. The minimum concentration of analyte that can be detected depends on phase noise of the system. For a given concentration of the incubated analyte, the adsorbed mass per unit area of bound analyte in the interrogation volume can be quantified as [71],

$$\eta = \frac{\Delta\varphi_m}{\Delta\varphi_t} \times \frac{w_m}{A_m} \qquad (4)$$

where $\Delta\varphi_m$ is phase change due to a given concentration of analyte, $\Delta\varphi_t$ is total phase change due to monolayer of analyte on sensor chip, w_m is weight of the analyte molecule and A_m is the cross-section area of the analyte molecule that is perpendicular to optical interrogation axis.

2.1.2 SD-PSI Optical Setup

The setup consists of superluminescent diode (SLD), 635 nm visible light source, 90:10 fiber coupler, 50:50 fiber coupler and home built spectrometer. The broadband SLD light source operates at 800-nm center wavelength with full-wave half-maximum (FWHW) and coherence length of 20nm and 14 μm respectively. The isolator in the system is incorporated to protect SLD source from back reflections that can damage or create instability in performance of SLD source. After isolator light is input in single axis fiber bench. This is used to attenuate the power on the sample when signal goes in saturation. The output port of fiber bench acts as input to 90:10 fiber coupler. To other input arm of coupler, 635nm red light source is connected to visualize the light focused on the sample. The arm with 90 % of power is inputted to 2x2 50:50 fiber coupler. The second coupler splits power equally in two sample paths. However, in figure

2.4 only one path is used for sensing. The light is collimated and then focused on the sample surface. The light is reflected back from reflective surfaces of the sensor surface. The interference signal caused due to the light reflecting back from the reflective surfaces of the sample is coupled to a home built spectrometer.

In home built spectrometer, light input to spectrometer is first collimated and is then directed to diffraction grating (1200 lines/mm). Diffraction grating splits the light into its frequency components. Focusing lens is used to focus light on CCD camera. The spectrally dispersed output of spectrometer is captured by attached 12-bit line scan camera. CCD records the amount of light that hits each pixel and converts to voltage level. As camera is 12 bit, each pixel in the camera can handle 4096 brightness units. The camera communicates with NI 1428 camera link acquiring digital frames and stores them on system hard drive. The spectrometer can acquire 20K spectra/sec with a resolution of 0.06nm.

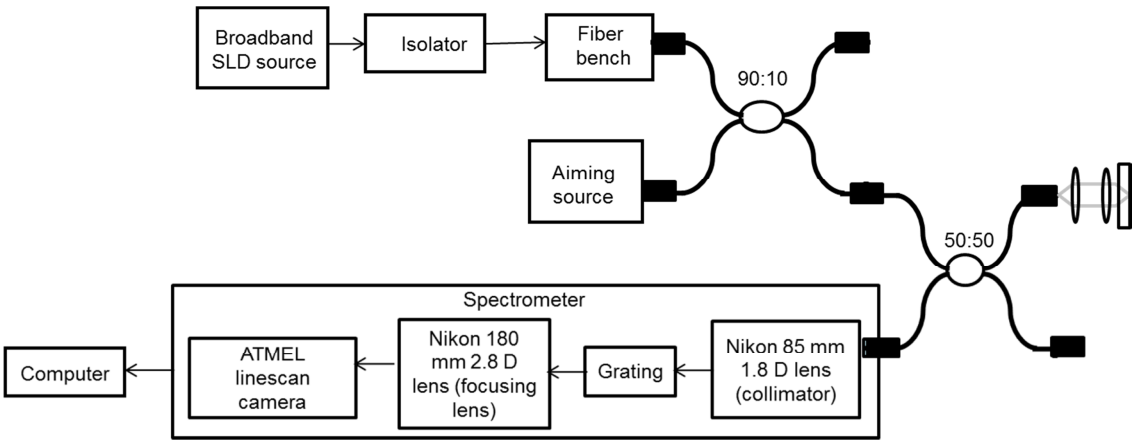

Figure 2.4 Optical setup of spectral domain phase sensitive interferometer. 90:10 coupler splits combined power of 800nm and 635 nm Laser in 90:10 ratio. 90% is input to 50:50 coupler which after reflecting back from sensor surface is detected by spectrometer. Computer stores acquired interference spectrums.

2.2 Characterization of Spectral Domain-Phase Sensitive Interferometry (SD-PSI)

The SD-PSI system is characterized for signal to noise ratio, phase noise, limit of determination and spectral resolution.

2.2.1 Signal to Noise Ratio (SNR)

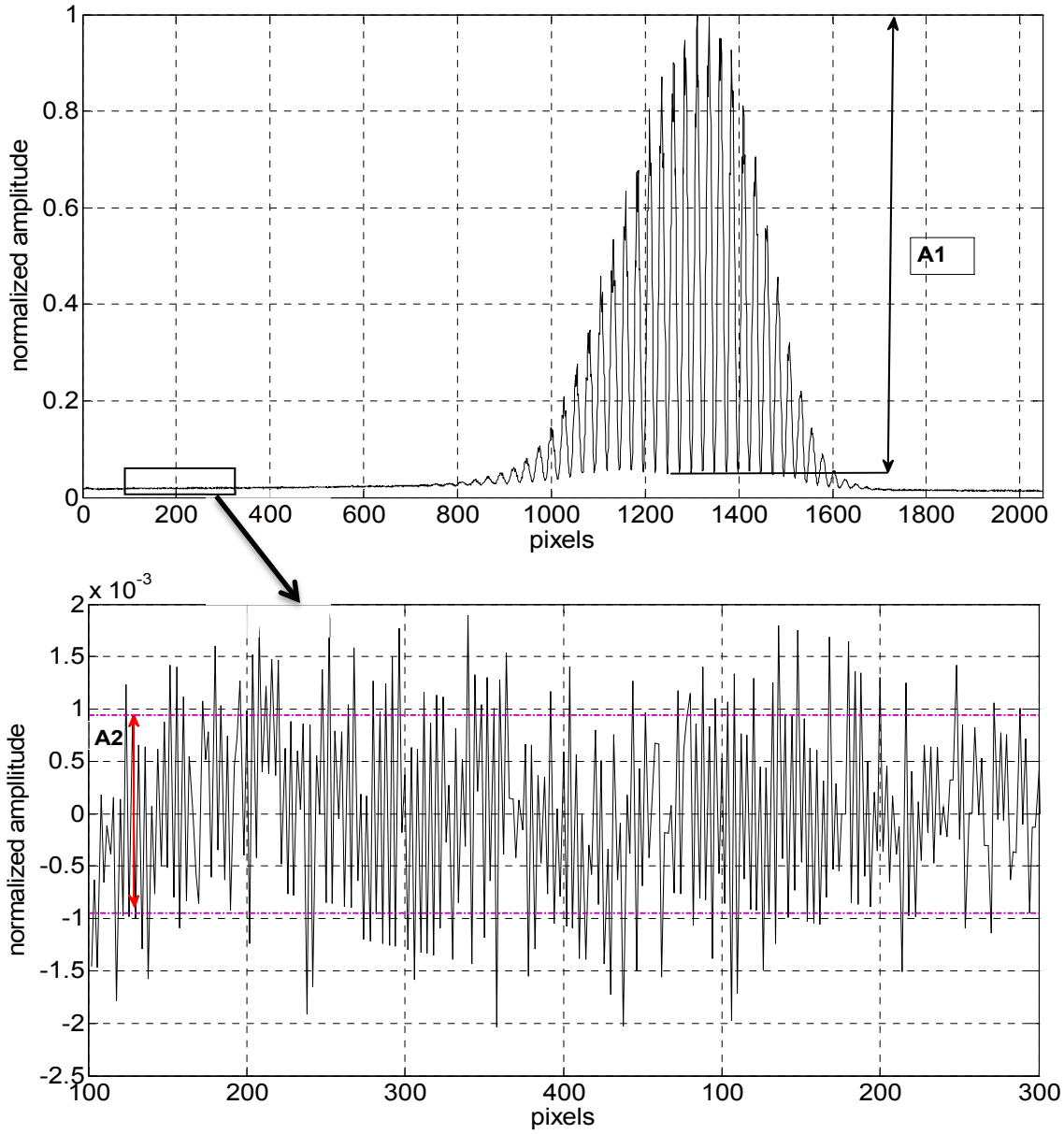

Figure 2.5 Calculation of signal to noise ratio (SNR) of SD-PSI for a coverslip of given thickness. The top panel shows interference spectrum with modulation depth A1 and bottom panel shows baseline standard deviation quantified as A2

Figure 2.5 shows procedure that is used to calculate signal to noise ratio experimentally. Coverslip with PBS (buffer) is used as the sample. The interference pattern

obtained is used to calculate signal to noise ratio of the system relevant to biosensing experiments. The signal is normalized to calculate the modulation depth. The modulation depth is considered as the signal rather than peak amplitude of the interference signal. This is because as the depth (thickness) of coverslip increases, the modulation depth decreases. The arrow on the top panel of the figure 2.5 shows the modulation depth (A1), which is (1-0.05) 95%. The RMS noise (A2) is calculated as standard deviation (0.014) of the baseline signal as shown by bottom panel of figure 2.5. The SNR calculated for this case is found out to be 56.6 dB.

$$(\mathrm{SNR})\mathrm{dB} = 20\log_{10}\left(\frac{\mathrm{A1}}{\mathrm{A2}}\right) \qquad (5)$$

2.2.2: Phase Noise

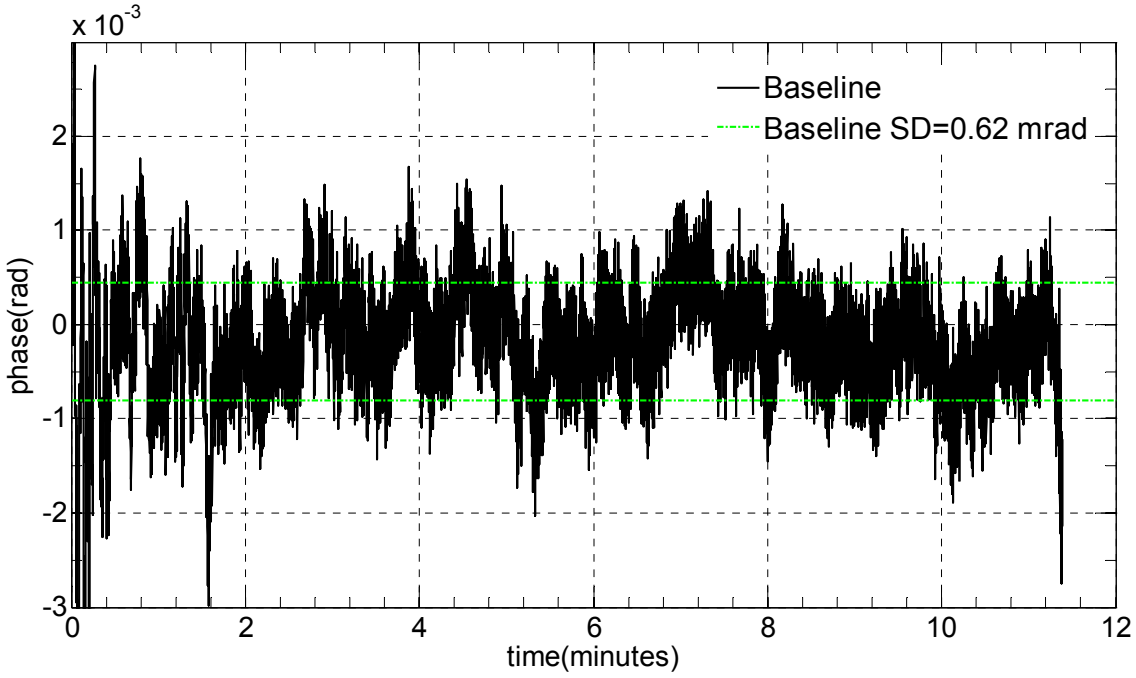

Figure 2.6 Phase noise of SD-PSI. The plot shows baseline phase signal and green lines show standard deviation of baseline signal.

The phase noise in SD-PSI varies with thickness of coverslip used, integration time, and the interface from which light is reflected to generate interference signal. Figure 2.6 shows

baseline signal acquired from SD-PSI system. Phase signal is acquired with coverslip # 0 as sample. The integration time and acquisition rate used is 36μs and 20Hz respectively. The phase noise is quantified as standard deviation in the baseline signal. After baseline stabilization, standard deviation (σ) of phase plot (figure 2.6) is calculated to be 0.62 milli-radians, which is phase noise floor of the system.

The phase noise of SD-PSI changes as a function of coverslip thickness used. Figure 2.7 shows phase noise as a function of coverslip thickness used. Coverslip # 0, 1, 1.5 and 2 have average thickness of 65,127,190,254 μm respectively. As thickness increases, the modulation depth of interference signal decreases which in turn increases the phase noise. The figure shows increase in phase noise with increase in coverslip thickness. The figure also shows the dependence of phase noise on the nature of the interface from where light is reflected for generating interference signal. It is seen that phase noise is higher for glass-PBS interface as compared to glass-air interface. However, the glass-PBS interface phase noise is more relevant as biosensing experiments are done with PBS as buffer.

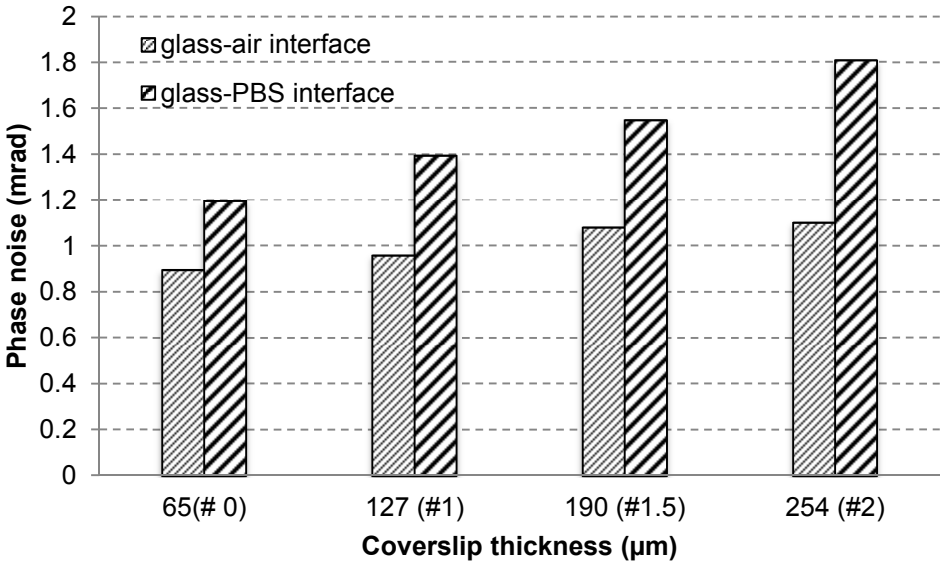

Figure 2.7 Phase noise of SD-PSI as a function of coverslip thickness. The bar plots shows baseline signal for glass-PBS interface and glass-air interface.

The reflectivity of the surface can be quantified by using the formula

$$R = \left(\frac{n_1 - n_2}{n_1 + n_2}\right)^2 \qquad (6)$$

For air-glass interface, the reflectivity is 4%. For PBS-glass interface, the reflectivity reduces to 0.36% (RI_{water} = 1.33, RI_{glass} = 1.5, RI_{air} = 1). From equation 2, the interference signal is a function of reflectivity of two surfaces of coverslip (R_1 and R_2). Hence reduced reflectivity at air-PBS interface increases the phase noise as evident from figure 2.7.

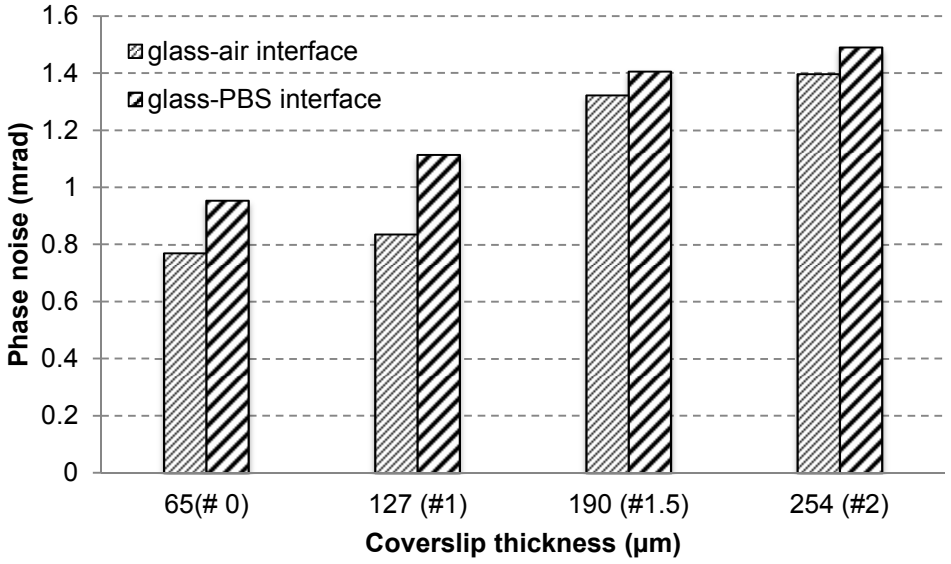

Figure 2.8 Phase noise of SD-PSI as a function of coverslip thickness coated with titanium dioxide (TiO_2). The bar plots show baseline signal for glass-PBS interface and glass-air interface.

However, if the reflectivity of the air-buffer surface is increased, the phase noise can be improved. Coating the glass surface with an optically clear material with higher reflectivity can improve phase noise. One material that can be used for coating is titanium dioxide. Titanium dioxide is spin coated on coverslips at 3000rpm for 60 seconds. The coated coverslips are heated at 450^0C for 10 minutes. This process sinters titanium dioxide on the coverslip. Figure 2.8 shows results for titanium dioxide coated coverslips. Again the phase noise is compared for

coverslips of 4 different thicknesses all coated with titanium dioxide. Also phase noise for glass-air and glass-water interface are plotted.

As seen from figure 2.8, with the increase in coverslip thickness, phase noise increases. Also, it is seen that phase noise is higher for glass-PBS interface as compared to glass-air interface. Also by comparing figure 2.7 and 2.8, it can be seen that phase noise for both coverslip thickness and interfaces decreases after titanium dioxide coating. For air-glass (TiO_2) interface, the reflectivity is increased to 18.3% (RI_{water} = 1.33, RI_{TiO2} = 2.5, RI_{glass} = 1.5, RI_{air} = 1). For PBS-glass (TiO_2) interface, the reflectivity increases to 9%.

2.2.3: Limit of Determination (LOD)

The phase noise dictates the limit of detection of protein of interest. Hence, ways of reducing the phase noise can help in improving the sensitivity of the system. If the detectable signal is defined to be 3σ, then the resolution of the sensor which is limit of determination (LOD) is defined as [72]

$$\mathrm{LOD} = \frac{3\sigma}{\mathrm{sensitivity}} \qquad (7)$$

As will be seen in chapter 3, for anti-rabbit IgG sensitivity is found to be 33 ng/ml in static setup. Using equation 7, resolution is calculated to be 86.7 pg/ml. This means that a change in the concentration by 86.7 pg/ml can be detected by SD-PSI for anti-rabbit IgG molecule.

2.2.4: Spectral Resolution

Experimentally, spectral resolution of the spectrometer is found by calculating number of pixels that image FWHM of source spectrum. The CCD used in the system is linescan camera having 2048 pixels with each square pixel 14μm in dimension. Spectrum of the source is measured by using mirror as sample. FWHM of reflected spectrum is imaged on 342 pixels. Hence the spectrometer resolution is calculated as

$$\delta\nu = \frac{\Delta\lambda}{\mathrm{N}} \qquad (8)$$

Here, Δλ is bandwidth of the source and N is number of pixels that image the reflected spectrum. Some of the specifications of SD-PSI are tabulated below

Table 2.1 Specifications of SD-PSI system for biosensing application

Parameter	Units	Specifications
Output power (at sample)	μW	230
Spectral resolution	nm	0.06
Spectral range and BW	nm	792-812, 20
Coherence length	μm	14
Signal to noise ratio	dB	56
Max sensor thickness	mm	1.17

2.3 Calibration of Spectral Domain-Phase Sensitive Interferometry (SD-PSI)

OPL changes can occur either due to change in length on sensor surface or due to change in refractive index (RI) in the interrogation volume. Quantification of physical length change can be achieved by assuming constant refractive index and quantification of refractive index change can be achieved by assuming constant length. For calibration both platforms are tested.

2.3.1 Quantification of Physical Length Change Assuming Constant Refractive Index

In this platform, refractive index of any material or biomolecule attaching to reflective surface is assumed constant. The changes in OPL are seen due to change in physical length increase on the surface of sensor. Figure 2.9 shows source of interference signal from two reflective surfaces of the coverslip. The light reflects from top and bottom surface of coverslip of thickness *l*. As biomolecules immobilize on interface 1, the reflective properties of interface 1 will change. In this geometry, the surface is modified so that it can physically attach biomolecules on its surface.

When biomolecules attach to interface 1, there is a change in OPL. If a constant RI of protein is assumed [73], then any change in phase of interference signal is caused due to physical change in length of interface 1 due to protein attachment. Using this geometry, it is possible to quantify the physical length change (l) due to attachment of biomolecules.

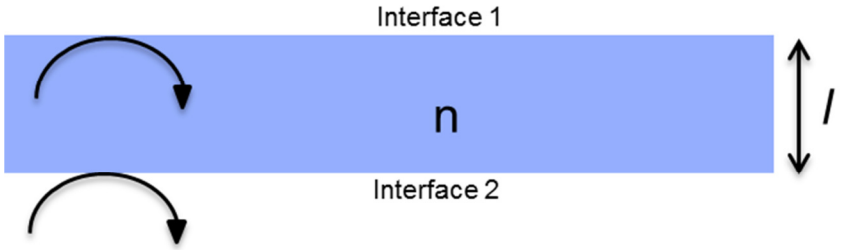

Figure 2.9 Source of reflective surfaces (interface 1 and interface 2) from a coverslip. Interface 1 is functionalized with ligand to capture analyte. This geometry quantifies physical length change, if refractive index of protein is assumed constant.

Equation 9 gives quantification formula for measuring physical length change (Δl) due to attachment of protein on sensor determined from change in phase of interference spectrum ($\Delta\varphi$). Here the refractive index of protein is assumed constant ($n = 1.45$) [73]. λ_o is center wavelength of the light source.

$$\Delta\varphi = \frac{4\pi n \Delta l}{\lambda_o} \qquad (9)$$

For calibration studies using this geometry, steps are created on coverslips of various heights. Steps are created by deposition of optically clear material over half portion of coverslip. The samples provided by collaborator, have unknown refractive index and unknown step size. The material deposition is done for three different thicknesses in nanometer range. Since, both refractive index and step size of samples is unknown, SD-PSI measurements are shown in OPL. Physical thickness of steps is quantified using profilometer. From these two measurements, refractive index change of the material is quantified. For quantification of protein attachment on functionalized coverslip, protein monolayer is deposited on a portion of sensor. The monolayer of protein quantification is done using SD-PSI and profilometer.

2.3.1.1: Measurement of step sizes formed from deposition of optically clear material

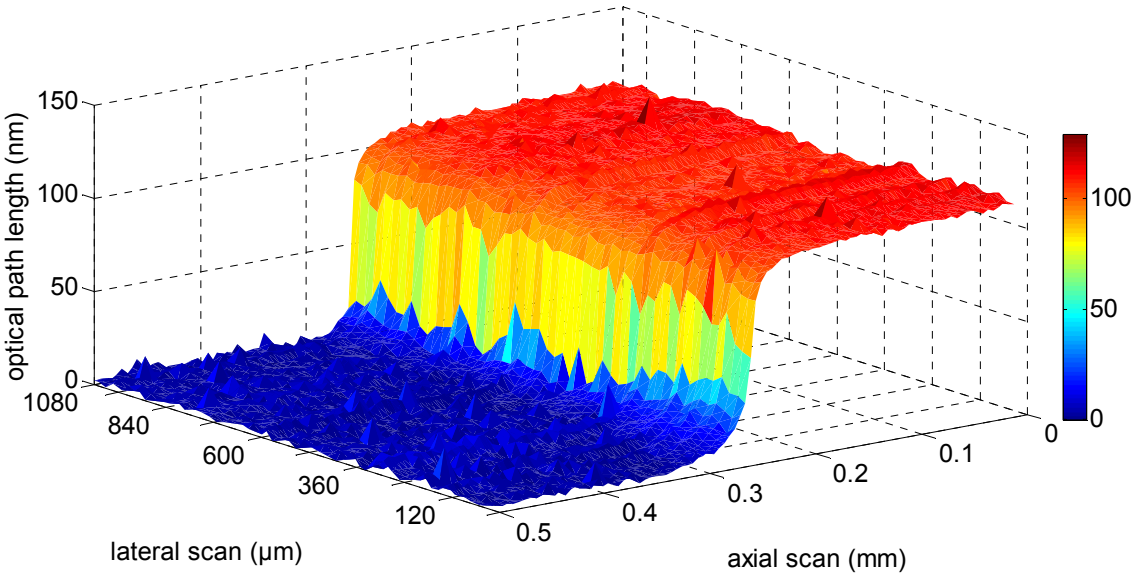

Figure 2.10 Optical path length measurement for sample 1 (1.0 mm x 0.5 mm) using SD-PSI for a step size estimated to have physical step size of 44.5 nm using profilometer.

The samples are glass coverslips with half portion of the coverslip coated with optically clear material of different heights. Using SD-PSI, three-dimensional plot is obtained by scanning across the step of 1mm x 0.5 mm section. The lateral step increment for these plots is 20µm. Using SD-PSI the optical path length of the samples is obtained which is a product of physical length of the step and refractive index of the material coated. The refractive index of the coated step is unknown; hence the step sizes using SD-PSI are reported as product of refractive index and physical step size. The step sizes are also measured using VEECO profilometer, which measured the physical step size.

Figure 2.10 shows the results for the thin film step sample 1. The optical path length obtained using SD-PSI show an average step size of 100nm. Figure 2.11a shows, the 3D plot of the same sample measured using profilometer. Figure 2.11b show a single line scan of the step. The profilometer line scans show an average physical step size of 44.5nm. Taking

profilometer height measurement as standard, the refractive index of the material is calculated to be 2.25.

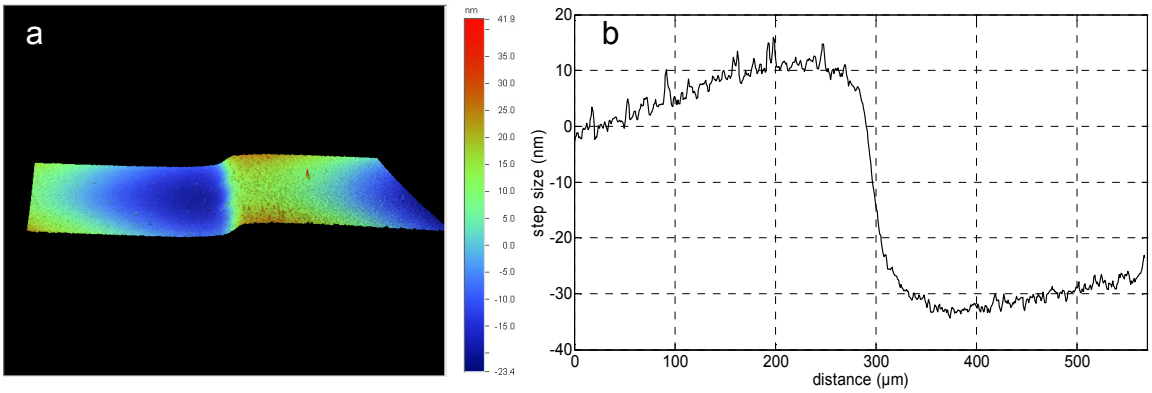

Figure 2.11 Physical length measurement using profilometer for sample 1. a) 3D plot showing step measured b) single line scan showing the step size measured using profilometer.

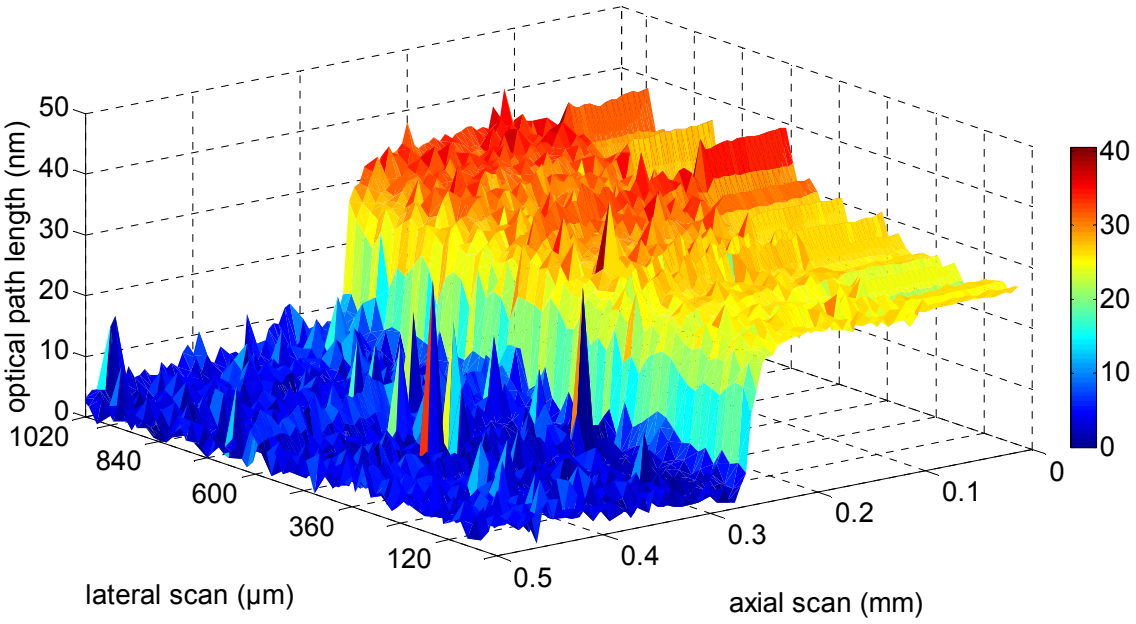

Figure 2.12 Optical path length measurement for sample 2 using SD-PSI (1.0 mm x 0.5 mm) for a step size estimated to have physical step size of 11.2 nm using profilometer

Figure 2.12 shows the results for the thin film step sample 2. Optical path length obtained using SD-PSI show an average step size of 25 nm. Sample physical step thickness

measured with profilometer is 11.2 nm. This gives refractive index of the coated material to be 2.23. Figure 2.13a gives 3D plot of same sample measured with profilometer and figure 2.13b gives one line scan of the step size.

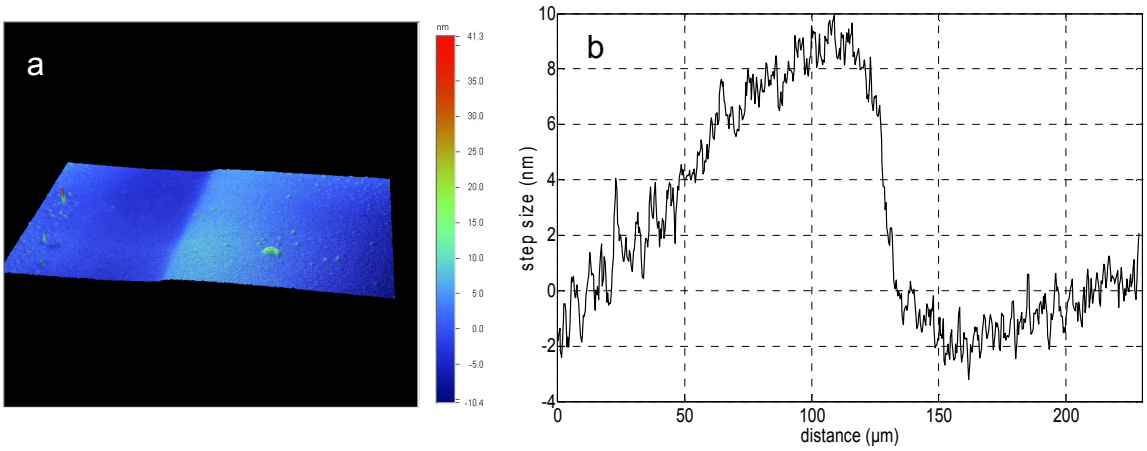

Figure 2.13 Physical length measurement using profilometer for sample 2. a) 3D plot showing step measured b) single line scan showing the step size measured using profilometer.

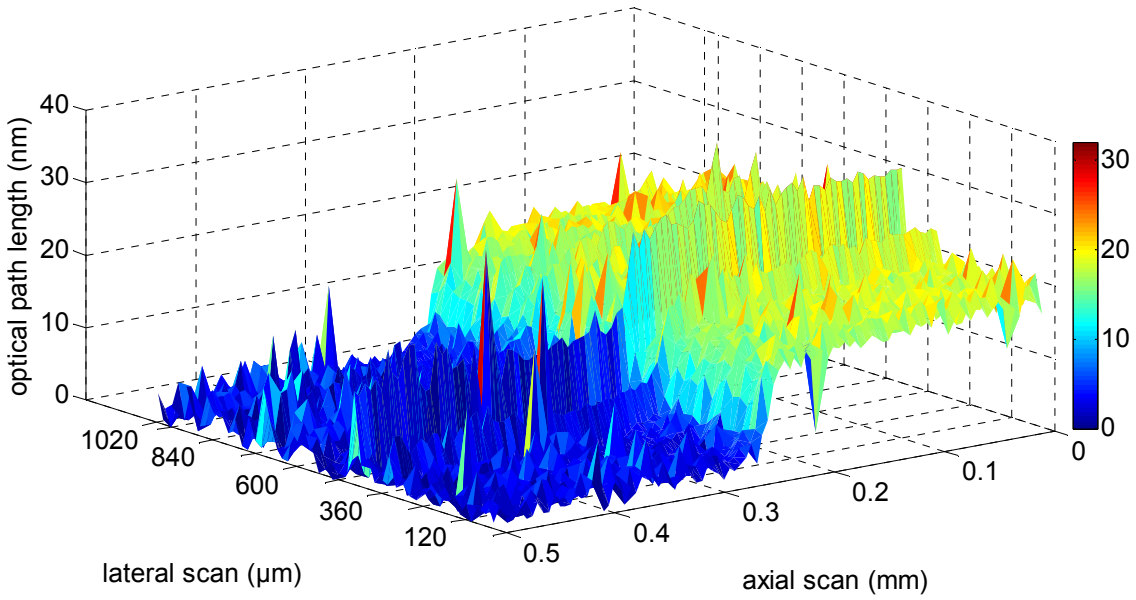

Figure 2.14 Optical path length measurement for sample 3 using SD-PSI (1.0 mm x 0.5 mm) for a step size estimated to have physical step size of 7.4 nm using profilometer

Figure 2.14 shows the results for the thin film step sample 3. The optical path length obtained using SD-PSI shows an average step size of 17 nm. Figure 2.15a shows the result of 3D scans of the sample measured using profilometer and figure 2.15b shows the single line scan of the same sample measured with profilometer. The physical step size measured using profilometer is 7.4nm. Using these measurements, the refractive index of the material is 2.29.

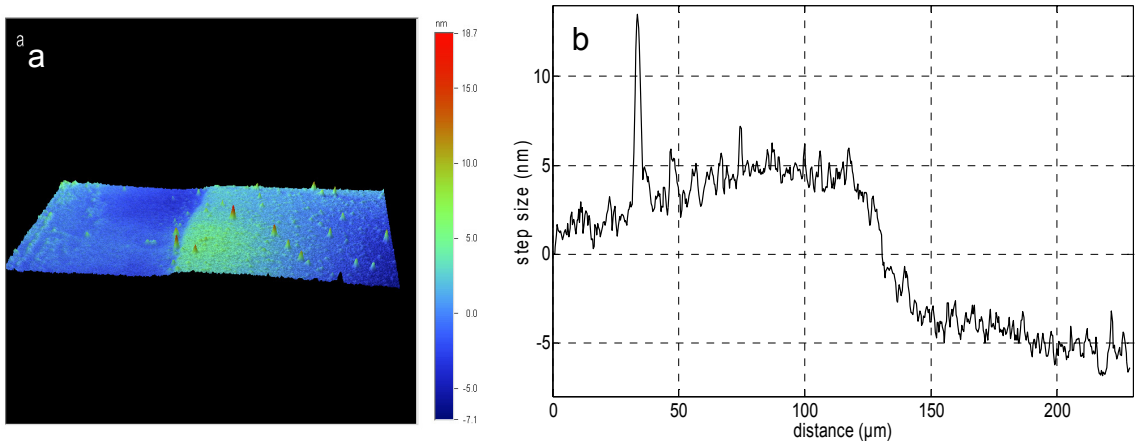

Figure 2.15 Physical length measurement using profilometer for sample 3. a) 3D plot showing step measured b) single line scan showing the step size measured using profilometer.

As seen from both SD-PSI step sizes (figure 2.14 and 2.15), profilometer step size and single line scan, there are spikes in the signal. These spikes could be due to variation in deposition of step layer or some dust/debris deposited on the surface of coverslip. The spikes although are seen in all three step sizes become more dominant in smaller step as the spikes are almost of the same order of magnitude as the step itself.

From all the above step sizes, the refractive index of the material deposited on the coverslip is calculated to be approximately 2.2, which verifies that the SD-PSI is measuring the accurate step size dimensions and can be used for measurement of step sizes or height changes in nanometer range.

2.3.1.2: Measurement of step sizes formed from deposition of protein on sensor coverslips

This section is devoted to see if the protein attaches to coverslips with aldehyde chemistry. Coverslips with chemistry to covalently attach amino containing molecules are purchased. Binding capacity for these surfaces is 250 ng/cm^2 for an IgG molecule as per manufacturer specifications. To test these sensor surfaces for attachment of protein, interaction of rabbit IgG with anti rabbit IgG is used. IgG is a large biomolecule with molecular weight of 150 kDa [74].

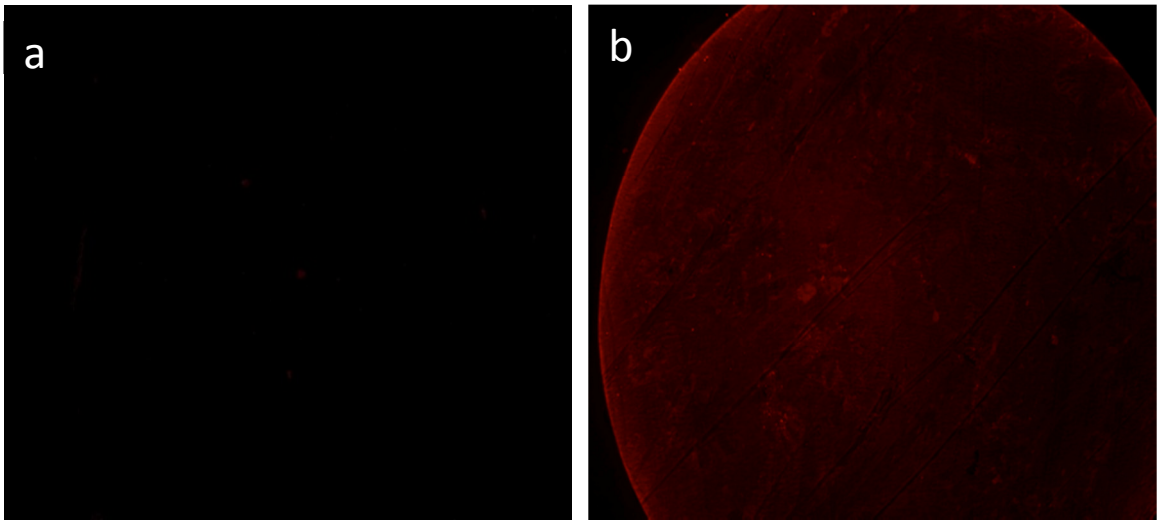

Figure 2.16 Fluorescence images of rabbit IgG-anti rabbit IgG interaction. a) Control well shows no background fluorescence, b) the global view of the spotted protein on the sensor coverslip.

Rabbit antigen is first incubated on the coverslip for 1 hour. After 1 hour, the coverslip is washed to remove any unattached antigen. 0.05% BSA is used for blocking the sensor surface for 30 minutes. After that fluorescently labeled anti-rabbit IgG (Dylight 594) is incubated on the coverslip for two hours. Following this step, the coverslip is washed 3 times with 0.05% PBST and 3 times with PBS to get rid of any unattached antibody. Figure 2.16b shows the fluorescent images (FS 00) of the attached antibody on immobilized antigen. Figure 2.16a shows the control well in which antibody was not incubated, and hence no background fluorescence signal is detected.

For confirmation, the antigen-antibody interaction spot is also imaged using profilometer. Figure 2.17 shows the 3D image of the portion of binding area, which shows increase in height (red spots) as result of antigen-antibody binding.

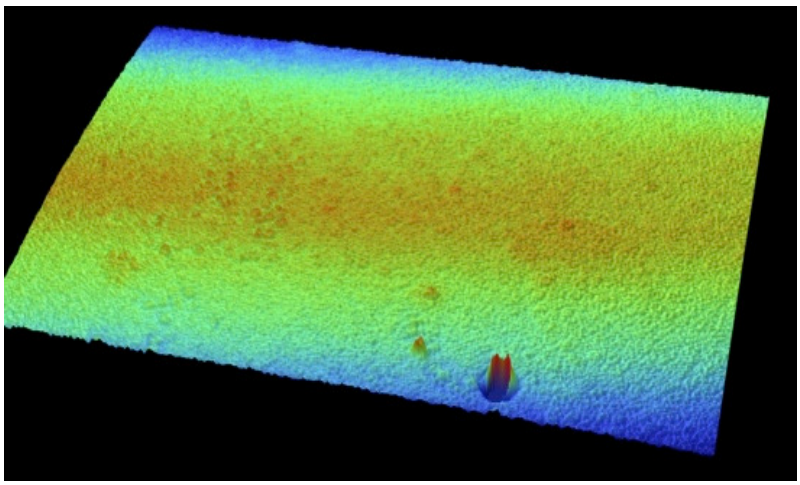

Figure 2.17 3D image of the portion of antigen-antibody binding spot generated using profilometer. Red spots show increased physical length due to interaction.

The antigen-antibody interaction spot is also scanned using SD-PSI. Figure 2.18 shows 3D scan of the protein spot. The figure shows increase in optical path length for protein binding. The SD-PSI measurement shows the global view of the spot. The lateral resolution is 40μm for the image. The plot also shows some variations and spikes over the interaction area. This might be due to debris or non-uniform binding of protein on the sensor chip.

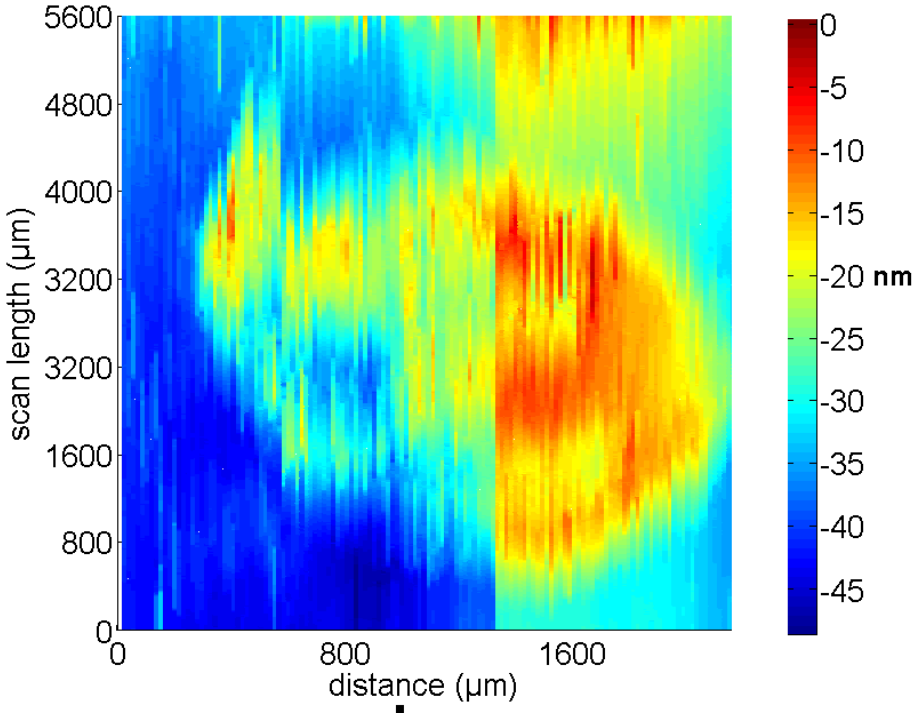

Figure 2.18 3D scan of the antigen-antibody protein immobilization on sensor generated using SD-PSI

2.3.2 Quantification of Refractive Index Change Assuming Constant Length

Measurement of refraction index with a fixed length is done using square capillary as a platform. Figure 2.19 shows, cross section of a square glass capillary. In this geometry there are multiple reflective surfaces that generate interference signal. Interference signal is generated from I_1 (black arrows), I_2 (brown arrows), I_3 (pink arrows) and I_4 (red arrows). In this diagram it is assumed that wall thickness of square capillary is same for both top and bottom plates and their interference signal overlap.

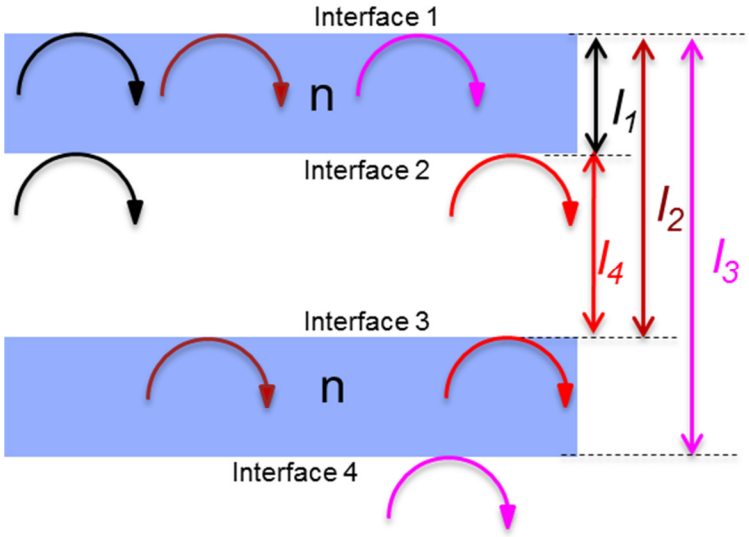

Figure 2.19 Source of reflective surfaces (interfaces 1,2,3 & 4) from a square capillary. The cartoon shows light reflecting from multiple surfaces and interfering. This generates a multiplexed interference signal. In this geometry none of the surfaces are functionalized with ligand.

In this geometry with air in the capillary, multiplexed interferogram is generated due to superimposition of interference signal from all reflective surfaces. When any other test sample with different refractive index is introduced in capillary, there is shift in phase of the multiplexed interference signal. This change is seen by all reflective surfaces that enclose the capillary cavity. In this example brown, pink and red interference pattern will show a phase shift. The phase change can be extracted from any of the above surfaces, to quantify the change in reflective index. As no surface is modified for physical attachment of the protein on the glass surface, a constant physical length is assumed. Hence any shift in phase signal is attributed to change in refractive index that occurs in the capillary cavity. Equation 10 gives the quantification formula for measuring refractive index change (Δn) that occurs when test sample flows through the capillary tube. Here the physical length of the capillary is assumed constant (l) at 254µm. λ_o is center wavelength of the light source.

$$\Delta\varphi = \frac{4\pi\Delta n l}{\lambda_o} \qquad (10)$$

2.3.2.1 Testing platform for refractive index change detection for glycerol dilution

To test system for detection of refractive index, quantification of refractive index change as a function of glycerol concentration is quantified. Concentration of glycerol is detected from 0.001% to 2.66%. The smallest refractive index change seen in figure 2.20 is 1.3102E-05 RIU. However with a phase sensitivity of 1milliradians, refractive index change of 2.6E-07 RIU is possible. The plot shows the linear increase in refractive index as a function of increase in glycerol concentration. The linear fit to the points gives regression coefficient of 0.99942.

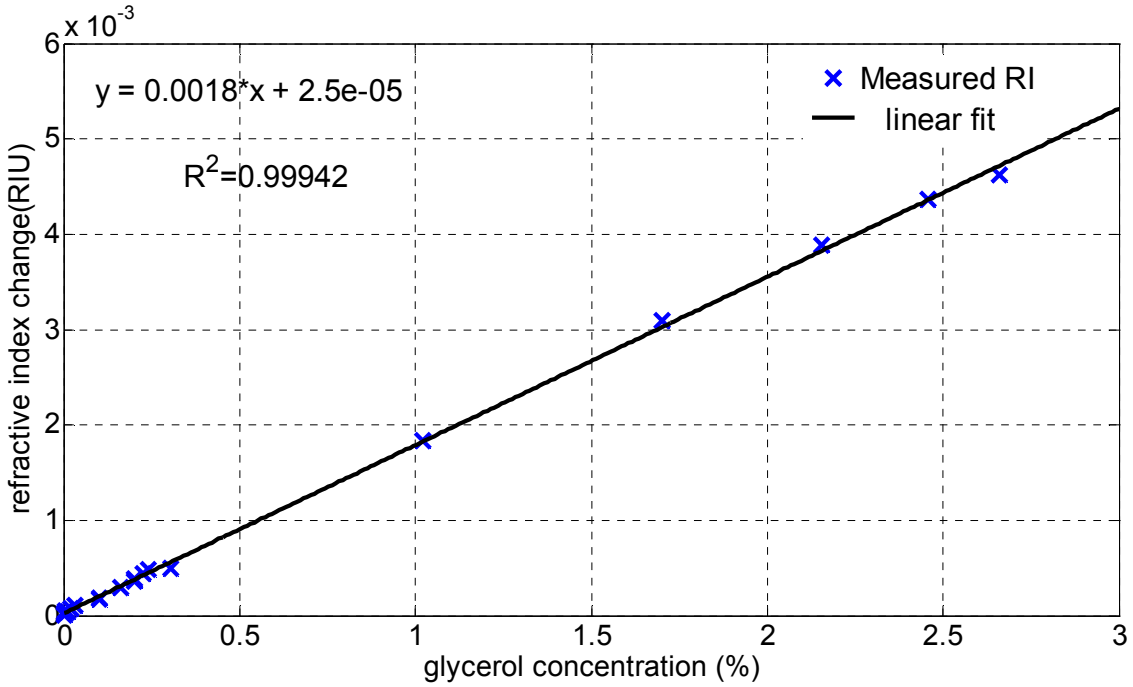

Figure 2.20 Refractive index change detection as a function of glycerol dilution. Blue points represent measured RI values as a function of glycerol concentration. Black line shows linear fit to data points

In summary, the focus of this chapter is to optimize, characterize and calibrate SD-PSI for BIA studies. Implementing SD-PSI in common mode geometry allowed for ultrasensitive phase detection. Calibration with measurement of thin films demonstrated precise OPL quantification capability of SD-PSI. Phase noise of SD-PSI can be improved by coating sensor surface with titanium dioxide, which can increase sensitivity of biomolecule detection. SD-PSI

can also be configured to measure refractive index changes as a function of concentration gradient of test sample.

CHAPTER 3

SPECTRAL DOMAIN PHASE SENSITIVE INTERFEROMETRIC BIOSENSING PLATFORMS

Label free technologies for biosensing and biomolecular interaction analysis use various platforms compatible to respective detection modalities. Currently available platforms used are flow cell, well plate, fiber tip, microarray, cassette and BioCD. Platform manufactured by *Attana* uses continuous flow based platform integrated with Quartz crystal microbalance (QCM). Analyte flows over QCM platform and BIA is performed as molecules bind and change vibration frequency of the crystal. Platform by *Bio-rad laboratories* uses microfluidic flow cell with alginate polymer coating on gold layer. Platform used by *ForteBio* is no fluidics dip and read method for BIA. Fiber tips functionalized with different chemistry are sensors that are dipped in well plate containing samples to be measured. Platform from *TTP LabTech's* is sensor cassette integrated with quartz crystal as the platform [3, 75].

Sensing platforms have stringent fabrication and functionalization requirements and can work only with that specific instrumentation. This restricts the choice of using multi platforms for various applications on a given system. Platform from *Fujifilm* have consumable sensor sticks integrated with plastic prism and immobilization chemistry. Well plate from *Corning epic* system uses resonant waveguide grating technology with patented optical sensor integrated in each well. *ForteBio* uses functionalized fiber tip with internally fabricated reflective layer for creating interference signal. Aim of this chapter is to demonstrate compatibility of SD-PSI with wider number of platforms.

SD-PSI is compatible with different platforms for performing BIA. SD-PSI can be integrated with flow cell, multi-well plate, fiber tip, or petridish. SD-PSI requires an optical interrogation window to perform BIA. The platforms for optical interrogation require glass or plastic window for SD-PSI technique to work. Laboratory grade coverslips with functionalization

chemistry are used as sensors for flow cell and static multi-well platforms. Petridishes with glass and plastic bottom are commercially available. For fiber tip platform, fiber tip with functionalization chemistry is used for BIA studies. Glass or plastic surface functionalization is needed to capture ligand molecule without loss of its functionality. Fortunately, there is a body of work on surface modification for attachment of biomolecules [76-84]. There are also companies that sell glass with different functionalization chemistry to capture various molecules [85, 86].

The sample arm of SD-PSI can be configured using two designs, bulk system and fiber probe. In bulk system, sample path consists of bulk optics to focus and collect light from sensor surface. Platforms compatible with bulk system are flow cell and multi-well sensor. In order to miniaturize sample path, fiber optic probe is designed with all the integrated optics. Fiber probe can be integrated with flow cell, multi-well sensor or sensor chip can be directly attached to fiber probe (fiber probe 1) for BIA [87]. BIA can be performed directly on fiber tip (fiber probe 2) without any need for beam collimation or focusing.

3.1 Biomolecular Interaction In Static Multi-Well Platform

BIA and biosensing with multi-well platform is demonstrated. Glass coverslip with aldehyde functionalization chemistry is used as sensor for multi-well platform. Ligand binding capacity of aldehyde-coated coverslip is characterized for IgG molecule and sensor is also tested for non-specific binding. Dynamic range, sensitivity and concentration analysis for IgG antigen and antibody is characterized.

3.1.1 Fabrication of Multi-Well Sensor

Multi-well sensor platform consists of a glass coverslip with mounted Polydimethylsiloxane (PDMS) stamp for creating multiple wells. Purchased PDMS consists of base agent and curing agent that are mixed in 10:1 ratio by volume. Bubbles formed during mixing are removed by placing mixture in desiccator for 30 minutes. Desiccated solution is poured on silicon wafer and cured on hot plate for 10 minutes at 150°C. Cured PDMS is peeled

from silicon wafer and cut into stamps of 40mmx22mm to fit coverslips of size 50mmx24mm. Stamps are punched by biopsy punch to form reaction wells. 15 reaction wells in 5x3 format are formed by this method. Punched PDMS stamp is cleaned for debris by scotch tape and placed on coverslip followed by gentle press till stamp sticks to coverslip glass.

Figure 3.1 shows top and side view of fabricated multi-well platform. For real time binding experiments, PDMS stamp with punched holes is placed on commercially available aldehyde-coated coverslips. Aldehyde group on coverslips covalently attaches amine groups of incubated protein and immobilizes specific recognition layer (ligand) on the glass coverslip. Multi-well platform is tested for BIA and biosensing with two molecules. The biomolecular interaction between Rabbit IgG (ligand) and Goat anti-rabbit IgG (analyte), and Biotin (ligand) and streptavidin (analyte) are studied.

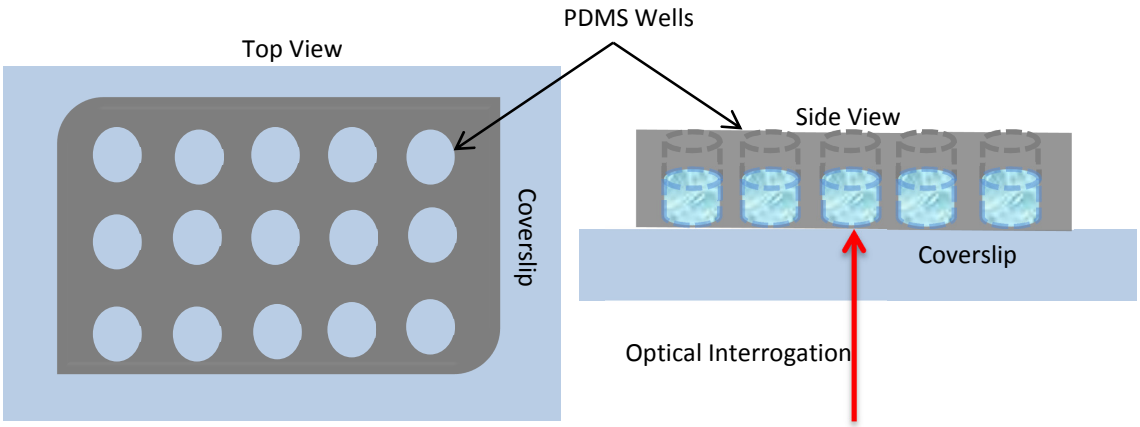

Figure 3.1 Top and side view of customized optically clear multi-well sensor chip platform. 15 reaction wells are obtained on a coverslip of 50mmx24mm

3.1.2 Binding Capacity of Sensor Coverslips

To determine ligand-binding capacity of the sensor coverslips, multi-well sensor chip is incubated with Rabbit IgG antigen (ligand) at varying concentrations (0.01-2000 µg/ml). Multi-well sensor chips is incubated at 4˚C overnight followed by 3 times wash with wash buffer (0.05% PBST and PBS). Wells are blocked with 0.5% BSA for 1 hour followed by three time

wash with wash buffer. For baseline acquisition, 40µl of PBS is incubated in interrogation well followed by incubation of 40µl of anti rabbit IgG (analyte) at 20µg/ml concentration for binding.

The final phase value after binding of antibody for each antigen concentration is plotted. Figure 3.2 shows log plot for final phase quantification of antigen-antibody interaction as a function of varying antigen concentration. As seen from the plot, saturation concentration of antigen is reached at 250µg/ml. Saturation coverage of antigen layer (ligand) is important, so that antibody (analyte) concentration quantification is independent of any discrepancy in the number of ligand sites available to analyte for binding. For analyte quantification, ligand is immobilized on sensor surface with saturation concentration to achieve saturated monolayer of ligand with almost 100% coverage. When analyte is incubated, it is ensured that quantification of analyte is only a function of concentration and is not affected by varying ligand coverage on coverslip. For all the biosensing experiments, IgG antigen is immobilized on sensor in saturation region with concentration of 2mg/ml.

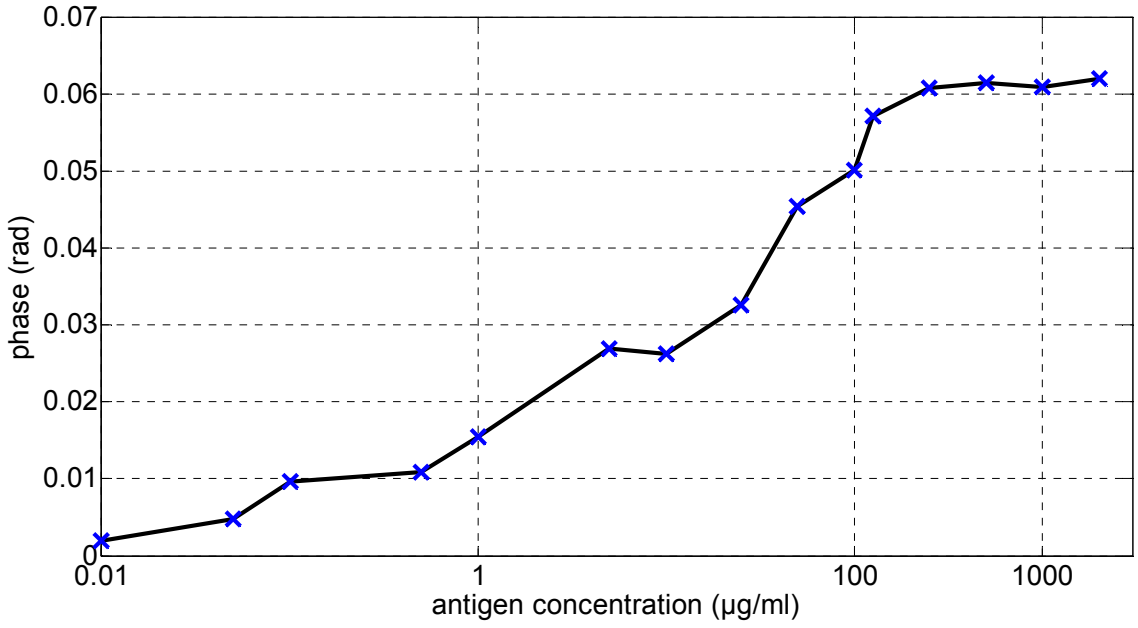

Figure 3.2 Plot showing rabbit IgG antigen binding capacity on aldehyde coated sensor coverslips. Saturation concentration is reached at 250µg/ml.

3.1.3 Sensor Chip Testing

Sensor chip is tested for non-specific binding, buffer refractive index changes and weight of test sample incubated. After incubating sensor surface with saturation coverage of ligand (antigen), wells are washed three times with wash buffer. Data acquisition is started after incubation of 20µl of PBS. As seen in figure 3.3, after baseline stabilization (6 minutes), non-specific analytes are added. The perturbation seen at 6 minutes is due to mechanical movement of the sensor chip that occurs as analyte is pipetted in the sensor well. As seen from the figure 3.3, the plots return to baseline. Glycerol is added at three different concentrations (85,10 & 1 %) to see if there is any affect of the RI change in the buffer or the weight of analyte. Irrespective of the concentration of the glycerol added, all curves settle down close to baseline. BSA is added to test non-specific binding of sensor coverslip.

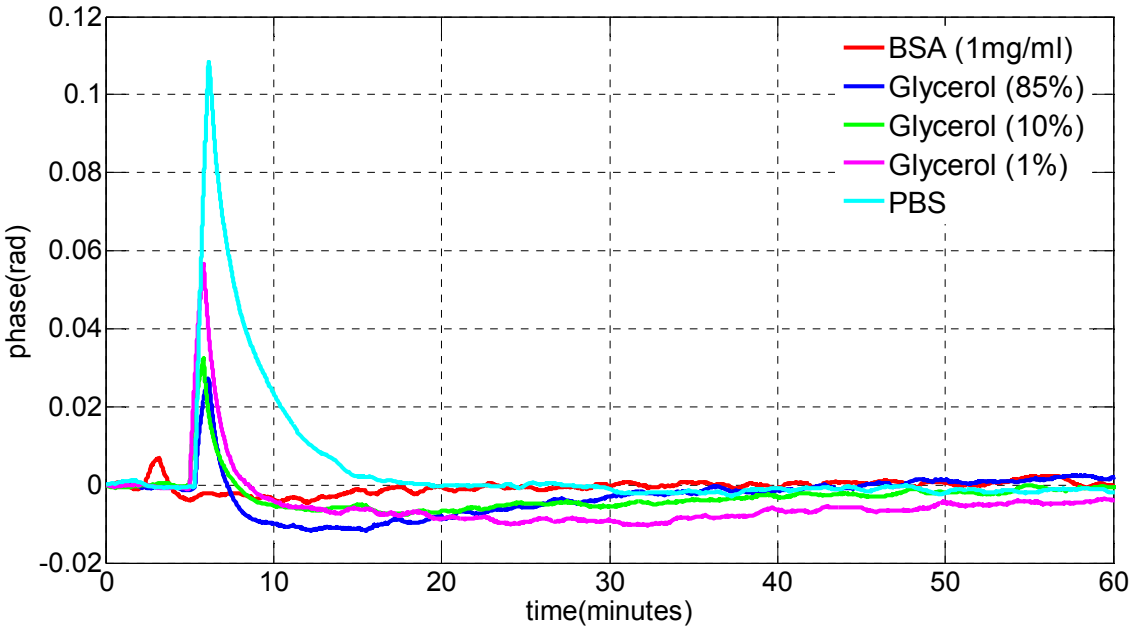

Figure 3.3 Multi-well platform testing for non-specific binding (BSA), buffer refractive index change (Glycerol) and weight of incubated analyte (1,10 and 85 % Glycerol and PBS).

3.1.4 Platform Testing For Biosensing and BIA In Multi-Well Sensor

Platform is tested for biosensing and BIA for rabbit IgG and anti rabbit IgG interaction. Binding curves for biotin and streptavidin are also studied.

3.1.4.1 Rabbit IgG antigen and Goat anti Rabbit IgG antibody interaction

Rabbit IgG is incubated in the wells at concentration of 2 mg/ml and stored at 4^0C overnight. Higher concentration of ligand is used to create 100% coverage of recognition layer. Multi-well sensor is washed three times with wash buffer to remove unattached antigen. All wells are filled with PBS for hydration. PBS buffer from interrogation well is removed and 20 µl of PBS is added to the well. Multi-well sensor is placed on sample holder and beam is focused on the sensor surface for acquisition of baseline signal. After baseline stabilization (5-10 minutes), anti-rabbit IgG at a given concentration is pipetted in the interrogation well. After antibody incubation, binding data is acquired until phase for a given concentration reaches steady value (1 hour). Figure 3.4 shows binding curve of rabbit IgG with the anti Rabbit IgG for five different concentrations of anti Rabbit IgG. Figure 3.4 shows representative binding plots for each concentration.

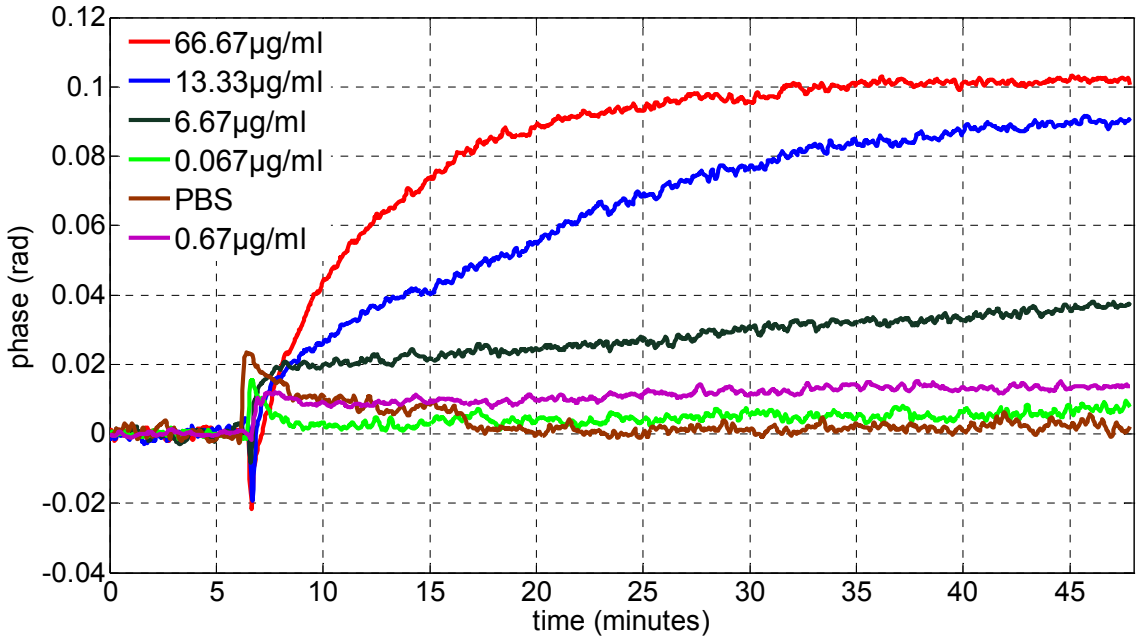

Figure 3.4 Binding interaction between immobilized rabbit IgG (antigen) on coverslip and anti-rabbit IgG (antibody). Different curves represent different concentrations of the antibody incubated. The plots settle at phase proportional to incubated antibody concentration. Curve shown in brown is control well, where buffer is incubated rather than antibody

The dip at 7 minutes is caused due to antibody incubation in the reaction well, which mechanically perturbs sensor surface. But it does not seem to affect final quantification of the phase since after incubation of PBS as control, baseline returns to its zero value.

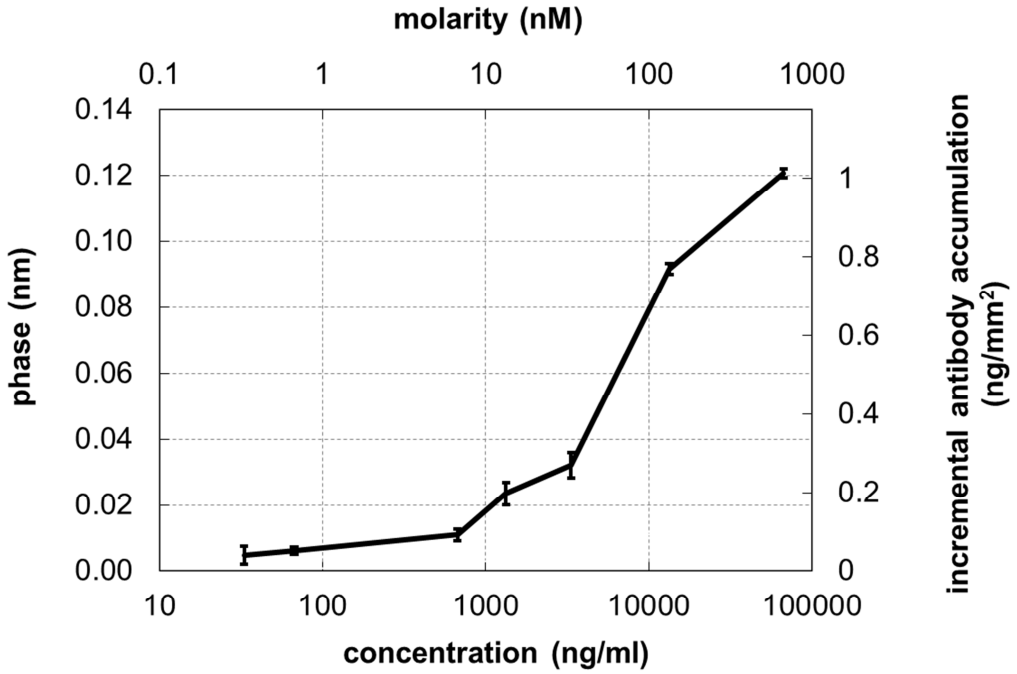

Figure 3.5 Dynamic range and limit of detection of the anti rabbit IgG antibody. The quantifiable concentration of anti-rabbit IgG is from 0.2nM to 440nM and has a sensitivity of 33 ng/ml. Secondary y axis (right) shows phase equivalent antibody accumulation on sensor and secondary x axis shows (top) Rabbit antibody concentration in moles

Goat anti-rabbit IgG antibody concentration is varied and quantifiable from 0.2 nM to 440 nM. Figure 3.5 shows dynamic range of the anti rabbit IgG detected. The quantification in terms of surface accumulation of anti rabbit IgG (ng/mm^2) is calculated and is shown on right y-axis. In calculating the mass coverage protein binding site density of 2.5 ng/mm^2 is used for IgG molecule as per manufacturers specifications. The surface accumulation varied from 0.05ng/mm^2 to 1.18ng/mm^2. Also, the cross-sectional area for the IgG antibody is calculated to be 3.14×10^{-12} mm^2 assuming IgG antibody to be of an ellipsoidal shape oriented along its major axis when bound to the antigen [88-90]. Measured sensitivity of detecting IgG antibodies is 33

ng/ml from a single detection spot. The change in mass coverage is a linear function of IgG antibody concentration up to 100 nM after which it shows nonlinear dependence.

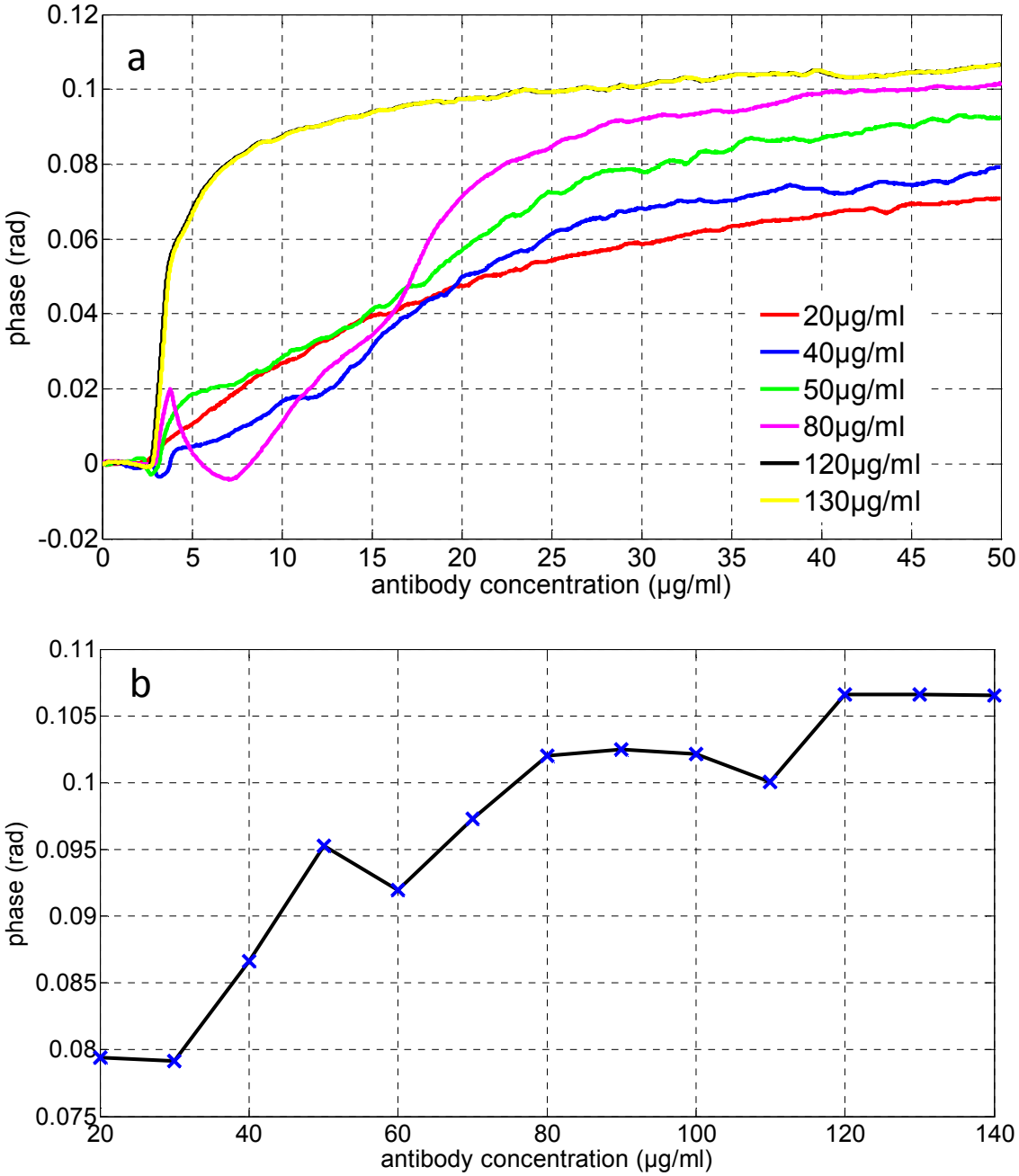

Figure 3.6 Rabbit IgG-anti rabbit IgG interaction in non-linear region. a) Binding curves for different concentrations b) plot of final phase values as a function of antibody concentration.

Figure 3.6a shows binding curves for rabbit IgG-anti rabbit IgG interaction for higher concentrations in non-linear region. As seen from plot 3.5, the response of phase change as a function of antibody concentration is linear until 20µg/ml. After this concentration, response of sensor is non linear. Figure 3.6a shows binding curves for antibody concentrations in non-linear region. The concentration of antibody is varied from 20µg/ml-140µg/ml. The sensor reaches saturation at 120µg/ml. Figure 3.6b shows plot of the final phase values as a function of concentration of antibody incubated.

3.1.4.2 Biotin and streptavidin biomolecular interaction

The second biomolecule interaction pair studied is biotin and streptavidin. Biotin has a molecular weight of 244.31 Da and streptavidin has a molecular weight of 52.8KDa. Biotin coated coverslips are purchased from commercial source (Xenopore).

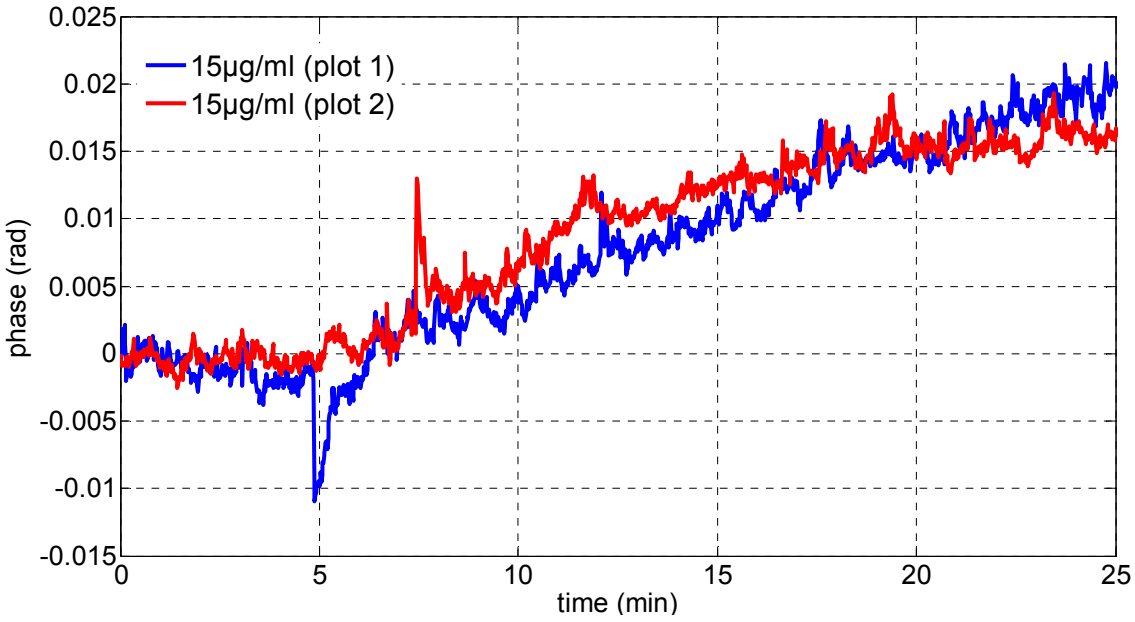

Figure 3.7 Binding interaction between biotin (ligand) coated on coverslip and streptavidin (analyte). The difference curves represent two trials of the same concentrations (250nM) of streptavidin detected.

After washing coverslips thoroughly with PBS, data acquisition is started with 20 µl of

PBS for baseline reading. After baseline stabilization, 15µg/ml of streptavidin is incubated. For both given plots in figure 3.7, concentration of streptavidin used is 15µg/ml. The plots show a calculated average OPL of 1.375 nm, which corresponds with the number, reported for this concentration by Joo et.al. [69].

3.2 Biomolecular Interaction in Flow Cell Platform

Using multi-well sensor chip, 15 interactions can be studied using one sensor chip (22 x40 mm). But there are some drawbacks using a static multi-well setup. First, during incubation of analyte there is mechanical perturbation in the chip that causes a spike in the signal. Second, the probability of incubated analyte to reach the immobilized ligand is dependent on the diffusion and Brownian motion of the analyte and hence the interaction takes longer time to reach the plateau value. In order to overcome these two drawbacks, flow cell is fabricated. Flow cell does not require pipetting of analyte and hence there is no incubation spike. Also, as the analyte is pumped inside the flow cell, the ligands comes in direct contact with analyte and interaction is just not dependent on diffusion and Brownian motion to interact.

3.2.1 Design of Flow Cell Platform

Figure 3.8 shows design of fabricated flow cell. The flow cell is fabricated from two aluminum plates. The bottom aluminum plate has two fluidic channels, each 250µm in depth and fluidic ports. On top of bottom plate, gasket (Viton) is placed to avoid any leakages from the flow cell. Coverslip (40mmx22mm) is placed on the square cut out on the flow cell top plate. The top cover is held in place on the bottom plate by threading in the 6 screws as shown in the figure 3.8. As there are two channels, one sensor chip can be used for studying two binding interactions. Flow cell is mounted on tip and tilt sample mount which helps in optimizing signal for maximum modulation depth of interference signal. The fluidic connectors are connected to input and output ports of the flow cell.

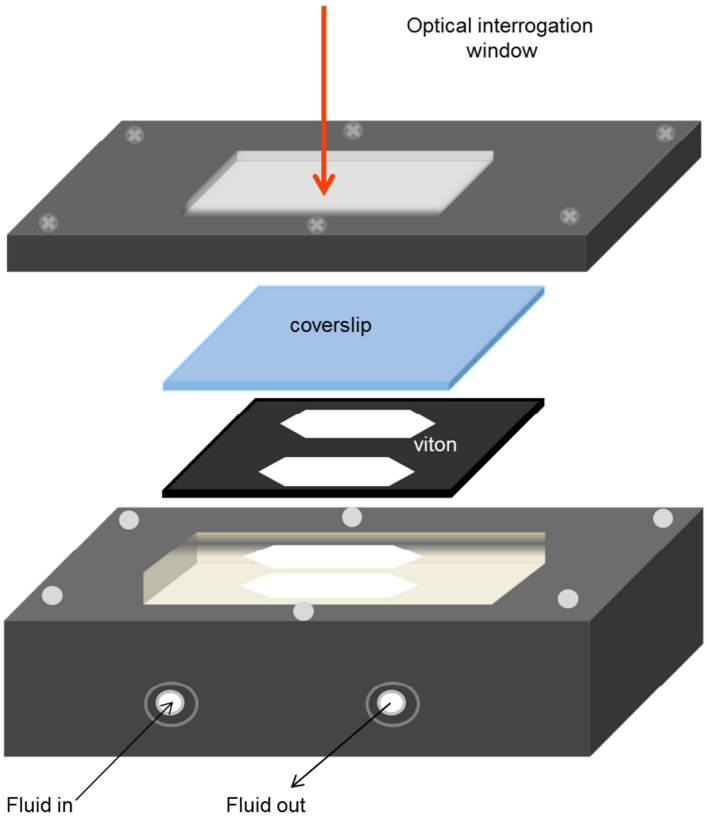

Figure 3.8 Flow cell showing different parts of flow cell. Flow cell base plate has two channels for fluidic connection. Gasket (Viton) is placed on the bottom plate to create fluidic seal. Top plate has a cutout for beam focusing on coverslip mounted on top plate.

3.2.2 Platform Testing for Biomolecular Interaction with Flow Cell

Figure 3.9 shows flow loop of the fluidic system. It comprises of peristaltic pump, injection valve and flow cell. Input sample of interest is placed in vial. Peristaltic pump has four channels; so four different fluids can be pumped simultaneously. The speed and direction of the peristaltic pump are controlled by LabView module. Changing voltage applied to peristaltic pump can control flow rate.

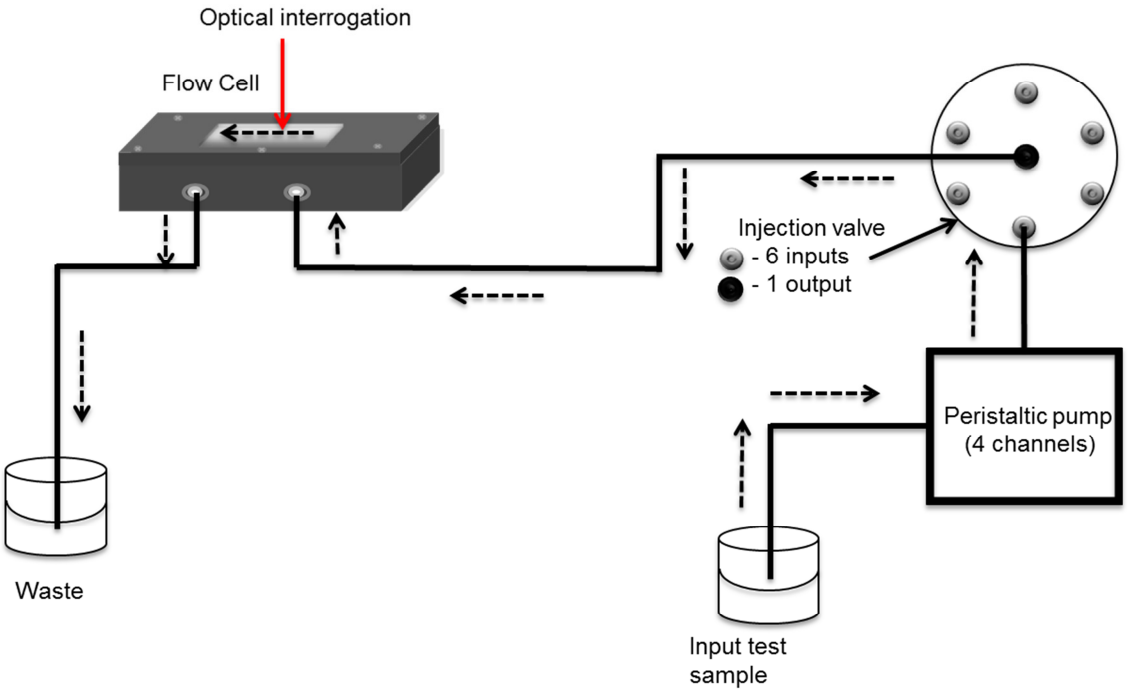

Figure 3.9 Fluidic loop for BIA studies. The required test sample is placed in a vial, which is input to peristaltic pump. Peristaltic pump introduces sample in the injection valve. The output of injection valve is connected to input port of flow cell. The fluid goes to waste from output port of flow cell. Dotted arrows indicate flow direction of test sample. Flow cell is placed on sample holder and integrated to interferometric system

In figure 3.9 only one channel is shown. The peristaltic pump, pumps fluid to the injection valve. Injection valve has 6 input switches so it can take 6 different samples. Based on user input, injection valve activates the selected input switch. Since there are four input channels on peristaltic pump, only four input channels of the injection valve can be used. Injection valve activates the input switch and fluid from it is pumped to output channel of injection valve. The output port of injection valve is connected to input port of the flow cell. The waste sample is collected at exit port of flow cell. Flow cell is immobilized on sample holder with fluidic ports connected. With test sample flowing through the flow cell, light is focused on the sensor coverslip of the flow-cell for BIA studies.

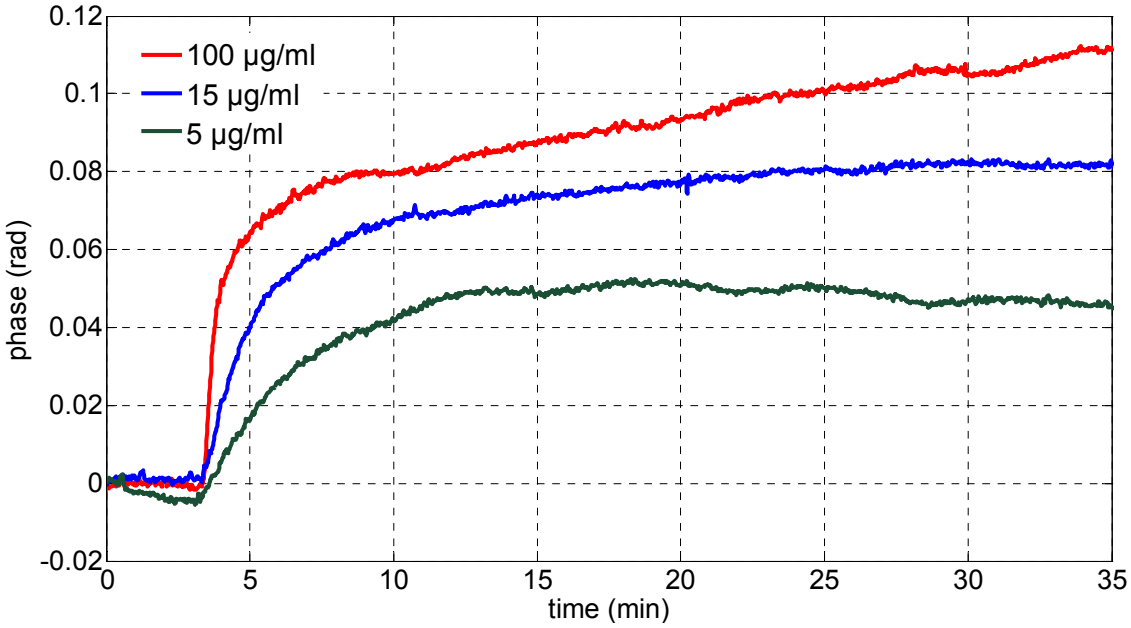

Figure 3.10 Binding curves obtained from flow cell. The figure show representative curves for Rabbit IgG antigen and goat anti rabbit IgG antibody. The antigen is incubated at 2mg/ml. The antibody concentration is shown for 5, 15 and 100 µg/ml.

Figure 3.10 shows binding curves of Rabbit IgG antigen and goat anti rabbit IgG antibody. The binding plots obtained have no incubation perturbance as seen with experiments done using PDMS multi-well sensor. The binding process is also faster as now the antibodies are brought in closer proximity by small dimensions of the channel. Also due to flow system, the biomolecular interaction is not just dependent on Brownian motion to interact. These two factors make binding process favorable and faster. However, the disadvantage of the flow system is that it requires more elaborate preparation and only two interactions can be studied using one sensor coverslip.

3.3 Fiber Probe with Integrated Optics for Biomolecular Interaction

To miniaturize the sample arm of the SD-PSI setup, fiber probe with integrated optics is fabricated. The miniaturization of sample arm is considered to reduce mechanical vibrations that occur in bulk sample arm. Also, fiber probe setup miniaturizes the setup and hence makes it

more convenient to handle sample. Fabricated fiber probe has an outer diameter of 2.1 mm. The fiber probe can be integrated with multi-well plate, flow cell platforms. The sensor chip can also be directly attached to the fiber end making it a single assembly (fiber probe 1).

3.3.1 Design of Fiber Probe

For fabrication of fiber probe heat sink tubing, sensor holder, steel tubing, GRIN lens, ferrule and single mode fiber are used. Their approximate dimensions are 20-mm sensor holder, 12 mm heat shrink tube, 28 mm steel tubing, 0.29-pitch GRIN lens (plano-plano, 0.46 NA, 1.8mm OD, 830nm), 12-mm fiber ferrule, and 60-cm single mode fiber.

The steel tubing is filled with index matching gel to approximately 2mm. After index-matching gel is in place, a thin layer of epoxy is coated on the outer edge of the lens and is pushed inside the steel tubing from the index matching gel side. This pushes the gel backwards. This step ensures that gel is in contact with the lens and also lens is immobilized on the steel capillary by epoxy. The GRIN lens stays flush with the steel tubing. This steel tubing assembly with GRIN lens with gel is put aside for epoxy to dry out. To prepare the fiber end, bare fiber is purchased from thorlabs. Fiber buffer is also purchased separately from thorlabs. About 5 inches of bare fiber is cut and is inserted inside buffer coating, which gives strength to the fiber. Using epoxy, bare fiber is immobilized on the buffer by applying epoxy to the distal terminal. From the proximal terminal, the bare fiber protrudes out from the buffer. The thin coating of the bare fiber is removed using thermal UV stripper. Fiber end is cleaned with acetone to remove any debris and is cleaved at 0°.

Next step is introducing the cleaved end of the fiber in ferrule. But since it is important to ensure that the cleaved tip is not destroyed in the process, reflectivity from the probe is monitored for rest of the probe fabrication process. In order to do that, the other side of the bare fiber is cleaved and spliced to a sample arm of 50:50 coupler. The other sample arm is unused and is dipped in water to avoid reflections coming from that surface.

The source arm of coupler is connected to 635 nm Laser to visualize the beam spot on the white paper. Detector end of the coupler is connected to silicon detector and the output of detector is connected to oscilloscope. Once, the source is turned on, light is distributed in two sample arms of the coupler. Some light is reflected from the cleaved end of the fiber tip that is monitored on the oscilloscope. At this point, the cleaved end is introduced in the ferrule till the bare fiber is about 2 mm out from the ferrule surface. If the cleaved end is not destroyed in this process, the reflectivity remains same as before. But if tip is destroyed in the process, reflectivity goes up, and hence the process needs to be repeated. Finally bare fiber is immobilized inside ferrule by epoxy. The next step is to introduce the fiber with ferrule assembly inside the steel tubing with immobilized GRIN lens.

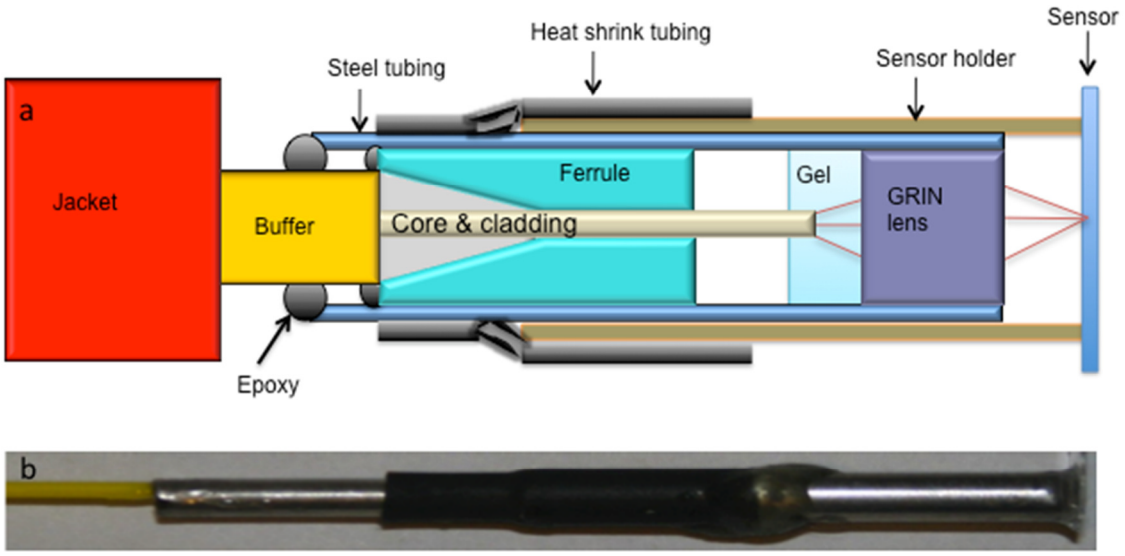

Figure 3.11 Cross section of fiber probe with integrated optics. a) The cartoon shows light from SMF fiber is focused by GRIN lens on the sensor surface. b) Shows the actual image of the fabricated probe.

For an image distance of 5mm, object distance is 150μm for the GRIN lens of pitch 0.29. To precisely immobilize fiber tip at a distance of 150 μm from the front face of the GRIN

lens following setup is used. The probe is plugged into one of the sample arm of the interferometer. The mirror is mounted at 5mm from the front end of the GRIN lens. The position of the mirror with respect to the grin lens mounted on steel tube is kept fixed. In the detector arm, silicon detector with the oscilloscope is connected to calculate the power output. The prepared fiber end with ferrule is mounted on the translation stage. The fiber end with ferrule is slowly inserted in the steel tubing containing GRIN lens with the help of translation stage. As soon as bare fiber tip touches the index matching gel, the reflectivity drastically goes down. The bare fiber end is further moved inside the steel tube till light focuses on mirror. When light focuses on the mirror, the beam will fold back and output signal to the detector will increase. Distance of fiber end from GRIN lens for maximum detector signal is the position of the object distance. At this point the ferrule is immobilized within the steel tubing that has a fixed image distance of 5 mm. Figure 3.11 shows the cross sectional cartoon view and picture of the probe fabricated. The fabricated probe at this point can be replaced by bulk sample path and can be integrated with flow cell or multi-well plate sensor. However for attaching sensor coverslip directly to probe end, sensor holder is fabricated and then integrated with fiber probe.

3.3.2 Platform Testing for Biomolecular Interaction with Fiber Probe 1

For this setup, next step is attachment of sensor to the probe. Aldehyde coated coverslips are cut into approximately 4mm x 4mm squares using diamond scribe. Square cutout coverslips are immersed in Rabbit IgG antigen solution (2mg/ml) overnight at 2-4˚C. Sensors are washed three times with wash buffer. The sensor is attached to the sensor holder steel rod using epoxy. This sensor holder has ID slightly higher than OD of fiber probe steel tubing. A heat shrink tubing is also attached to this steel tubing. The idea is to insert assembled probe inside the sensor holder that has sensor attached. The probe is connected to SD-PSI to determine the distance at which amplitude and modulation depth of the interference signal is highest. To do so, the probe is moved inside the sensor assembly tubing. Once the best signal is coupled back from the sensor, the sensor holder is immobilized to the optical probe. At this

point the probe and attached sensor are one single unit and biosensing experiments are started.

The probe assembly with sensor attachment is immobilized to the post on translation stage. The translation stage in moved in downward direction till the sensor surface is in contact with PBS. At this point, data acquisition is started for monitoring the baseline. After baseline acquisition, the known concentration of anti rabbit IgG is introduced in the PBS to make a final concentration of 100µg/ml. The binding is monitored till the steady state of binding curve is achieved as shown in figure 3.12.

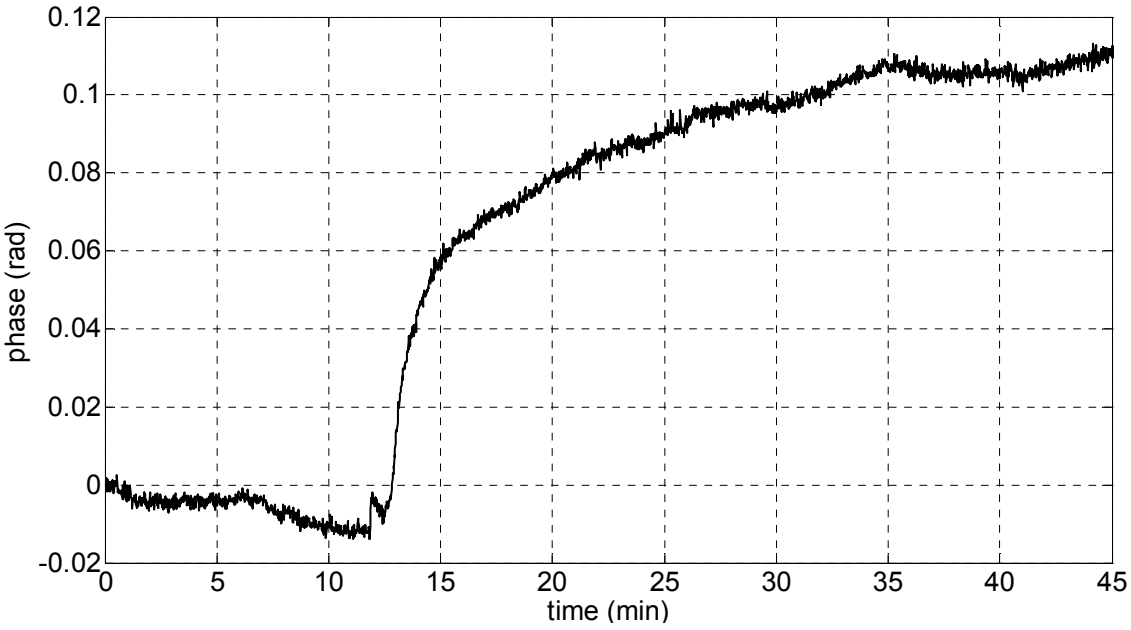

Figure 3.12 Binding curve obtained from fiber probe with attached sensor surface. The figure show representative curves for Rabbit IgG antigen and goat anti rabbit IgG antibody. The antigen is incubated with 2mg/ml. The antibody concentration is shown for 100 µg/ml.

One of the disadvantages of the fabricated fiber probe is that PBS reacts with epoxy that holds coverslip to sensor holder. This in turn loosens the contact point and changes the distance between fiber probe and coverslip that can increase the phase noise.

3.4 Biomolecular Interaction with Fiber Probe 2 Platform

In order to overcome limitations of assembled fiber optic probe, an alternative fabrication process is implemented. The physical attachments in the assembled fiber probe increase the phase noise due to mechanical movements of the assembled parts. Hence, there is a need to have a miniaturized fiber probe with minimal or no physical component attachments. The idea of fabricating this fiber probe is to make biosensing cost effective and reusable.

3.4.1 Fabrication of PDMS Mold for Holding Sensor Fibers

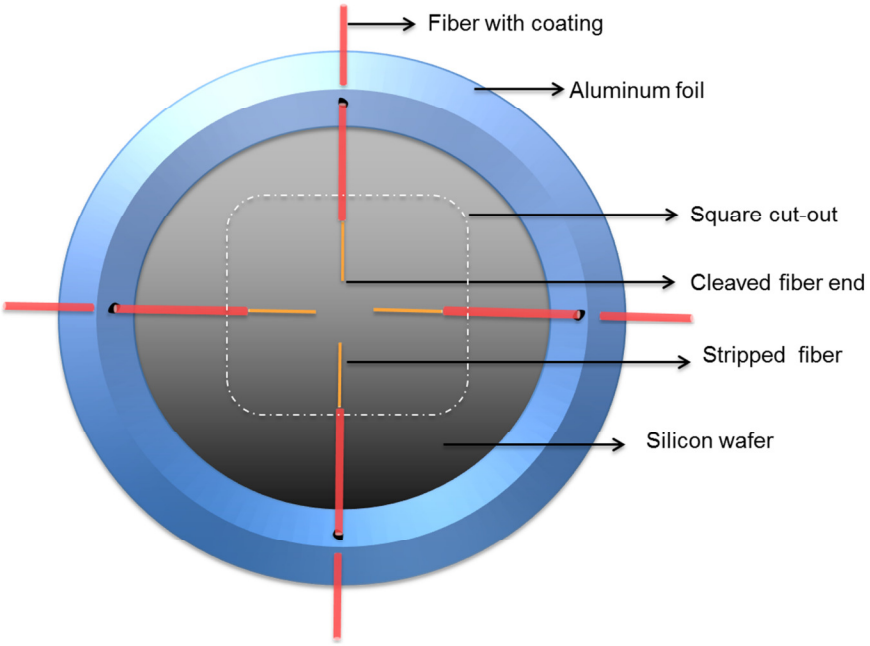

Figure 3.13 Fibers immobilized on the silicon wafer. Figure shows four fibers mounted on the silicon wafer inside aluminum foil holder. Part of fiber with coating is left outside wafer so that fiber can be pulled out after PDMS is cured.

The holder for immobilizing stripped optical fiber is designed. The single mode fiber (780-970nm) is purchased from Thorlabs (780HP). The bare fiber has a buffer diameter of 250 micrometers. The fiber is cut into 4 inch pieces each. Then, fiber coating is stripped for about 1 inch using fiber stripper. The entire fiber (4 inches) is not stripped because fiber handling

becomes difficult. The stripped end is cleaned using acetone to remove any debris and cleaved at 0˚. These cleaved fibers are immobilized on silicon wafer as shown in figure 3.13.

To make aluminum foil holder, silicon wafer is placed on the aluminum sheet. The edges are help in upright position to make wall enclosure for the wafer. Then, four holes are created in the aluminum container walls as shown in figure 3.13. The prepared fibers are inserted through these holes and placed on silicon wafer.

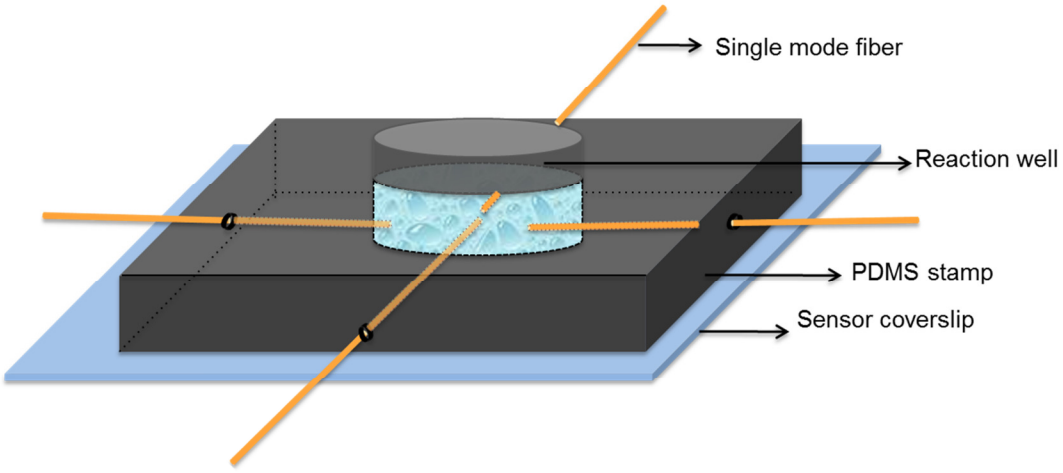

Figure 3.14 The PDMS stamp with fiber mold and hole punched at center is immobilized on glass slide. The etched cavity fibers are inserted inside the holes created from the fiber mold. This immobilizes the fiber inside the PDMS stamp providing it protection and support.

This aluminum wall enclosure holds the PDMS in un-cured state. Prepared PDMS solution is slowly poured in silicon wafer with immobilized fiber probes. After pouring PDMS, fiber probes are readjusted if needed. This assembly is placed on hot plate to cure PDMS for 45 minutes at 65 ˚C. Lower temperature for curing PDMS is chosen because higher temperature can damage coating of the un-stripped portion of fiber. Alternatively, the entire assemble with un-cured PDMS can be left at room temperature overnight to be cured. After PDMS is cured, the fiber is held from the part that is protruding out from aluminum holder and pulled. Once all the fibers are pulled out of the PDMS holder, the mold for fibers inside the PDMS stamp is created. The PDMS stamp is peeled from the silicon wafer. The mold has a diameter of 125μm

near the stripped portion of the fiber and 250μm diameter near the fiber with coating. After all the embedded fibers for creating the mold are removed, the PDMS stamp is cleaned using scotch tape.

In the next step, square/rectangular cutout is created in the PDMS fiber holder as shown in figure 3.13 (dotted square). This square cutout is removed from rest of the mold and cleaned to remove any debris. In the center of this square cutout, 6mm hole is punched. This assembly with a square PDMS stamp with a 6 mm hole in the center is cleaned with scotch tape to ensure there is no remaining debris. After cleaning, the PDMS stamp is mounted on the glass slide. The PDMS sticks very well to the glass surface and creates a water leak resistant seal. The stamp immobilized on glass slide is shown in figure 3.14. This assembly is set aside till optical fibers with etched cavity are fabricated.

3.4.2 Fabrication of Etched Fiber (Fiber Probe 2)

Four inch pieces of bare fiber are used. Coating on fibers is removed for one inch. Stripped fiber end is cleaned using acetone to remove any debris and then cleaved at 0°. The cleaved fiber tips are immersed in etchant solution. The etchant consists of ammonium fluoride, hydrofluoric acid and water. The etching process used is as described in [84]. The ratio used is NH_4F: HF: H_2O=0.5:1:1. The fibers are immersed in this solution. This etchant dissolved core at a higher rate as compared to cladding because the core of optical fiber is germanium doped while as cladding is pure silica. The chemical reaction between etchant and cladding and core respectively is [84]

$$SiO_2 + 4HF + 2NH_4F \rightarrow (NH_4)_2SiF_6 + 2H_2O \quad (1)$$

$$GeO_2 + 4HF + 2NH_4F \rightarrow (NH_4)_2GeF_6 + 2H_2O \quad (2)$$

It is resultant difference in solubility of (NH4) SiF_6 and (NH4) GeF_6 that gives differential etching rate for core and cladding [84]. Depending on the time the fibers are immersed in the etchant, the differential etching between core and cladding changes. For designed fibers, fibers are etched for 30 minutes. Fibers are removed and washed with DI water twice to remove any

etchant solution on the fiber probes. The fiber probes are air-dried and then spliced to another cleaved un-etched fiber (bare fiber). This process creates a discontinuity in the core, which is seen as a bubble in the figure 3.15(d).

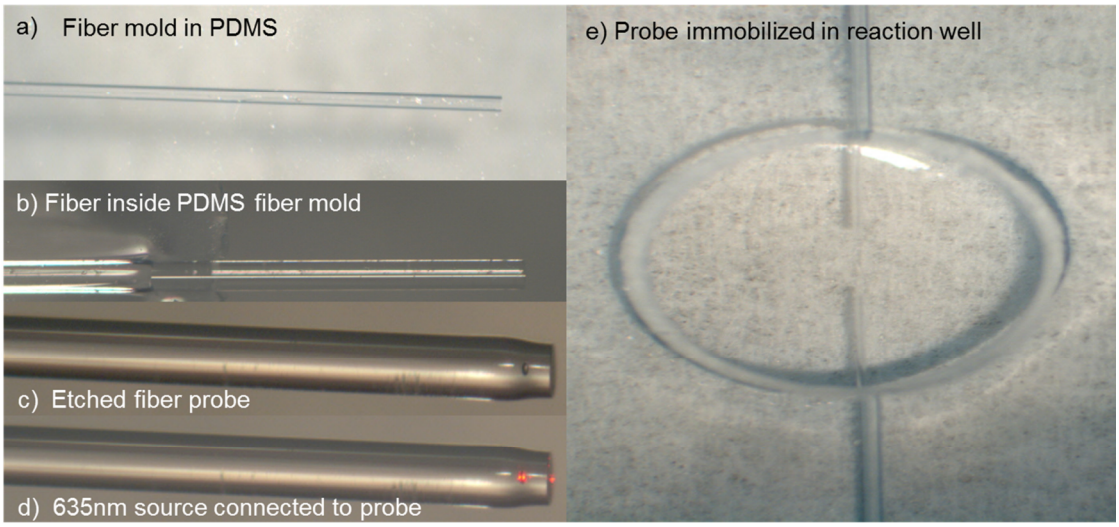

Figure 3.15 Images of a) Fiber mold on PDMS, b) Fiber inserted in fiber mold, c) Etched fiber probe showing cavity, d) Etched fiber probe showing red light reflecting from cavity, e) Two fiber probes immobilized in reaction well

Figure 3.15a shows image of fabricated PDMS fiber mold, Figure 3.15b shows bare fiber inserted in PDMS mold, figure 3.15c shows etched fiber probe with a cavity. To visualize cavity clearly, fiber probe is connected to 635 nm Laser source. Figure 3.15d shows red light reflecting from fabricated cavity in fiber. Figure 3.15e shows two fibers immobilized inside PDMS mold with fiber sensor tips inside reaction well.

For splicing the etched fiber to un-etched fiber, the splicing power is changed from 12 bits (14.45 mW) to 20 bits (14.8 mW) in the splicer. As seen from figure 3.16 as bit power of splicer is decreased, more power is coupled in the fiber. Increasing splicer power seems to increase the losses occurring in the cavity.

Once cavity is formed, the bare fiber is spliced to connectorized SMF. To do this, single

mode FC/APC patch cables (780-970 nm) is used. These fibers are connectorized at both ends. The fiber was split in two single connectorized fibers. The non-connectorized end of fiber is prepared by removing the outer jacket followed by removal of strength fibers and then buffer jacket for nearly 4 inches. After this, a bare fiber with protective coating is exposed. The protective coating is removed for about 1 inch fiber using fiber stripper followed by acetone cleaning and then cleaved at 0˚. Prepared fiber is spliced with the etched fiber after which it is cleaved at a certain distance from the bubble. For multiplexing, this length is varied for different fibers for simultaneous detection of biomolecules.

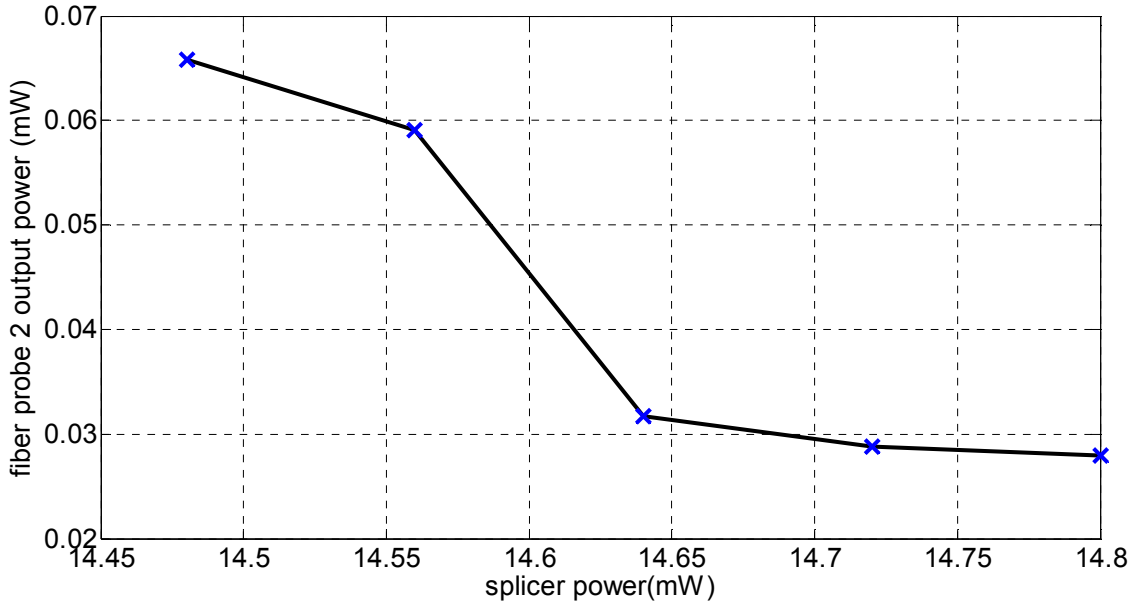

Figure 3.16 Plot for output power of etched cavity fiber as a function of splicing power.

At this point, the connectorized fiber with etched cavity (fiber probe 2) is ready. The prepared probes are integrated to the PDMS fiber holder stamp. Fiber probes are carefully inserted in the fiber holder and protruded by 1 mm in the reaction well as shown in figure 3.15e. It should be ensured that fiber end is not damaged after inserting the probe in the PDMS holder. This assembly holds fiber still in the reaction well.

3.4.3 Functionalization of Fiber Tip

After inserting fiber probes in reaction well, probe tips are washed with acqa regia for 15 minutes to remove any organic debris on fiber tip. Fibers are washed 3 times with DI water to remove any acid on the fiber tip. The next step is to functionalize fiber tip so that proteins can directly attach without loss of functionality. The proteins are adsorbed on the glass without any surface modifications, but they lose functionality as the hydrogen bonds break, which causes protein to denature [84, 91-96]. Hence, there is a need for surface modification of glass surface, so that protein can attach without losing functionality. There are various glass surface modifications techniques available [97-99]. Electrostatic-self-assembly (ESA) is one of the surface modification techniques. Proteins adsorb on the polyelectrolyte layer due to electrostatic and hydrophobic interactions [84, 100]. By alternately dipping the fiber in cationic and anionic solution, a polyelectrolyte film is created on the fiber tip. This layer can adsorb protein without changing their functionality.

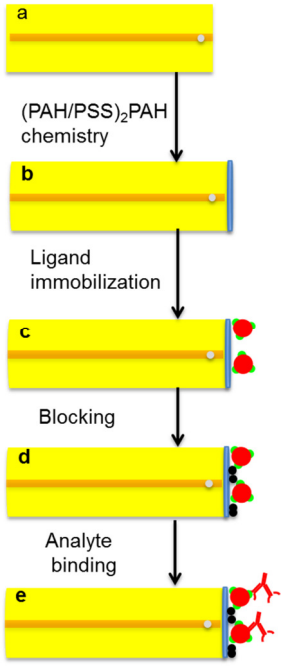

Figure 3.17 Process of functionalizing single mode fiber tip. The steps involve cleaning, surface chemistry, ligand immobilization, blocking and analyte binding.

The cationic solution polyallylamine hydrochloride (PAH) and anionic solution polysodium 4-styrenesulfonate (PSS) are used to create polyelectrolyte multilayer thin films on the fiber tip. The PAH and PSS are dissolved in DI water at concentration of 4mg/ml each. Functionalization process is initiated by adding PAH to the reaction well. After 5 minutes, PAH is removed and well is thoroughly washed by DI water to remove any loosely bound PAH on fiber tip. After this PSS is introduced in the well for 5 minutes followed by DI water wash. The another layer of each PAH and PSS is coated on the fiber for 5 minutes each followed by DI water wash after each layer formation. The last layer of PAH is introduced for 3 minutes and well washed with DI water. The steps involved in functionalization are shown in figure 3.17. This process creates 5 layers of polyelectrolyte solution, which can be represented as $(PAH/PSS)_2PAH$. This step is shown by a blue multilayer polyelectrolyte growth on fiber by figure 3.17b. The characterization and more detailed fabrication processes of these multilayer functionalization are documented in dissertation by Yan Zhang [84] .

3.4.4 Platform Testing for Biomolecular Interaction with Fiber Probe 2

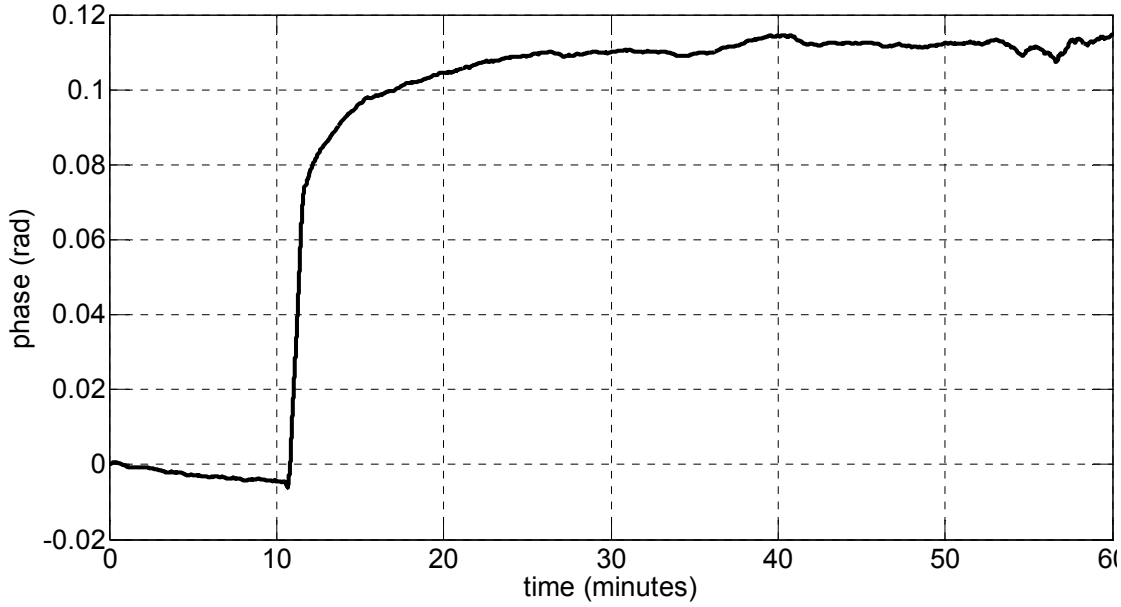

Figure 3.18 Binding curve showing attachment of rabbit IgG antigen (2mg/ml) on the $(PAH/PSS)_2PAH$ coated fiber tip

The next step is to immobilize receptor molecule or recognition protein molecule on the fiber tip. To immobilize as well as to monitor the binding process of ligand, the reaction well is incubated with 20µl of PBS and data acquisition is initiated. Once baseline is stable, 40µl of rabbit IgG antigen (2mg/ml) is incubated in the reaction well. This step is shown by figure 3.17c of the flow chart and binding plot is shown in figure 3.18.

After monitoring the binding curve for about 1 hour (when binding reaches steady state), the acquisition is stopped. The reaction well is washed three times with wash buffer to remove any loosely bound and unattached protein on fiber tip. After this step, blocking by BSA (0.5%) is done. Again for blocking step, 20µl of PBS is introduced in the reaction well and data acquisition is started. After baseline stabilization 40µl of 0.5 % BSA is added and data is acquired till steady state of binding curve is reached. This step is demonstrated in flowchart part 3.17d and binding curve is shown in figure 3.19.

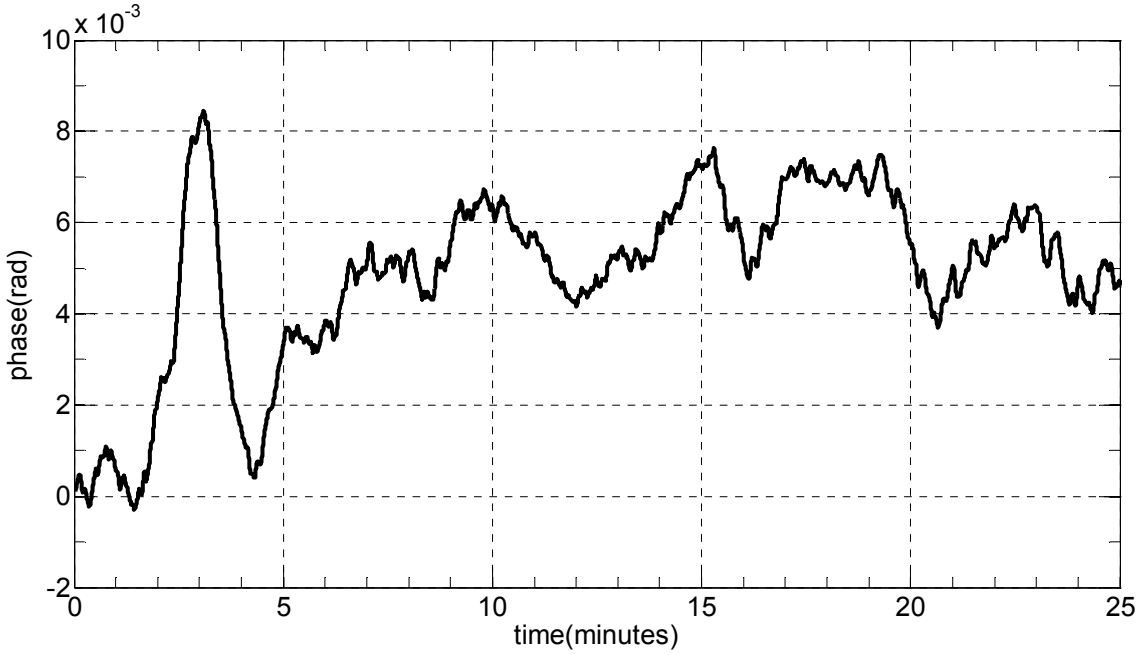

Figure 3.19 Non-specific binding, curve showing attachment of 0.5% BSA to the antigen immobilized fiber tip.

It can be seen from the figure 3.19, that BSA blocks any left out spaces on the fiber tip. This step is necessary because, the self-assembled monolayer of polyelectrolyte can attach any protein on its surface. But we are interested in studying and quantifying the interaction between ligand and analyte interaction only. If blocking step is not used, the analyte might directly attach to the polyelectrolyte layer and hence give incorrect quantification results. The blocking step might also cause some non-specific binding and hence increase in optical path length is seen.

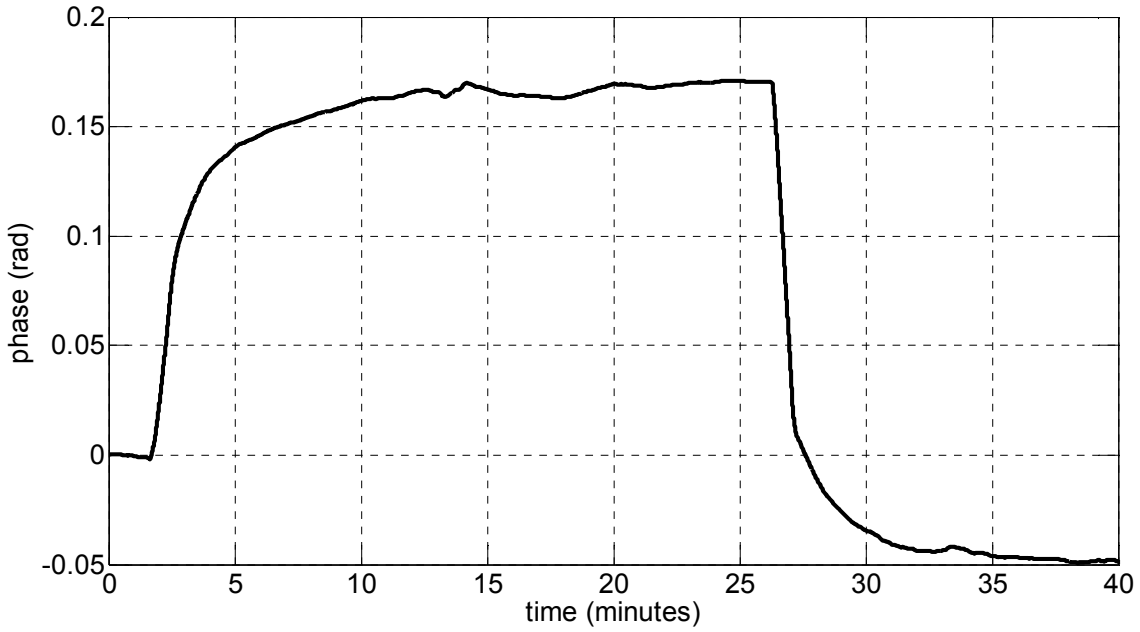

Figure 3.20 Binding curve showing attachment of anti rabbit IgG antibody (100µg/ml) to the antigen immobilized on fiber tip.

Again after blocking step, reaction well is washed 3 times with PBS. At this point the sensor probe is ready for quantification of analyte (antibody). Data acquisition is started after incubation of 20µl of PBS, after baseline stabilization, anti rabbit antibody (100µg/ml) is incubated in the well. After binding curve reaches steady state (27 minutes in figure 3.20), 1M HCL is introduced in the well. It can be seen from figure 3.20, the phase decreased abruptly and goes below 0. This shows that HCL removed the protein as well as the functionalization layer of the fiber probe. Cleaning probes with HCL and eventually with acqa regia, removes all the

binding chemistry from the optical probe and the probe can be reused after every biosensing experiment, which is one of the strength of this fabrication technique. This platform is miniature with sensor diameter of 125µm and is fluidics free.

3.5 Refractive Index Change Detection with Square Capillary

Using SD-PSI, it is also possible to detect refractive index changes when physical length in the interrogation volume is constant. The concept is explained in chapter 2, where test sample of interest in pumped through the capillary and RI change is detected.

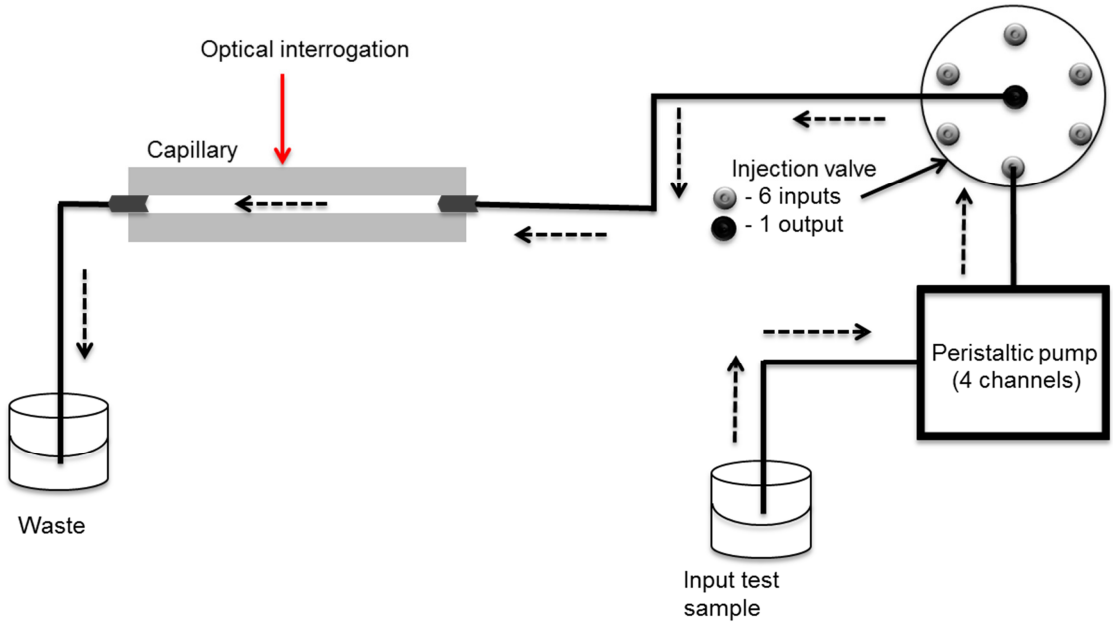

Figure 3.21 Flow setup for detecting refractive index changes in the test sample. The required test sample is placed in a vial, which is input to peristaltic pump. Peristaltic pump introduces sample in the injection valve. The output of injection valve is connected to input port of square capillary. The fluid goes to waste from output port of capillary. Dotted arrows indicate flow direction of test sample. Square capillary is placed on sample holder and integrated to interferometric system

Figure 3.21 shows the flow loop of the fluidic system. It comprises of peristaltic pump, injection valve, glass capillary and SD-PSI system. The sample of interest is placed in the vial. The peristaltic pump, pumps this fluid in the injection valve. The injection valve lets in the fluid from the selected channel and sends it to output channel. The output channel is connected to

input port of the glass capillary. The fluid flows through the capillary and is eliminated at the exit port of the capillary. As the fluid is flowing through the flow cell, light from the SD-PSI system is focused on the core of the capillary cavity.

3.5.1 Testing Platform for Refractive Index Change Detection for Biomolecules

For proof of principle, figure 3.22 shows the change in phase of interference signal for BSA at three concentrations (250, 500 and 1000µg/ml). Since, the physical length of capillary is constant, changes in phase are due to change in refractive index at different concentrations of BSA. The RI detection of BSA shows proof of principle experiment for concentration quantification based on RI change. The phase change is linear is a function of BSA concentration. The advantage with this platform is that surface immobilization chemistry is not required.

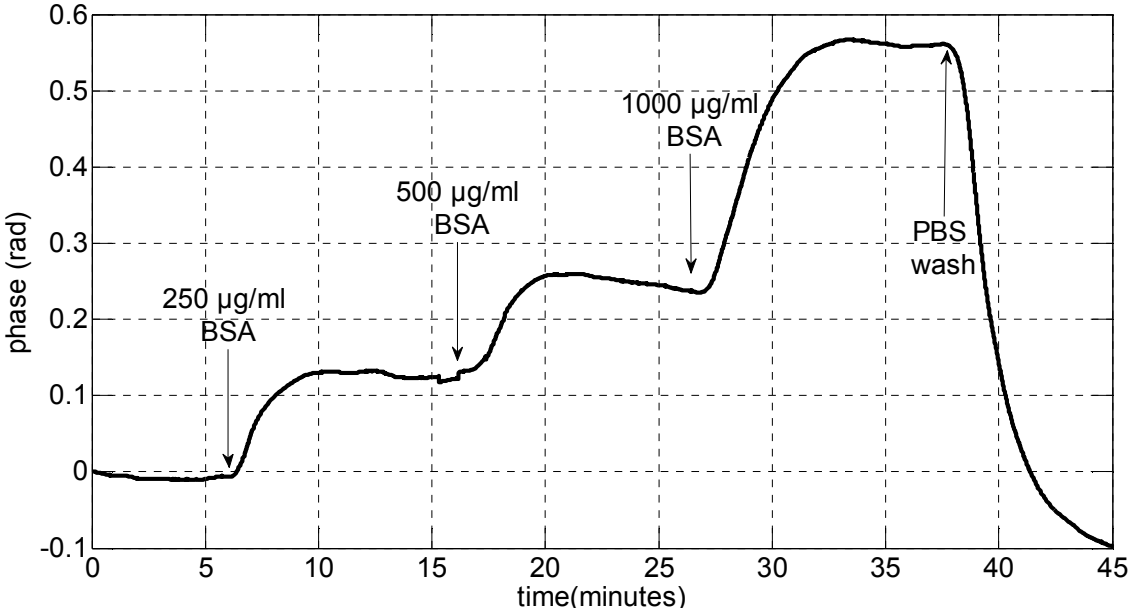

Figure 3.22 Phase change due to refractive index change of 3 different concentrations of bovine serum albumin (BSA).

Figure 3.23, shows phase change as a result of RI change for antigen, antibody and antigen-antibody complex all at concentration of 1mg/ml. As seen from figure, the phase change

occurring due to 1mg/ml of antigen is approximately 5 times lower than 1mg/ml of antibody. Phase change for complex formed by mixing antigen and antibody at 1mg/ml is in between antigen and antibody. However, the complex is not exactly the average of two biomolecules.

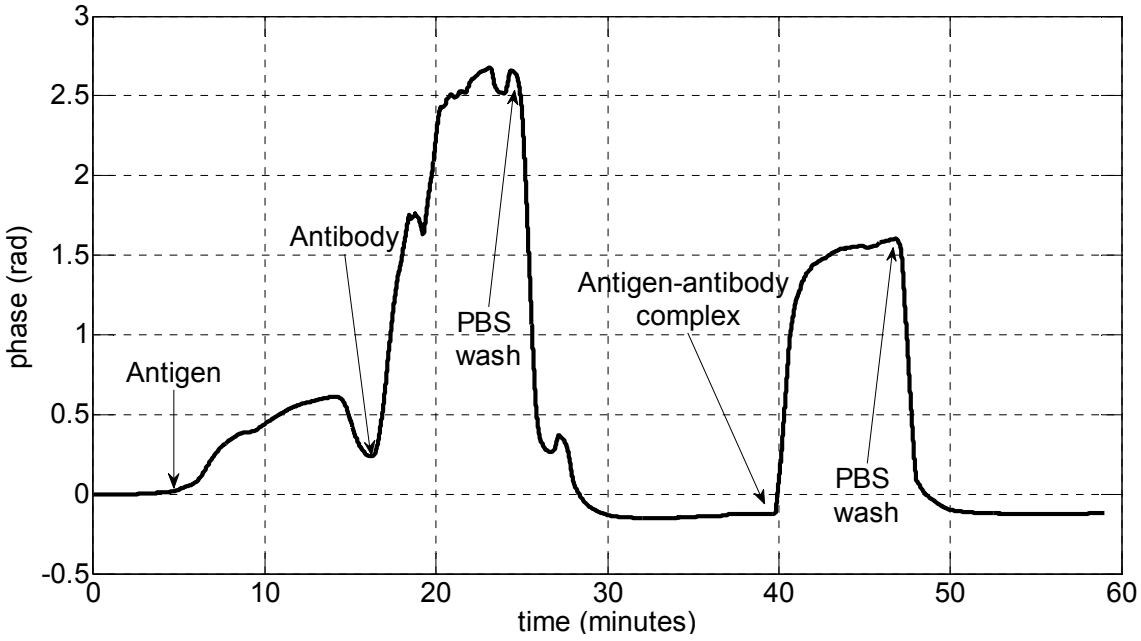

Figure 3.23 Phase change due to refractive index change of Rabbit IgG antigen, anti rabbit IgG antibody and antigen-antibody complex at concentration of 1mg/ml.

Figure 3.24 compares the phase change occurring between antigen, antibody and antigen-antibody complex at three different concentrations (250, 500, 1000µg/ml). This platform can provide information about conformational changes as binding occurs. Also, this platform does not require any immobilization chemistry for concentration quantification.

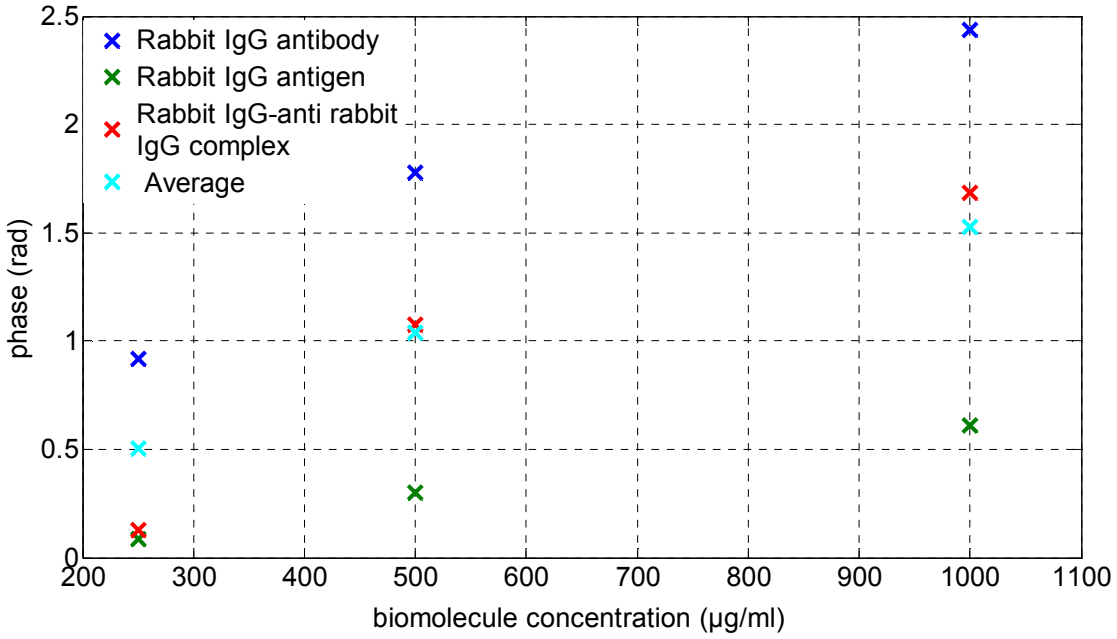

Figure 3.24 Plot shows phase change as a function of antigen, antibody and antigen-antibody complex at three different concentrations (250, 500, 1000µg/ml). The graph also shows calculated average of antigen and antibody to differentiate it from antigen-antibody complex.

In summary, four sensor platforms are fabricated for BIA studies. Fabricated platforms use laboratory grade coverslip with immobilization chemistry as sensor. Multi-well plate platform is cost efficient with small volume requirements. The drawback of analyte incubation perturbation in multi-well is overcome by flow cell platform. Flow cell platform can perform concentration and kinetics analysis of biomolecules with two interactions per sensor. For fluidics free interaction studies fiber probe 1 and fiber probe 2 are ideal. Fiber probe 1 with light focused on attached sensor allows for BIA by dipping sensor in analyte solution. Fiber probe 2 performs BIA directly on fiber tip without need of any integrated optics. Simple fabrication, miniature sensor, resistance to mechanical perturbations and sensor regenerations are some of the advantages of fiber probe 2 platform. However, there is a power loss in the cavity, which can be overcome by using higher power source if needed.

CHAPTER 4

MULTIPLEXED BIOMOLECULAR INTERACTION ANALYSIS

High throughput detection of biomolecules is required for drug screening, biomarker detection and food borne pathogen detection. For pharmaceutical drug discovery and screening, high throughput detection is required for identification, characterization and testing of potential drugs. This not only helps in cost reduction but also makes drug availability in market a faster process [101-104].

New technologies are trying to address limited throughput issues by incorporating highly multiplexed biosensing platforms. The idea is to study multiple interactions in parallel, to save time and resources. The EPIC system by *corning* marketed high throughput label free screening platform that can study 40,000 wells in 8 hours. The Octet system by *Forte´Bio* can study 96 samples in 20 minutes or 384 samples in 75 minutes. However they can study 16 samples in parallel. The *Biacore's* system Biacore 4000, can study 16 interactions in parallel. It can study up to 4800 interactions in 24 hours.

High sensitivity, label free, high throughput, faster response and simple sensor fabrication are some of the desired characteristics of biosensing platform. The SD-PSI is label free technique that requires simple sensor preparation. Plain Laboratory grade coverslip can be used as biosensor without any prior calibration. Using single channel biosensing, sensitivity of 33 ng/ml for IgG antibody is demonstrated. The system can be configured for high throughput detection. Coherence multiplexing, time division multiplexing or a combination of both multiplexing techniques can be utilized for high throughput detection. Also as demonstrated in chapter 3, SD-PSI system is compatible with range of sensor formats. Biosensing can be done in well plate, flow cell and fiber based platforms. This system provides additional advantage of miniaturization that can have potential for patient screening at point of care.

4.1 Coherence Multiplexing with SD-PSI

The multiplexing techniques that can be used for high throughput detection are time division multiplexing (TDM), wavelength division multiplexing (FDM) and coherence multiplexing (CM). Briefly, in TDM optical input is pulsed and each sensor produces output pulse, which is separated in time. In FDM, frequency of source is ramped linearly and system is setup in a way that OPD for each sensor is different [105]. In coherence multiplexing, high throughput is achieved from single optical signal and does not need complex time or frequency domain instrumentation [105, 106]. Simultaneous biosensing from multiple channels in a fiber-based instrument is done using coherence multiplexing, which is an advantage compared to other multiplexing techniques. The sensors used in CM are such that each sensor generates OPL that is distinct for other sensor. Coherence multiplexing capability can be integrated with time division multiplexing to further increase throughput of SD-PSI.

4.1.1 Range of Sensor Thickness for Coherence Multiplexing

For creating different optical path length differences for each sensor, coverslips of different thicknesses are used. The range of coverslip thickness that can be used as sensor is a function of coherence length of the source, spectral resolution and center wavelength of the source. Continuous super luminescent diode with short coherence length (14μm) is used as a light source. The coherence length of the light source with center wavelength λ_0 and full width half maximum bandwidth of source, $\Delta\lambda$ is calculated by

$$l_c = \frac{2\ln 2}{\pi}\frac{\lambda_0^2}{\Delta\lambda} \qquad (1)$$

The optical path length difference for each sensor needs to be much higher than coherence length of the source so that interference between two waves from different sensors does not occur [107]. The thinnest sensor that can be used depends on coherence length of the source. For the system to identify two reflective surfaces of coverslip for interference signal, the coverslip thickness has to be higher than coherence length of the source, which is 14μm. But since the thinnest coverslip commercially available is # 00 corresponding to average thickness

of 60μm, this thickness dictates the lower limit on sensor thickness. The thickest sample that can be used is a function of center wavelength of source and spectral resolution of source and is calculated as 1.17 mm by using equation 2 [108].

$$Z_{max} = \frac{\ln(2)}{2\pi} \frac{\lambda_0^2}{\delta v} \quad (2)$$

Where, $\lambda_0$is the wavelength of the source and δv is the spectral resolution. Hence, the range of coverslips from 70 μm-1170 μm thicknesses can be used for coherence multiplexing. The coverslips numbers 00 (55-80μm), 0 (80-120μm), 1(130-160μm), 1.5(160-190μm), 2(190-230μm), 3(280-320μm), 4(380-420μm) 5(500-600μm) are commercially available. The maximum number of channels that can be used for coherence multiplexing is given by

$$N_{max} = \frac{\Delta\lambda}{2\delta v} \quad (3)$$

Where $\Delta\lambda$ is bandwidth of the source and δv is the spectral resolution. Using equation 3, the maximum multiplexed channels used can be 166. However, as there is a limitation on commercially available coverslip thicknesses, different combinations of commercially available coverslips can be sandwiched to get the desired sensor thicknesses. Commercially available index matching epoxy can be spin coated on coverslip to give a thin coating of epoxy to which another coverslip can be attached.

4.1.2 Working Principle of High Throughput Detection for Biosensing

The working principle for high throughout detection of an N channel coherence multiplexed label-free biosensing using a phase sensitive spectral domain interferometric setup is shown figure 4.1. Each channel is a coherence separated interference channel. For each channel, the coherence separation is done using sensors of different thickness in each channel. The thinner coverslip will produce slower sinusoidal spectral oscillation and its output can be extracted from lowest spatial frequency in Fourier domain. The higher thickness coverslip will produce spectral oscillations at higher frequency and can be extracted from higher spatial frequency in Fourier domain [67].

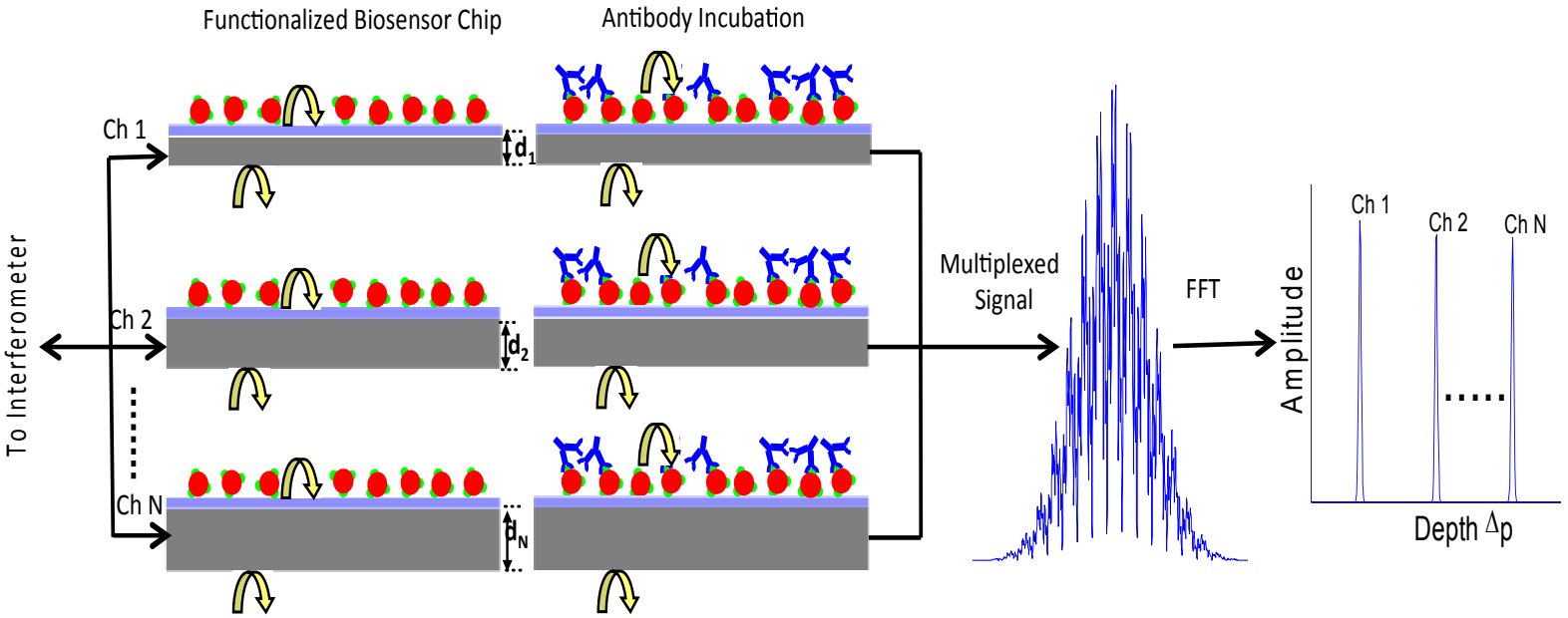

Figure 4.1 Cartoon illustrating implementation of N coherence multiplexing to detect different molecules simultaneously and data analysis technique. Each biosensor chip is attached to a separate output port of the interferometer. Fourier transform of the multiplexed spectral interference signal (middle panel) separates the signal in different channels (right panel).

The capture molecule/ligand (red) is immobilized on the aldehyde-coated coverslips of different thicknesses. The sensor thickness varies from d_1 to d_N for channels 1 to N. During optical interrogation, light incident on the coverslip is reflected (yellow arrows) from bottom of the coverslip (air-glass interface) and top of attached protein (ligand-buffer interface) as shown in figure 4.1. Two beams of reflected light for each sensor interfere and produce interference pattern for each channel. N interference signals form all N channels add up and are shown as multiplexed signal on figure 4.1. After incubation of analyte (blue) and binding with ligand, the source of reflective surface change for each biosensor. Reflections now occur at the glass-air interface and the analyte-buffer interface resulting in the interference signal, which is shifted with respect to the previous multiplexed interference pattern. The shift occurs due to the increase in the optical path length as a result of the physical increase in thickness caused by the analyte binding onto the ligand. The multiplexed signal detected by interferometer is given by [65, 68-70, 109]

$$S(k) = \alpha S_0(k)\left\{R_r + R_s + \sqrt{R_r R_s}|\mu(k)| \sum_{m=1}^{N} \cos(4\pi \Delta p_m k)\right\} \qquad (4)$$

$S_0(k)$ is incident spectral intensity, R_r and R_s are reflectivity of the two surfaces of the biosensor in consideration , $\mu(k)$ is the spectral degree of coherence which is assumed one as light exiting single mode fiber is spatially coherent, Δp_m is optical path length difference between two surfaces of the mth biosensor and k is the wave number. The cosine term is equation 4 causes the modulation in the signal and this modulation is the function of optical path length difference between the two reflective surfaces of the coverslip.

The sub nanometer change in the length due to binding on each sensor can be precisely quantified as change in phase. From the multiplexed signal (equation 4), the relation between phase shift and change in optical path length can be quantified. Fourier transform of equation 4 yields magnitude of reflected light as a function of optical path length difference between the two reflective surfaces of each sensor, which can be quantified by equation 5.

$$\varphi_m(t) = \tan^{-1}\left\{\frac{\mathrm{Im}\,\Im[S(k)]}{\mathrm{Re}\,\Im[S(k)]}\right\}|_{z=\Delta p_m} = \frac{4\pi\Delta p_m}{\lambda_0} \qquad (5)$$

From equation 5, the change in the phase of the interference signal as analyte binds to the captured protein can be precisely quantified which can eventually be related to the change in the optical path length due to binding. Here λ_0 is center wavelength of the low coherence source.

4.1.2 Optical Setup of SD-PSI Four Channel Multiplexed Detection

Figure 4.2 shows optical setup for multiplexing by simultaneous detection of four sensors. However, to increase the number of samples for detection, 1:N fiber coupler can be used to give N biosensing channels. The setup consists of superluminescent diode (SLD), 635 nm visible light source, 90:10 fiber coupler, 50:50 fiber coupler and home built spectrometer. The broadband SLD light source operates at 800-nm center wavelength with full-wave half-maximum (FWHW) and coherence length of 20nm and 14 μm respectively. The coherence length of 14 μm indicates that the interference will occur only if the optical path length difference between the sample signal and reference signal is less than 14 μm. And this dictates the spatial resolution of the system. The 635 nm red light source is used in the system for visualization of beam on the sample. The light from SLD and 635 laser sources are input to 90:10 fiber coupler. The fiber coupler splits the combined power in ratio of 90:10. The arm with 90 % of power is inputted to 2x2 50:50 fiber coupler. The second coupler splits power equally in two output paths. To each output path, one more 2x2 (50:50) coupler is used. This geometry gives four sample paths. The light is collimated and then focused on the each sample surface. The light is reflected back from reflective surfaces of the sensor surface. The interference signal caused due to the light reflecting back from the reflective surfaces of the respective samples is coupled back to a home built spectrometer.

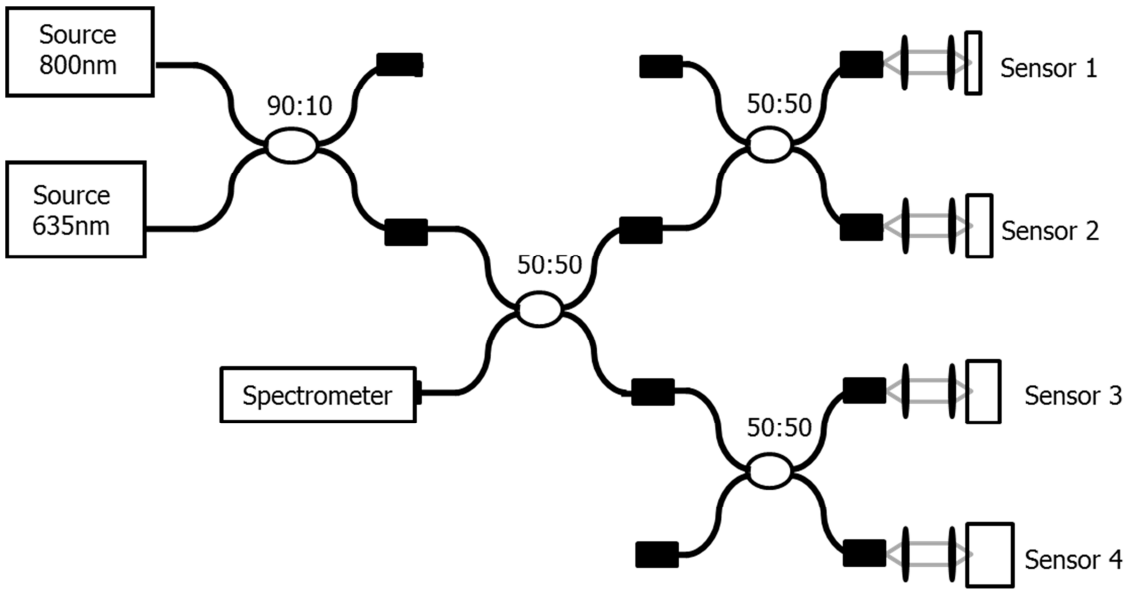

Figure 4.2 Optical setup for multiplexed detection of four biosensors simultaneously. Four sensors with different thicknesses are shown. Each biosensor chip is attached to a separate output port of the interferometer.

As shown in chapter 2, the SNR drops off as a function of increase in sensor thickness. As, the biosensor gets thicker, its sensitivity of biomolecule detection decreases. The sensitivity of detection also depends on size and refractive index of molecule. Hence, the interaction studies of small molecules and large molecules can be done on thinner and thicker sensors respectively to compensate for SNR variation to some extend. Another way to compensate for SNR fall for higher thickness sensors is to coat the sensor surface with titanium dioxide. Comparing figure 2.7 and 2.8 from chapter 2, it can be seen that titanium dioxide coating decreases the phase noise. Hence, thicker sensors can be coated with higher refractive index coating of titanium dioxide to improve detection sensitivity.

4.2 Multiplexed Detection of Biomolecules in Different Platforms

For proof of principle, 4-channel multiplexed detection of biomolecules is demonstrated. This can be extended to N channels as shown in figure 4.1. The multiplexed detection is tested on different platforms such as static multi-well plate, flow cell, fiber probe 1 and fiber probe 2.

4.2.1 Multiplexed Detection of Biomolecules in Static Setup

The sample preparation from static experiments is same as described in chapter 3. Four PDMS stamps with punched holes are immobilized on coverslips. The coverslips used are of 4 different thicknesses. Coverslip # 0, 1, 1.5 and 2 are used. These coverslips are commercially available with aldehyde chemistry. Multi-well sensors are placed on sample holder with tip and tilt mount for optical interrogation.

Figure 4.3 shows multiplexing results with two channels. Figure 4.3a shows binding of anti rabbit IgG to immobilized rabbit IgG on the sensor surface. The concentration of anti rabbit IgG in one channel is 13.33µg/ml and in other channel is 3.33µg/ml. The incubation of anti-rabbit IgG is done at different time points to see if there is any cross talk between two channels. However as seen from the figure, the incubation of anti-rabbit IgG at concentration of 3.33µg/ml at later time point of 9 minutes does not affect the binding curve of earlier incubated antibody at concentration of 13.33µg/ml. Again figure 4.3b shows two different sensors measuring same concentration of anti-rabbit IgG. Concentration of anti rabbit IgG in both channels is 13.33µg/ml. From these two plots it can seen that binding response of one channel is independent and unaffected by binding response of another channel.

The plots for same concentration (figure 4.3b), the phase value at 50 minutes is same, but settle at two different valves at 55 minutes. The discrepancy in final settling for same concentration can be attributed to the random Brownian motion of analytes after incubation. In this setup as there is no pump or stirring to increase the probability of analytes to get in proximity of ligands, the quantification is dependent on Brownian motion. Hence, also the biomolecular interaction in static setup takes longer time to reach final steady state quantification phase value.

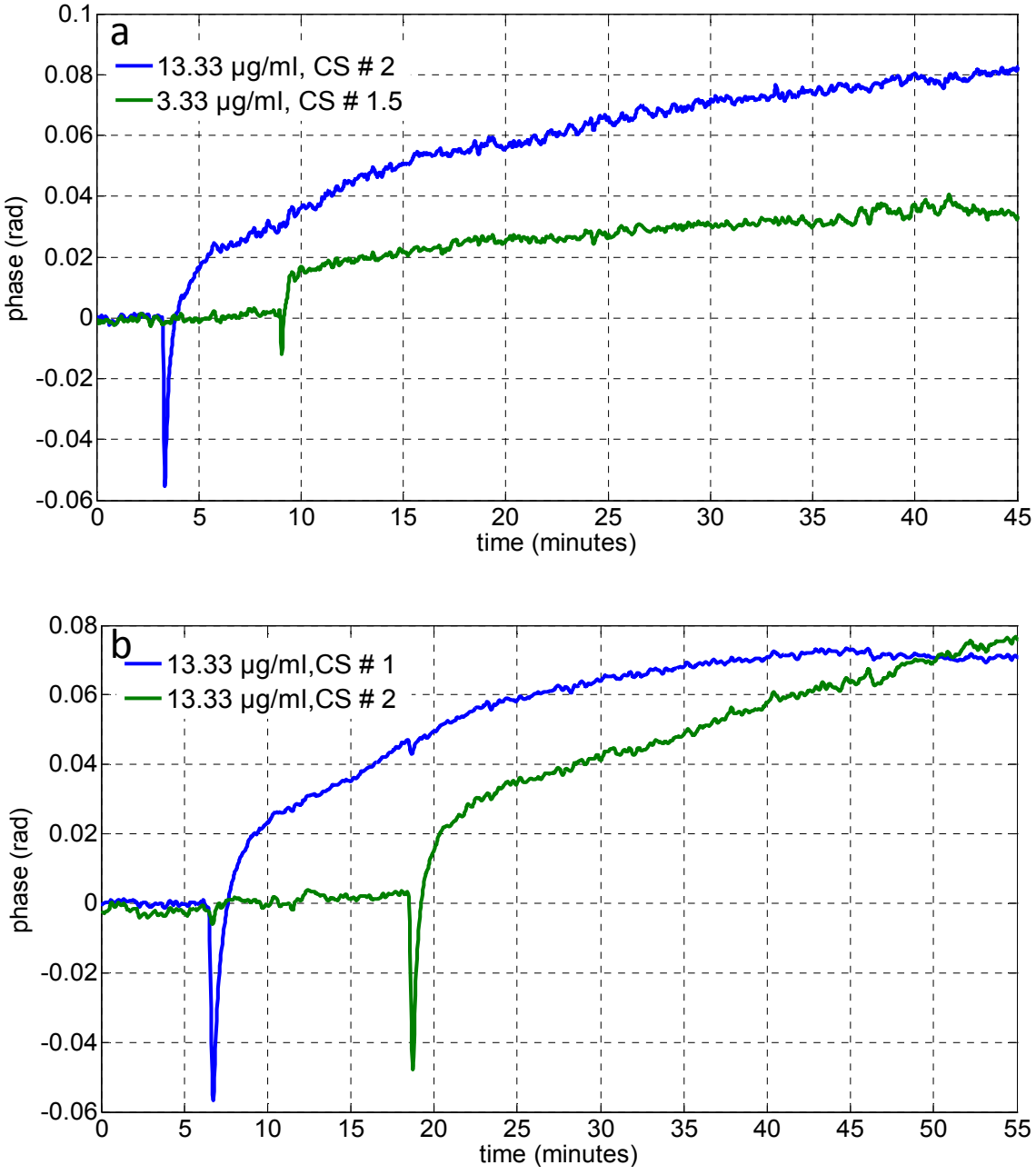

Figure 4.3 Multiplexing capability of SD-PSI demonstrated by showing binding interaction between immobilized Rabbit IgG and anti-rabbit IgG. a) Two different concentrations in both channels, b) Same concentration in both channels

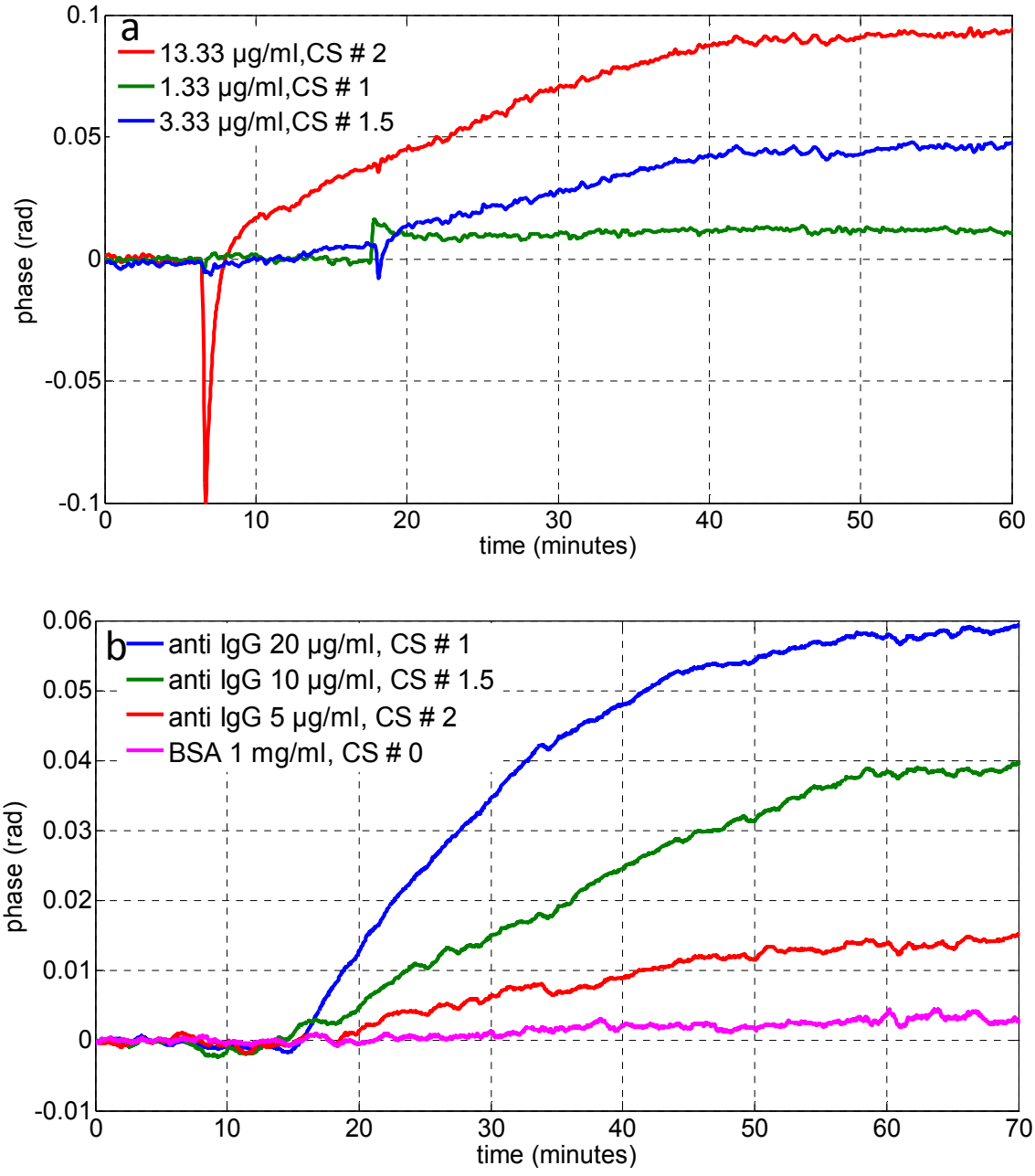

Figure 4.4 Multiplexing capability of SD-PSI with multi-well sensor platform. a) Three channel multiplexing, b) Four channel multiplexing

Figure 4.4a shows multiplexed detection using three channels. The concentration of

anti rabbit IgG in channel one is 3.33µg/ml, in channel two is 1.33µg/ml and in channel three is 13.33µg/ml. The anti-rabbit IgG is incubated at same time for sensor 1.5 and 1, again demonstrating no cross talk between the channels. Figure 4.4b shows 4-channel multiplexing. In this plot for coverslip 0, interaction of bovine serum albumin (BSA) is studied on polylysine-coated coverslip. This is done, as coverslip 0 is not commercially available with aldehyde coating to study rabbit IgG-anti rabbit IgG interaction.

4.2.2 Multiplexed Detection of Biomolecules in Flow Cell Platform

The coverslips (CS) # 1, 1.5 and 2 are placed as sensor in 3 different flow cells. The peristaltic pump is used to pump analyte in all three-flow cells at same speed. The flow rate in the channel is calculated to be 460 nl/sec. After baseline data acquisition for 10-15 minutes, the analyte is flowed through the channels.

In figure 4.5a, the same concentration of analyte is flowed through all three-flow cells. As seen from the figure, the flow cell cells show higher repeatability as compared to static step as analyte in brought in close proximity to ligand from flow and micrometer size channel. The binding kinetics also shows repeatability and the interaction takes lesser time to reach final steady phase quantification value. Figure 4.5b shows binding kinetics at three difference concentrations of analyte that settle at three different phase values.

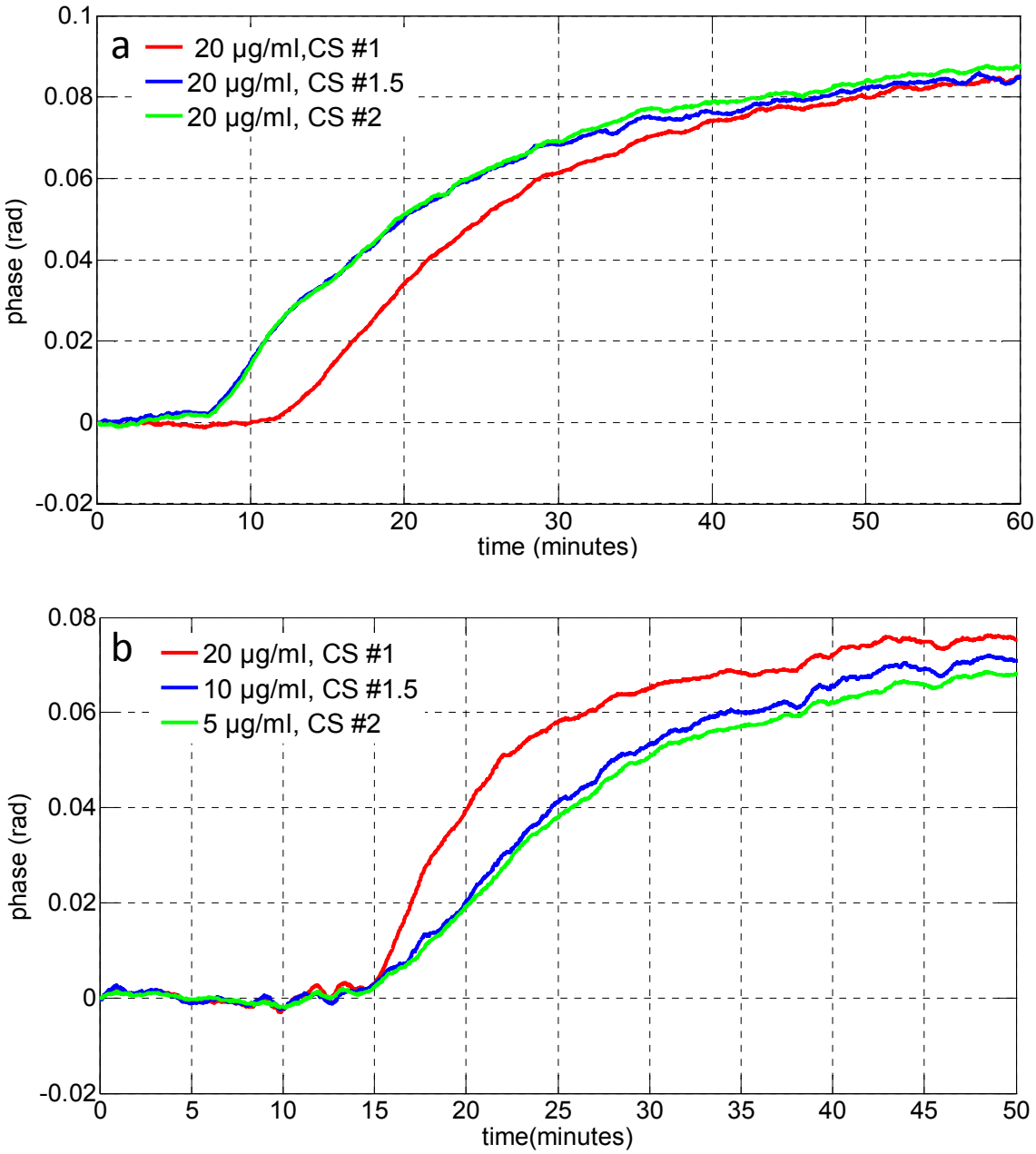

Figure 4.5 Multiplexing capability of SD-PSI with flow cell platform demonstrating 3 channel multiplexing. a) Same concentration of analyte (anti-rabbit IgG concentration 20µg/ml), b) Different concentration of analyte (anti-rabbit IgG concentration 20, 10 and 5 µg/ml)

4.2.3 Multiplexed Detection of Biomolecules using Fiber Probe 1

For this set of experiments, the bulk optical sample arm cage system is replaced by miniature fiber probe. The light from coupler is directed to GRIN lens in the fiber probe that focuses the light on the sample. The sample is immobilized on the fiber tip, making the entire sample arm one assembly. Fiber probes are prepared and functionalized sensor of different thickness with rabbit IgG is attached directly to the fiber probe. Fiber probe is then immersed in the PBS solution and baseline data is acquired. After the baseline stabilization, anti-rabbit IgG is added to PBS solution. From figure 4.6, it can be seen that noise level for two probes is different. One disadvantage with this setup is that when epoxy gets in contact with PBS, the salts in PBS start affecting epoxy. This causes some mechanical movement in the sensor, affecting the focus position. The advantage with miniaturized fiber probe is that many such probes can be packaged in a single assembly for high throughput detection. The radius of the miniaturized probe is 1.05 mm, which means approximately 25 such probes can be packed in a cylinder of 0.5mm radius which can identify 25 different proteins in sample simultaneously.

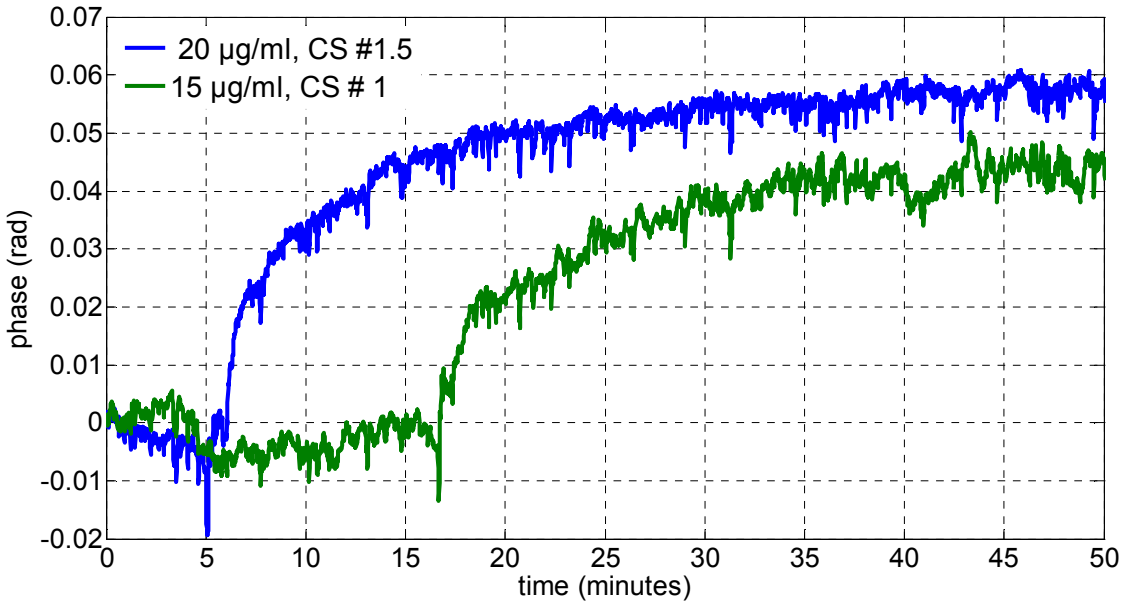

Figure 4.6 Multiplexing capability of SD-PSI demonstrated by two different fiber probes 1 detecting two different concentrations.

4.2.4 Multiplexed Detection of Biomolecules with Fiber Probe 2

In this setup the coherence multiplexing is achieved by cleaving the fibers at different lengths from the etched fiber interface. This is shown by varying distance of the fiber tip from the cavity. This gives rise to different thicknesses of the sensor that are essential for coherence multiplexing. The probes are inserted in the PDMS fiber mold with a reaction well as shown in figure 4.7.

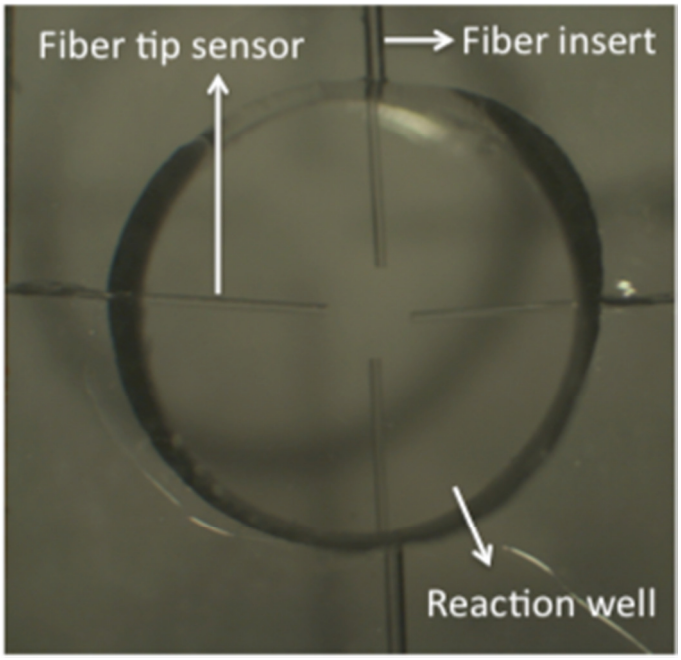

Figure 4.7 Four-channel fiber tips immobilized in PDMS fiber insert. The image shows all four probes inserted in single reaction well.

Each fiber is functionalized with $(PAH/PSS)_2PAH$ chemistry to attach to ligand of interest as described in chapter 3. As seen from figure 4.8, the cartoon shows four fiber probes each functionalized with Goat IgG, Rabbit IgG, Laminin and Biotin as ligands. After baseline stabilization with PBS in the reaction well, the mixture of analytes in incubated in the reaction well. The analytes mixtures incubated are anti goat IgG, anti rabbit IgG, anti-laminin and streptavidin.

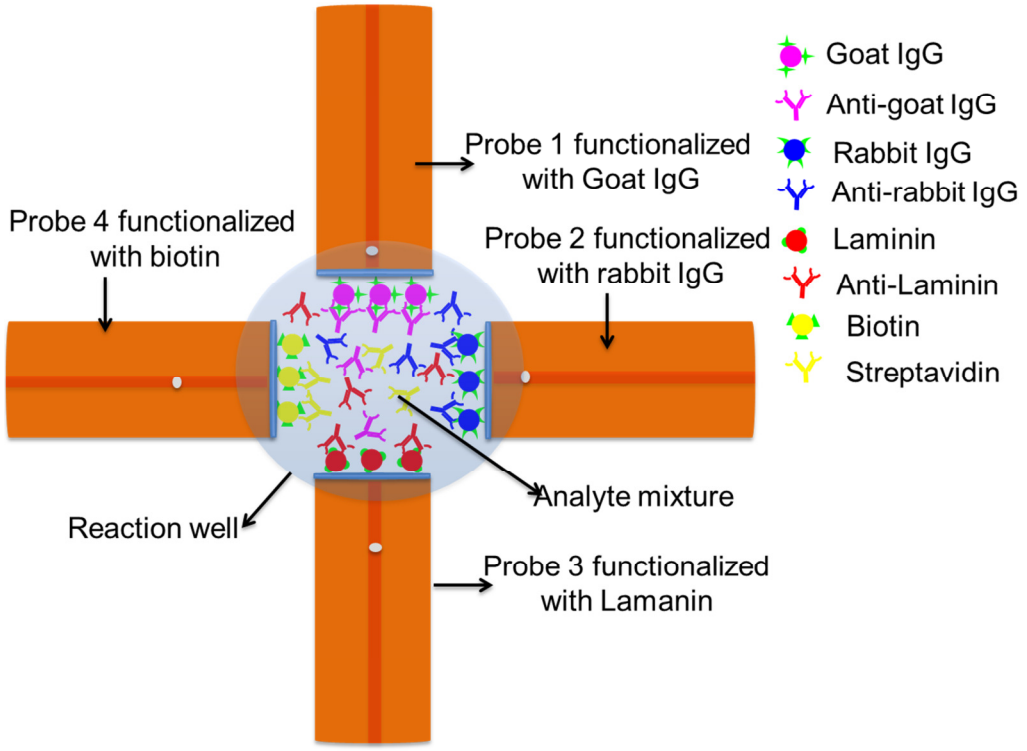

Figure 4.8 Cartoon of four-channel fiber probe 2 biosensing. Coherence multiplexing is achieved by cleaving fibers are different lengths. Four probes are functionalized with four different ligands to identify 4 corresponding analytes in the reaction well

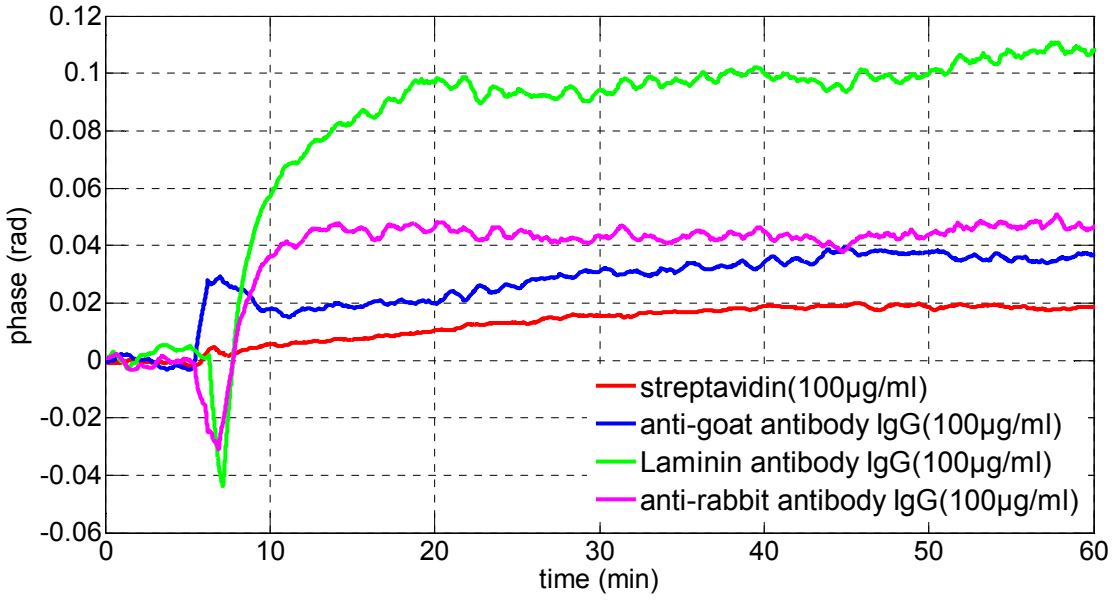

Figure 4.9 Binding curves obtained from incubation of different analytes in the reaction well.

Figure 4.9 shows the binding curve for 4 different analytes binding to the corresponding immobilized ligands. The concentration of all the analytes is 100µg/ml but depending on the size and refractive index of the molecule, the final settling values for all four pairs is different.

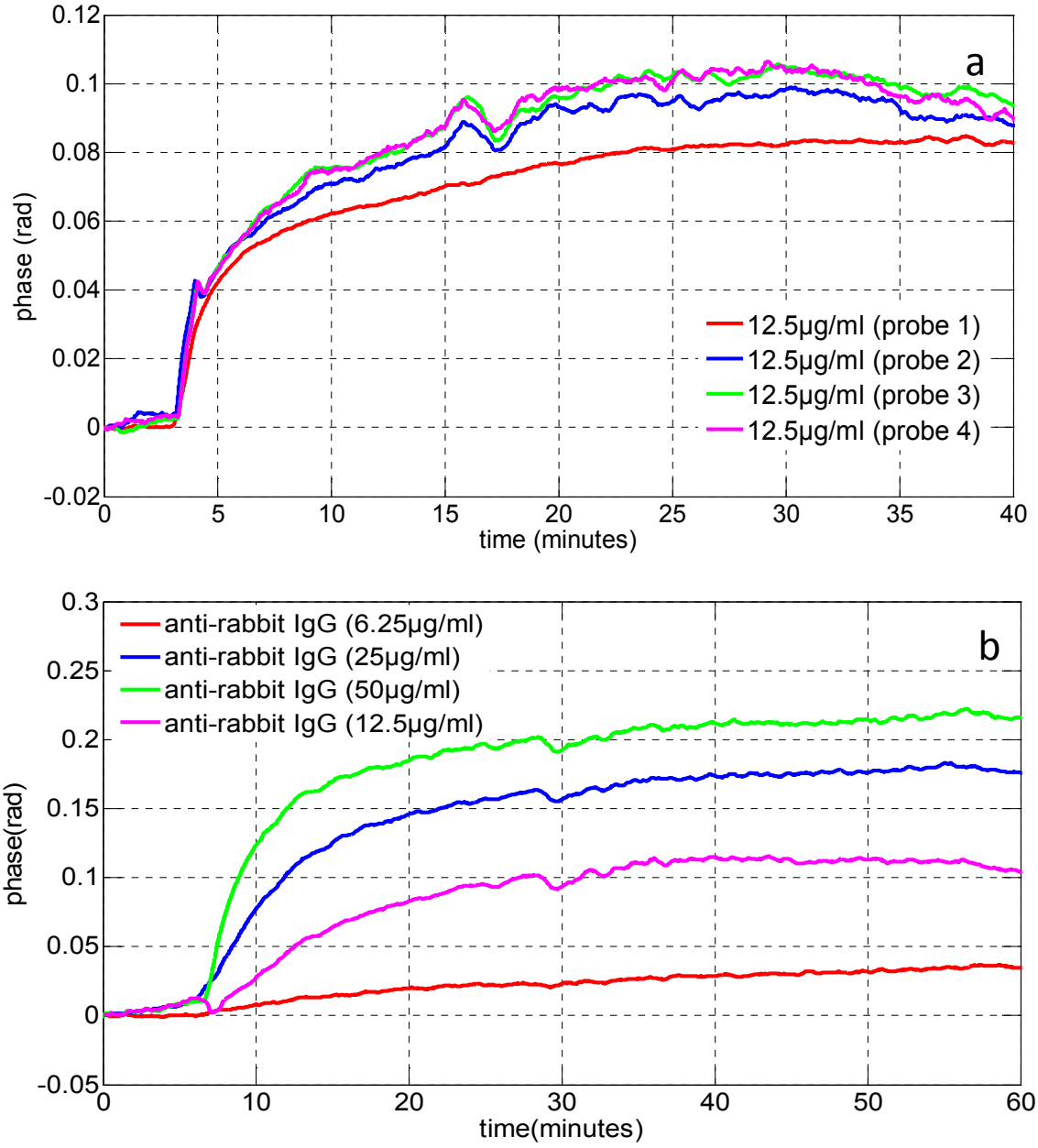

Figure 4.10 Binding curves obtained from incubation of anti rabbit IgG. a) At same concentration of analyte (12.5µg/ml) b) At different concentration of analyte

Figure 4.10 shows binding curve for multiplexed detection of anti rabbit IgG for two cases. In figure 4.10a, the concentration of incubated anti rabbit IgG is 12.5µg/ml for all four probes. Figure 4.10b shows different concentration of anti rabbit IgG for all four probes. For this set of experiment, each fiber probe has a separate reaction well in order to study different analyte concentration.

Incorporating time division multiplexing in addition to coherence multiplexing can further increase the high throughput capability of SD-PSI. If 166 coherence channels are integrated with 16 time division channels, detection of simultaneous 2656 BIA channels is possible.

In summary, high throughput capability of SD-PSI is demonstrated by implementing 4 coherence multiplexed channels. With designed SD-PSI specifications, 166 coherence channels can be implemented with maximum sensor thickness of 1.17 mm. Four platforms are tested for coherence multiplexing by incorporating coverslips of different thicknesses. For fiber probe 2, cleaving fiber at different lengths from etched interface varies thickness of sensor. BIA of 4 different analytes from analyte mixture is also demonstrated. This has an application in multi-biomolecule detection in patient test sample such as blood, serum or saliva.

CHAPTER 5

CONCLUSIONS AND FUTURE WORK

The feasibility of SD-PSI for biomolecular interaction analysis and biosensing is demonstrated. As demonstrated in the experiments, laboratory grade coverslip is used as sensor for BIA. Use of coverslip as sensor makes SD-PSI cost effective BIA modality. Multi-platform compatibility of SD-PSI is tested with multi-well plate, flow cell and fiber probe platforms. For proof of principle, each fabricated platform is tested for BIA between rabbit IgG and anti rabbit IgG.

With the fabricated design of multi-well platform, 15 interactions can be studied using one sensor chip. 50µl of analyte is required for the interaction. However, as the interaction is dependent on Brownian motion and diffusion for analyte to interact with immobilized ligand, sensorgram takes longer time to reach steady state. Multi-well platform can be used for applications requiring cost effective and low volume reagents for concentration analysis studies.

With designed flow cell platform, two BIA can be performed from single sensor. With constant flow of analyte in fluidic circuit, analyte is brought in close proximity to attached ligand for binding interaction. Flow cell platform can be used for applications requiring binding kinetics information as well as concentration analysis. However, designed flow cell requires higher volume of analyte as compared to multi-well platform.

Two fiber probes for BIA studies are fabricated. Fiber probe platform 1 with integrated optics enables miniaturization of sensing platform. Fabricated probe has an outer diameter of 2.1 mm, which is dipped in analyte solution for BIA allowing for fluidics free detection. Fiber probe 2 is capable for performing BIA directly on fiber tip. Advantages offered from fiber probe 2 include miniaturization with sensor diameter of 125µm, resistance to mechanical perturbations,

fluidics free and regeneration capability of fiber tip for reuse. Multiple fiber probe 2 platforms can be integrated to lab on chip for BIA studies of different ligands within a test sample.

High throughput detection capability of SD-PSI is demonstrated with coherence multiplexing with four channels. For proof of principle, fabricated platforms are tested for BIA by implementation of coherence multiplexing. Use of coverslips with different thicknesses as sensors helps in realization of coherence multiplexing. With the current spectrometer design and source bandwidth, 166 coherence channels can be implemented with maximum sensor thickness to be 1.17mm. To increase the range of available sensor thicknesses, index-matching epoxy can be used to epoxy commercially available coverslips in different combinations. To address the issue of decreasing signal to noise ratio as a function of increase in sensor thickness, thicker sensors can be coated with transparent material with higher reflectivity as compared to glass.

Future work involves systematic study of sensitivity, dynamic range and repeatability for each fabricated platform. With fabricated multi-well plate, sensitivity of 33 ng /ml for detection of anti-rabbit IgG is achieved. Detection sensitivity of SD-PSI can be improved either by reducing phase noise of SD-PSI or by conjugating analyte with nanospheres/nanoparticles to produce higher phase change for lower concentrations of analytes. From preliminary experiments with ligand conjugated gold nanoparticles, 25 ng/ml of antigen concentration gives phase change of 84 milli-radians. By linear scaling, the sensitivity of detection can be improved by three orders of magnitude allowing detection concentration in pg/ml.

Future work also involves BIA on live cell assays. BIA on live cell assays allows for study of interactions in natural biological environment without need for receptor extraction from cells. BIA can be performed using either OPL measurements or RI changes as analyte binds to cell receptor. For OPL measurements, adherent cells (20-50% confluent) can be grown on sensor surface. Light can be focused on single cell to take baseline measurement and BIA can be studied after incubating analyte. Binding of analyte on adherent live cell receptor changes

OPL that can be quantified. For detecting refractive index changes as a result of binding, cells can be immobilized inside a square capillary. Dynamic mass redistribution (DMR) [110] as result of analyte binding to cell receptor can be studied from cumulative refractive index change as a result of binding inside the square capillary.

REFERENCES

1. Gao, Y., et al., *Plasmonic Mach-Zehnder interferometer for ultrasensitive on-chip biosensing.* ACS nano, 2011. **5**(12): p. 9836-44.
2. Tanious, F.A., B. Nguyen, and W.D. Wilson, *Biosensor-surface plasmon resonance methods for quantitative analysis of biomolecular interactions.* Methods in cell biology, 2008. **84**: p. 53-77.
3. Comley, J., *Progress in the implementation of Label free detection, Part 2: Binding analysis Assays.* Drug Discovery World Fall 2008: p. 28-49.
4. Wu, G., *Label-free technologies in biological assays.* Trends in Bio/Pharmaceutical Industry p. 42-53.
5. Tothill, I.E., *Biosensors for cancer markers diagnosis.* Semin Cell Dev Biol, 2009. **20**(1): p. 55-62.
6. Soper, S.A., et al., *Point-of-care biosensor systems for cancer diagnostics/prognostics.* Biosensors & bioelectronics, 2006. **21**(10): p. 1932-42.
7. Notermans, S. and K. Wernars, *Immunological methods for detection of foodborne pathogens and their toxins.* Int J Food Microbiol, 1991. **12**(1): p. 91-102.
8. Gilbride, K.A., D.Y. Lee, and L.A. Beaudette, *Molecular techniques in wastewater: Understanding microbial communities, detecting pathogens, and real-time process control.* J Microbiol Methods, 2006. **66**(1): p. 1-20.
9. Cremonesi, P., et al., *Pathogen detection in milk samples by ligation detection reaction-mediated universal array method.* J Dairy Sci, 2009. **92**(7): p. 3027-39.
10. J, S., et al., *Biosensing*2006: Springer.
11. Keusgen, M., *Biosensors: new approaches in drug discovery.* Naturwissenschaften, 2002. **89**(10): p. 433-44.
12. Cooper, M.A., *Optical biosensors: where next and how soon?* Drug Discov Today, 2006. **11**(23-24): p. 1061-7.
13. Cooper, M.A., *Optical biosensors in drug discovery.* Nat Rev Drug Discov, 2002. **1**(7): p. 515-28.
14. Minghui Yang, et al., *Meeting current public health needs: optical biosensors for pathogen detection and analysis.* Proc. SPIE 2009. **7167 716702**: p. 1-14.
15. Attana. http://www.attana.com/.
16. Huber, W. and F. Mueller, *Biomolecular Interaction Analysis in Drug Discovery Using Surface Plasmon Resonance Technology*. Current Pharmaceutical Design. Vol. 12. 3999-4021.
17. Vo-Dinh, T. and B. Cullum, *Biosensors and biochips: advances in biological and medical diagnostics.* Fresenius' journal of analytical chemistry, 2000. **366**(6-7): p. 540-51.
18. Szwaya, J., et al., *A novel platform for accelerated pharmacodynamic profiling for lead optimization of anticancer drug candidates.* Journal of biomolecular screening, 2007. **12**(2): p. 159-66.
19. Sundberg, S.A., *High-throughput and ultra-high-throughput screening: solution- and cell-based approaches.* Current opinion in biotechnology, 2000. **11**(1): p. 47-53.
20. Barberis, A., *Cell-based high-throughput screens for drug discovery.* European Biopharmaceutical Review, 2002: p. 93-96.
21. Ji, H.F., et al., *Microcantilever biosensors based on conformational change of proteins.* The Analyst, 2008. **133**(4): p. 434-43.

22. Yan, X., et al., *Surface stress changes induced by the conformational change of proteins.* Langmuir : the ACS journal of surfaces and colloids, 2006. **22**(26): p. 11241-4.
23. Braun, T., et al., *Conformational change of bacteriorhodopsin quantitatively monitored by microcantilever sensors.* Biophysical Journal, 2006. **90**(8): p. 2970-7.
24. Ray, S., G. Mehta, and S. Srivastava, *Label-free detection techniques for protein microarrays: prospects, merits and challenges.* Proteomics, 2010. **10**(4): p. 731-48.
25. Endo, T., et al., *Multiple label-free detection of antigen-antibody reaction using localized surface plasmon resonance-based core-shell structured nanoparticle layer nanochip.* Analytical chemistry, 2006. **78**(18): p. 6465-75.
26. Tan, W., et al., *Optical protein sensor for detecting cancer markers in saliva.* Biosensors & bioelectronics, 2008. **24**(2): p. 266-71.
27. Joo, C., et al., *Spectral-domain optical coherence phase microscopy for label-free multiplexed protein microarray assay.* Biosensors & bioelectronics, 2009. **25**(2): p. 275-81.
28. Tomlinson, I.M. and L.J. Holt, *Protein profiling comes of age.* Genome Biol, 2001. **2**(2): p. REVIEWS1004.
29. Ozkumur, E., et al., *Quantification of DNA and protein adsorption by optical phase shift.* Biosensors & bioelectronics, 2009. **25**(1): p. 167-72.
30. Nath, N.; Available from: http://biosensing.wordpress.com/.
31. Gauglitz, G. and G. Proll, *Strategies for label-free optical detection.* Advances in biochemical engineering/biotechnology, 2008. **109**: p. 395-432.
32. Haake, H.M., A. Schutz, and G. Gauglitz, *Label-free detection of biomolecular interaction by optical sensors.* Fresenius' journal of analytical chemistry, 2000. **366**(6-7): p. 576-85.
33. Nirschl, M. and J. Vörös, *Review of Transducer Principles for Label-Free Biomolecular Interaction Analysis.* Biosensors 2011. **1**(3): p. 70-92.
34. Shiau, A.K., M.E. Massari, and C.C. Ozbal, *Back to basics: label-free technologies for small molecule screening.* Comb Chem High Throughput Screen, 2008. **11**(3): p. 231-7.
35. Rich, R.L. and D.G. Myszka, *Survey of the year 2000 commercial optical biosensor literature.* J Mol Recognit, 2001. **14**(5): p. 273-94.
36. Rich, R.L. and D.G. Myszka, *Grading the commercial optical biosensor literature-Class of 2008: 'The Mighty Binders'.* J Mol Recognit. **23**(1): p. 1-64.
37. Baird, C.L. and D.G. Myszka, *Current and emerging commercial optical biosensors.* J Mol Recognit, 2001. **14**(5): p. 261-8.
38. Nusz, G.J., et al., *Label-Free Plasmonic Detection of Biomolecular Binding by a Single Gold Nanorod.* Anal. Chem., 2008. **80**(4).
39. Skorobogatiy, M. and A.V. Kabashin, *Photonic crystal waveguide-based surface Plasmon resonance biosensor.* Appl. Phys. Lett., 2006. **89**.
40. Comley, J., *Progress in the implementation of label-free detection part 2: binding analysis assays.* Lead Discovery World Fall, 2008.
41. Fang, Y., *Label-free optical biosensors in drug discovery.* Trends in Bio/Pharmaceutical industry, 2007. **3**.
42. Merwe, P.A.v.d., *Surface plasmon resonance*, Biacore.
43. Birkert, O., et al., *Label-Free Parallel Screening of Combinatorial Triazine Libraries Using Reflectometric Interference Spectroscopy.* Anal. Chem., 2002. **74**(4).

44. Brecht, A., G. Gauglitza, and J. Polsterb, *Interferometric immunoassay in a FIA-system: a sensitive and rapid approach in label-free immunosensing.* Biosen. Bioelectron., 1993. **8**(7-8).
45. Vakhtin, A.B., et al., *Common-path interferometer for frequency-domain optical coherence tomography.* Appl. Opt., 2003. **42**(34).
46. Bouma, B.E. and G.J. Tearney, eds. *Handbook of optical coherence tomography*. 2002, Marcel Dekker, Inc.
47. Joo, C., et al., *Spectral-domain optical coherence phase microscopy for label-free multiplexed protein microarray assay.* Biosen. Bioelectron., 2009. **25**.
48. Joo, C. and J.F. de Boer, *Spectral-domain optical coherence reflectometric sensor for highly sensitive molecular detection.* Optics letters, 2007. **32**(16): p. 2426-8.
49. Joo, C., et al., *Spectral-domain optical coherence phase microscopy for quantitative phase-contrast imaging.* Optics letters, 2005. **30**(16): p. 2131-3.
50. Liu, B., S. Li, and J. Hu, *Technological advances in high-throughput screening.* Am J Pharmacogenomics, 2004. **4**(4): p. 263-76.
51. Hariharan, P., *Basics of Interferometry*2007.
52. Wolff, E.G., *Fundamentals of Optical Interferometry for Thermal Expansion Measurements.* For presentation at the 27th International Thermal Conductivity Conference and 15th International Thermal Expansion Symposium , October 26-29, 2003 Knoxville, Tennessee, 2003.
53. Harasaki, A. and J.C. Wyant, *Fringe modulation skewing effect in white-light vertical scanning interferometry.* Applied optics, 2000. **39**(13): p. 2101-6.
54. Wyant, J.C., *White Light Interferometry.* Optical Sciences Center, 2003.
55. Lee, C.E. and H.F. Taylor, *Fiber-optic Fabry-Perot Temperature Sensor Using a Low-Coherence Light Source.* Journal of Lightwave Technology, 1991. **9**(1): p. 129-134.
56. Ellerbee, A.K., T.L. Creazzo, and J.A. Izatt, *Investigating nanoscale cellular dynamics with cross-sectional spectral domain phase microscopy.* Optics express, 2007. **15**(13): p. 8115-24.
57. Ellerbee, A.K. and J.A. Izatt, *Phase retrieval in low-coherence interferometric microscopy.* Optics letters, 2007. **32**(4): p. 388-90.
58. Choma, M.A., et al., *Spectral-domain phase microscopy.* Optics letters, 2005. **30**(10): p. 1162-4.
59. Novacam. http://www.novacam.com/technology/how-lci-works/.
60. Morel, E.N. and J.R. Torga, *Spectral Low Coherence Interferometry: A Complete Analysis of the Detection System and the Signal Processing.* Universidad Tecnológica Nacional, Facultad Regional Delta Campana, Buenos Aires Argentina. **6**.
61. Shaked, N.T., et al., *Reflective interferometric chamber for quantitative phase imaging of biological sample dynamics.* Journal of biomedical optics, 2010. **15**(3): p. 030503.
62. http://www.optique-ingenieur.org/en/index.
63. Krstaji, N., et al., *Common path Michelson interferometer based on multiple reflections within the sample arm: sensor applications and imaging artefacts* Meas. Sci. Technol., 2011. **22**: p. 1-6.
64. Choma, M.A., et al., *Doppler flow imaging of cytoplasmic streaming using spectral domain phase microscopy.* Journal of biomedical optics, 2006. **11**(2): p. 024014.
65. Vakhtin, A.B., et al., *Common-path interferometer for frequency-domain optical coherence tomography.* Appl Opt, 2003. **42**(34): p. 6953-8.

66. de Boer, J.F., et al., *Improved signal-to-noise ratio in spectral-domain compared with time-domain optical coherence tomography.* Opt Lett, 2003. **28**(21): p. 2067-9.
67. Blazkiewicz, P., et al., *Signal-to-noise ratio study of full-field fourier-domain optical coherence tomography.* Appl Opt, 2005. **44**(36): p. 7722-9.
68. Joo, C., et al., *Spectral-domain optical coherence phase microscopy for label-free multiplexed protein microarray assay.* Biosens Bioelectron, 2009. **25**(2): p. 275-81.
69. Joo, C. and J.F. de Boer, *Spectral-domain optical coherence reflectometric sensor for highly sensitive molecular detection.* Opt Lett, 2007. **32**(16): p. 2426-8.
70. Dave, D.P., *Phase sensitive interferometry for biosensing applications.* Methods Mol Biol, 2009. **503**: p. 179-87.
71. Dave, D.P., *Phase sensitive interferometry for biosensing applications.* Methods in molecular biology, 2009. **503**: p. 179-87.
72. Cooper, M.A., *Label-free biosensors*. Vol. 1. 2009: Cambridge University press.
73. Ozkumur, E., et al., *Quantification of DNA and protein adsorption by optical phase shift.* Biosens Bioelectron, 2009. **25**(1): p. 167-72.
74. Pease, L.F., 3rd, et al., *Determination of protein aggregation with differential mobility analysis: application to IgG antibody.* Biotechnol Bioeng, 2008. **101**(6): p. 1214-22.
75. Comley, J., *Progress in the Implementation of Label-Free Detection - part 1: cell-based assays. Summer 08.* Lead Discovery World Summer, 2008.
76. Arumugam, S. and V.V. Popik, *Attach, Remove, or Replace: Reversible Surface Functionalization Using Thiol-Quinone Methide Photoclick Chemistry.* Journal of the American Chemical Society, 2012.
77. Rendl, M., et al., *Simple one-step process for immobilization of biomolecules on polymer substrates based on surface-attached polymer networks.* Langmuir : the ACS journal of surfaces and colloids, 2011. **27**(10): p. 6116-23.
78. Crespin, M., et al., *Surface properties and cell adhesion onto allylamine-plasma and amine-plasma coated glass coverslips.* Journal of materials science. Materials in medicine, 2011. **22**(3): p. 671-82.
79. Haensch, C., S. Hoeppener, and U.S. Schubert, *Chemical modification of self-assembled silane based monolayers by surface reactions.* Chemical Society reviews, 2010. **39**(6): p. 2323-34.
80. Nolte, A.J., et al., *In situ adhesion measurements utilizing layer-by-layer functionalized surfaces.* ACS applied materials & interfaces, 2009. **1**(2): p. 373-80.
81. Groll, J., et al., *A novel star PEG-derived surface coating for specific cell adhesion.* Journal of biomedical materials research. Part A, 2005. **74**(4): p. 607-17.
82. Fixe, F., et al., *Functionalization of poly(methyl methacrylate) (PMMA) as a substrate for DNA microarrays.* Nucleic acids research, 2004. **32**(1): p. e9.
83. Schlecht, C.A. and J.A. Maurer, *Functionalization of glass substrates: mechanistic insights into the surface reaction of trialkoxysilanes.* RSC Adv., 2011. **1**: p. 1446-1448.
84. Zhang, Y., et al., *Miniature fiber-optic multicavity Fabry-Perot interferometric biosensor.* Optics letters, 2005. **30**(9): p. 1021-3.
85. Inc, M. http://www.memsurface.com/.
86. Xenopore. http://www.xenopore.com/.
87. Kodoyianni, V., *Label-free analysis of biomolecular interactions using SPR imaging.* BioTechniques, 2011. **50**: p. 32-40.

88. Y, D. and S. C, *Heterogeneous immunosensing using antigen and antibody monolayers on gold surfaces with electrochemical and scanning probe detection.* Anal Chem, 2000. **72**(11): p. 2371-2376.
89. Murphy, R.M., et al., *Size and structure of antigen-antibody complexes: thermodynamic parameters.* Biochemistry, 1990. **29**(49): p. 10889-99.
90. Murphy, R.M., et al., *Size and structure of antigen-antibody complexes. Electron microscopy and light scattering studies.* Biophysical Journal, 1988. **54**(1): p. 45-56.
91. Holtz, B., et al., *Denaturing and refolding of protein molecules on surfaces.* Proteomics, 2007. **7**(11): p. 1771-4.
92. Doster, W., *The protein-solvent glass transition.* Biochimica et biophysica acta, 2010. **1804**(1): p. 3-14.
93. Ngai, K.L., S. Capaccioli, and N. Shinyashiki, *The protein "glass" transition and the role of the solvent.* The journal of physical chemistry. B, 2008. **112**(12): p. 3826-32.
94. Weik, M., et al., *Specific protein dynamics near the solvent glass transition assayed by radiation-induced structural changes.* Protein science : a publication of the Protein Society, 2001. **10**(10): p. 1953-61.
95. Vitkup, D., et al., *Solvent mobility and the protein 'glass' transition.* Nature structural biology, 2000. **7**(1): p. 34-8.
96. Porter, D. and F. Vollrath, *Water mobility, denaturation and the glass transition in proteins.* Biochimica et biophysica acta, 2012. **1824**(6): p. 785-91.
97. Hlady, V., J. Buijs, and H.P. Jennissen, *Methods for studying protein adsorption.* Methods in enzymology, 1999. **309**: p. 402-29.
98. Squires, T.M., R.J. Messinger, and S.R. Manalis, *Making it stick: convection, reaction and diffusion in surface-based biosensors.* Nature biotechnology, 2008. **26**(4): p. 417-26.
99. Schlecht, C.A. and J.A. Maurer, *Functionalization of glass substrates: mechanistic insights into the surface reaction of trialkoxysilanes.* RSC Adv., 2011(1): p. 1446-1448.
100. Bosch, M.E., et al., *Recent Development in Optical Fiber Biosensors.* Sensors and Actuators, 2007. **7**.
101. Bleicher, K.H., et al., *Hit and lead generation: beyond high-throughput screening.* Nature reviews. Drug discovery, 2003. **2**(5): p. 369-78.
102. Macarron, R., et al., *Impact of high-throughput screening in biomedical research.* Nature reviews. Drug discovery, 2011. **10**(3): p. 188-95.
103. Liu, B., S. Li, and J. Hu, *Technological advances in high-throughput screening.* American journal of pharmacogenomics : genomics-related research in drug development and clinical practice, 2004. **4**(4): p. 263-76.
104. Fernandes, P.B., *Technological advances in high-throughput screening.* Current opinion in chemical biology, 1998. **2**(5): p. 597-603.
105. Guan, Z.G., D. Chen, and S. HE, *Coherence Multiplexing of Distributed Sensors Based on Pairs of Fiber Bragg Gratings of Low Reflectivity.* Journal of Lightwave Technology, 2007. **25**(8): p. 2143-2148.
106. Sorin, W. and D. Baney, *Multiplexed Sensing using Optical Low-Coherence Retlectometry.* Hewlett Packard, 1995.
107. Lo, Y.L., *Study of cross-talk of parallel Fabry Perot sensors in path-matching differential interferometry.* Optics and Lasers in Engineering 1999. **31**: p. 401-410.

108. Drake, T.K., F.E. Robles, and A. Wax, *Multiplexed low coherence interferometry instrument for measuring microbicide gel thickness distribution.* Applied optics, 2009. **48**(10): p. D14-9.
109. Chirvi, S., Z. Qiang, and D.P. Davé, *Coherence multiplexed label-free biomolecular interaction analysis.* Optics letters, 2012.
110. Fang, Y., *Live cell optical sensing for high throughput applications.* Advances in biochemical engineering/biotechnology, 2010. **118**: p. 153-63.

BIOGRAPHICAL INFORMATION

Sajal Chirvi was born on 17th May, 1983 in Srinagar, Jammu and Kashmir, India. She completed her Bachelor of Engineering in Biomedical Engineering from Mumbai (Bombay) University, India in May 2004. She served as research trainee engineer at biomedical wing of Bhaba Atomic Research Center, Mumbai, India for one year.

She joined University of Texas at Arlington in spring 2007 to pursue Masters of Science in Biomedical Engineering. After completion of her Masters in 2008, she continued with her Ph.D in Biomedical Engineering with joint program between University of Texas at Arlington and University of Texas Southwestern Medical Center at Dallas.

Her research interests include biomolecular interaction studies and biosensing using interferometric techniques. She is also interested in platform miniaturization for point of care diagnostics and lab on chip applications.